SOCRATES

Table of Contents

1. Overview

The NCAR interactive chemical dynamical radiative two-dimensional (2-D) model has undergone substantial changes since its description was last published (Brasseur et al 1990). This report presents the details of the most recent version SOCRATES (**S**imulation **o**f **C**hemistry, **R**adiation, **a**nd **T**ransport of **E**nvironmentally important **S**pecies). Major changes in SOCRATES from the previous version include :

- Model domain extended up to 120 km altitude to include mesospheric and thermospheric processes (molecular diffusion, simplified ionic productions, tidal wave forcing etc.).
- UV Radiative transfer that accounts for multiple scattering by air molecules, aerosols and clouds.
- Parameterization of aerosol and cloud radiative effects in the infrared.
- Non-LTE infrared radiation for the mesosphere.
- Planetary wave model to parameterize interactions between planetary wave and mean flow.
- Update of the gravity wave forcing parameterization.
- Option of imposing QBO forcing.
- Circulation boundary condition moved down to 2 km and determined from physical principles.
- Tropospheric winds and temperature calculated interactively with specified forcing.
- Semi-Lagrangian transport scheme used to solve for chemical transport.
- Tropospheric hydrocarbon chemistry.
- Diurnal averaging scheme that allows for diurnal variation for chemical species.
- Parameterization of convective and frontal induced vertical transport in the troposphere.

The model domain extends from the surface to 120 km with a 1 km vertical resolution, and from -85º to 85º latitude with a 5º latitudinal resolution. Time step for the thermodynamic and the chemical transport equations can be varied, but for a general run,

a time step of 1 day is being used. The radiative heating is calculated every 5 days. Different time steps can also be assigned for the time integration of the planetary wave model. Currently, a time step of 1 day for the wave model is used. In order to describe approximately the diurnal variation of chemical species, the chemical equation without the effect of transport is time integrated with 8 timesteps per day, with 4 timesteps per daytime, and 4 timesteps per nighttime.

SOCRATES has the capability of accounting for multiple-scattering of air molecules, aerosols and clouds in the calculation of the solar heating rate and photolysis rates. This is performed by solving a multiple-scattering radiative transfer equation using the two-stream delta-Eddington method. Absorption cross sections of chemical compounds have been updated to more recent data, and improved parameterization of the Schumann-Runge bands for O2 photolysis rates and the delta bands for NO photolysis rates were implemented.

In order to facilitate mesospheric studies of the model, a non-LTE CO2 infrared radiative code of the mesosphere is incorporated in the model in place of the simple Newtonian cooling formulation. Solar heating from chemical recombination and solar energy loss to airglow process which are important in the mesosphere are taken into account. To consider the effect of molecular diffusion on the chemical species and heat budget, molecular diffusion and thermal conductivity are implemented in the chemical transport and the thermodynamic calculations.

New methods to estimate the dynamical forcing from planetary and gravity waves have been implemented. Planetary wave momentum forcing is calculated from a quasi-geostrophic wave model that takes into account dissipation caused by Newtonian cooling, Rayleigh friction, and wave breaking. For grravity wave forcing, the standard run utilizes the Lindzen (1981) formulation, although another option of a parameterization scheme that utilizes the observed energy spectral characteristic of gravity wave motions is available. Another update in the dynamic aspect of the model is the option of including a quasi-biennial oscillation (QBO) type forcing (deduced from observed zonal wind oscillation) in the temperature and circulation fields.

The lower boundary of the circulation and temperature has been moved from the tropopause level down to 2 km altitude. In addition, the lower boundary condition of the stream function at 2 km is interactive with the model-derived wave forcings. The temperature in the troposphere is explicitly calculated from thermodynamics consideration, through the specification of tropospheric wave momentum flux and latent heating according to climatology. This lessens the constraint of the lower stratospheric circulation to the lower boundary condition, and allows some degree of interaction between the troposphere and the stratosphere.

The most significant improvement made in the chemical module of the model is in treating explicitly the diurnal variation affecting chemical species. For this purpose, the timestep in the chemical equation has been shortened (8 timesteps per day). This eliminates the need to diurnally average the photolysis rates for the chemical time integration. In addition, the chemical family technique used in the previous version of the model has been replaced by a formulation in which each chemical compound is treated seperately. Another improvement made is in the representation of tropospheric chemistry, in particular hydrocarbon chemistry. Chemical species and reactions important in the troposphere which may have non-negligible consequences in the stratosphere were added, including the chemistry of C2H6, C3H6, CH2O, PAN etc. In addition, a simple parameterization of vertical tropospheric tracer transport in convective and frontal regions is included in the model.

The logistical structure of SOCRATES (shown in Figure 1) is slightly modified from the previous version of the model in that solar heating rate is estimated along with the photolysis calculation instead of being separately calculated. The model starts off with using initial temperature and concentrations of chemical species to calculate the zonal wind (from geostrophic approximation), solar heating and infrared cooling rates. The planetary and gravity wave forcing, along with the eddy diffusivity, is then estimated according to the zonal wind profile. With this wave forcing and heating information, the circulation is derived. Subsequently, the model calculates the temperature for the next time step, according to thermodynamic principles from the circulation and heating rates. From here on, it

calculates the photolysis rates, solar heating rate, and the concentration of the chemical species, and then continues on to the next time loop.

---

1. Overview

The NCAR interactive chemical dynamical radiative two-dimensional (2-D) model has undergone substantial changes since its description was last published (Brasseur et al 1990). This report presents the details of the most recent version SOCRATES (**S**imulation **o**f **C**hemistry, **R**adiation, **a**nd **T**ransport of **E**nvironmentally important **S**pecies). Major changes in SOCRATES from the previous version include :

- Model domain extended up to 120 km altitude to include mesospheric and thermospheric processes (molecular diffusion, simplified ionic productions, tidal wave forcing etc.).
- UV Radiative transfer that accounts for multiple scattering by air molecules, aerosols and clouds.
- Parameterization of aerosol and cloud radiative effects in the infrared.
- Non-LTE infrared radiation for the mesosphere.
- Planetary wave model to parameterize interactions between planetary wave and mean flow.
- Update of the gravity wave forcing parameterization.
- Option of imposing QBO forcing.
- Circulation boundary condition moved down to 2 km and determined from physical principles.
- Tropospheric winds and temperature calculated interactively with specified forcing.
- Semi-Lagrangian transport scheme used to solve for chemical transport.
- Tropospheric hydrocarbon chemistry.
- Diurnal averaging scheme that allows for diurnal variation for chemical species.
- Parameterization of convective and frontal induced vertical transport in the troposphere.

The model domain extends from the surface to 120 km with a 1 km vertical resolution, and from -85º to 85º latitude with a 5º latitudinal resolution. Time step for the thermodynamic and the chemical transport equations can be varied, but for a general run, a time step of 1 day is being used. The radiative heating is calculated every 5 days. Different time steps can also be assigned for the time integration of the planetary wave model. Currently, a time step of 1 day for the wave model is

used. In order to describe approximately the diurnal variation of chemical species, the chemical equation without the effect of transport is time integrated with 8 timesteps per day, with 4 timesteps per daytime, and 4 timesteps per nighttime.

SOCRATES has the capability of accounting for multiple-scattering of air molecules, aerosols and clouds in the calculation of the solar heating rate and photolysis rates. This is performed by solving a multiple-scattering radiative transfer equation using the two-stream delta-Eddington method. Absorption cross sections of chemical compounds have been updated to more recent data, and improved parameterization of the Schumann-Runge bands for O2 photolysis rates and the delta bands for NO photolysis rates were implemented.

In order to facilitate mesospheric studies of the model, a non-LTE CO2 infrared radiative code of the mesosphere is incorporated in the model in place of the simple Newtonian cooling formulation. Solar heating from chemical recombination and solar energy loss to airglow process which are important in the mesosphere are taken into account. To consider the effect of molecular diffusion on the chemical species and heat budget, molecular diffusion and thermal conductivity are implemented in the chemical transport and the thermodynamic calculations.

New methods to estimate the dynamical forcing from planetary and gravity waves have been implemented. Planetary wave momentum forcing is calculated from a quasi-geostrophic wave model that takes into account dissipation caused by Newtonian cooling, Rayleigh friction, and wave breaking. For grravity wave forcing, the standard run utilizes the Lindzen (1981) formulation, although another option of a parameterization scheme that utilizes the observed energy spectral characteristic of gravity wave motions is available. Another update in the dynamic aspect of the model is the option of including a quasi-biennial oscillation (QBO) type forcing (deduced from observed zonal wind oscillation) in the temperature and circulation fields.

The lower boundary of the circulation and temperature has been moved from the tropopause level down to 2 km altitude. In addition, the lower boundary condition of the stream function at 2 km is interactive with the model-derived wave forcings. The temperature in the troposphere is explicitly calculated from thermodynamics consideration, through the specification of tropospheric wave momentum flux and latent heating according to climatology. This lessens the constraint of the lower

stratospheric circulation to the lower boundary condition, and allows some degree of interaction between the troposphere and the stratosphere.

The most significant improvement made in the chemical module of the model is in treating explicitly the diurnal variation affecting chemical species. For this purpose, the timestep in the chemical equation has been shortened (8 timesteps per day). This eliminates the need to diurnally average the photolysis rates for the chemical time integration. In addition, the chemical family technique used in the previous version of the model has been replaced by a formulation in which each chemical compound is treated seperately. Another improvement made is in the representation of tropospheric chemistry, in particular hydrocarbon chemistry. Chemical species and reactions important in the troposphere which may have non-negligible consequences in the stratosphere were added, including the chemistry of C2H6, C3H6, CH2O, PAN etc. In addition, a simple parameterization of vertical tropospheric tracer transport in convective and frontal regions is included in the model.

The logistical structure of SOCRATES (shown in Figure 1) is slightly modified from the previous version of the model in that solar heating rate is estimated along with the photolysis calculation instead of being separately calculated. The model starts off with using initial temperature and concentrations of chemical species to calculate the zonal wind (from geostrophic approximation), solar heating and infrared cooling rates. The planetary and gravity wave forcing, along with the eddy diffusivity, is then estimated according to the zonal wind profile. With this wave forcing and heating information, the circulation is derived. Subsequently, the model calculates the temperature for the next time step, according to thermodynamic principles from the circulation and heating rates. From here on, it calculates the photolysis rates, solar heating rate, and the concentration of the chemical species, and then continues on to the next time loop.

---

2. Model Physics and Chemistry.

The 2-D model extends vertically from the surface up to 120 km with a vertical resolution of 1 km, and latitudinally from -85 to 85 with a 5º resolution. Log-pressure height is used as the vertical coordinate. As in Garcia and Solomon (1983), the dynamical fields and temperature are governed by a set of zonally-averaged quasi-geostropic equations of thermodynamics, momentum, and mass continuity, expressed in the transformed Eulerian mean (TEM) framework (symbol definition listed in Appendix A).

$$\frac{\partial \overline{\theta}}{\partial t} + \overline{v}^{*} \frac{\partial \overline{\theta}}{\partial y} + \overline{w}^{*} \frac{\partial \overline{\theta}}{\partial z} = Q_S + Q_{IR} + D_\theta \qquad (1)$$

$$\frac{\partial \overline{u}}{\partial t} - \eta \overline{v}^{*} + \frac{\partial \overline{u}}{\partial z} \overline{w}^{*} = F_R + F_G + F_T \qquad (2)$$

$$\frac{1}{\cos\phi} \frac{\partial}{\partial y} (\overline{v}^{*} \cos\phi) + \frac{1}{\rho_0} \frac{\partial}{\partial z} (\rho_0 \overline{w}^{*}) = 0 \qquad (3)$$

$$(f + 2\overline{u} \frac{\tan\phi}{a}) \frac{\partial \overline{u}}{\partial z} = -\frac{g}{\theta} \frac{\partial \overline{\theta}}{\partial y} \qquad (4)$$

where

$$\eta = f - \frac{1}{\cos\phi} \frac{\partial}{\partial y} (\overline{u} \cos\phi) \quad . \qquad (5)$$

Note that in these equations, z represents the pressure altitude defined as $z = 7 \ln(p/p_0)$ where p_0 is the surface pressure. In Equation (1), thermodynamics is driven by solar heating (Q_S), infrared heating (Q_{IR}), and small scale diffusive transport of heat (D_q) by wave and molecular diffusion processes, given as:

$$D_\theta = \frac{1}{\cos\phi} \frac{\partial}{\partial y} (K_{yy} \cos\phi \frac{\partial \overline{\theta}}{\partial y}) + \frac{1}{\rho_0} \frac{\partial}{\partial z} (K_{zz} \rho_0 \frac{\partial \overline{\theta}}{\partial z}) + \frac{1}{\rho_0} \frac{\partial}{\partial z} (K_T \rho_0 \frac{\partial \overline{\theta}}{\partial z}). \qquad (6)$$

where K_{yy} is the meridional eddy diffusivity coefficient, K_{zz} the vertical diffusivity

coefficient, and K_T is the molecular thermal conductivity coefficient. The temperature and wind fields are advected by the transformed Eulerian mean circulation (v^* and w^*, also called residual circulation), a quantity that is more representative of the actual motions of air parcels in the meridional plane (see discussions in Andrews et al. 1987).The zonal momentum forcing (Equation (2)) is caused by planetary wave (F_R), gravity (F_G), and tidal wave (F_T) dissipation and breaking.

The governing equations can be combined to form a diagnostic equation for the mean circulation, represented by the streamfunction χ(Garcia and Solomon, 1983):

$$C_{yy}\frac{\partial^2\chi}{\partial y^2}+C_{yz}\frac{\partial^2\chi}{\partial y\partial z}+C_{zz}\frac{\partial^2\chi}{\partial z^2}+C_y\frac{\partial\chi}{\partial y}+C_z\frac{\partial\chi}{\partial z}=C_F\cos\phi \qquad (7)$$

where χ is related to the residual velocities as:

$$\overline{v}^* = -\frac{1}{\rho_0\cos\phi}\frac{\partial}{\partial z}(\rho_0\chi) \qquad (8a)$$

$$\overline{w}^* = \frac{1}{\rho_0\cos\phi}\frac{\partial}{\partial y}(\rho_0\chi) \qquad (8b)$$

The coefficients of the stream function equation (7) are functions of the mean zonal wind and temperature:

$$C_{yy} = N^2 \qquad (9a)$$

$$C_{yz} = 2f\frac{\partial\overline{u}}{\partial z} \qquad (9b)$$

$$C_{zz} = f(f+\overline{u}\frac{\tan\phi}{a}-\frac{\partial\overline{u}}{\partial y}) \qquad (9c)$$

$$C_y = N^2\frac{\tan\phi}{a}-\frac{f}{H}\frac{\partial\overline{u}}{\partial z} \qquad (9d)$$

$$C_z = -\frac{f}{H}(f+\overline{u}\frac{\tan\phi}{a}-\frac{\partial\overline{u}}{\partial y})+\frac{\partial\overline{u}}{\partial z}(2f\frac{\tan\phi}{a}+\frac{\partial f}{\partial y}). \qquad (9e)$$

The forcing term C_F on the right-hand side of Equation (7):

$$C_F = \frac{R}{H}\frac{\partial}{\partial y}(Q_S + Q_{IR} + D_\theta) + f\frac{\partial}{\partial z}(F_R + F_G + F_T) \qquad (10)$$

Therefore, the circulation determined by Equation (7) is driven by the latitudinal gradient of the diabatic heating and the vertical gradient of the wave momentum forcing. Central to the improvements made in SOCRATES are the different ways in which these radiative and dynamic forcings are derived; these will be described in detail in the next section.

2.1 Radiation

2.1.1 Ultraviolet (UV) and visible radiative region (117 - 730 nm)

The 2-D model has a total of 170 wavelength bands: a resolution of 500 cm^{-1} wavenumber between 116.3 and 307.7 nm, a resolution of 5 nm in wavelength between 307.7 and 655 nm, and a resolution of 10 nm in wavelength between 655 and 735 nm (see Table 1). At each wavelength, the actinic flux is obtained by solving the equation of radiative transfer with the delta-Eddington method (Shettle and Wienman 1970, Joseph et al.1976), which is a two-stream method (Meador and Weavor 1980; Toon et al., 1989).

The general equation for absorption and scattering of solar radiation in a plane-parallel atmosphere for each wavelength interval can be written as:

$$\mu \frac{dI(\tau,\mu)}{d\tau} = I(\tau,\mu) - \frac{\varpi(\tau)}{2}\int_{-1}^{1} d\mu' \, p(\mu;\mu')I(\tau,\mu') - \frac{\varpi(\tau)I^0}{4\pi} p(\mu;\mu_0)\, e^{-\tau/\mu_0} \qquad (11)$$

where I is the mean radiance, τ is the optical depth, ϖ is the single scattering albedo (ratio of scattering extinction and total extinction), p is the scattering phase function, μ is the cosine of the zenith angle, μ_0 is the cosine of the zenith angle for the direct solar beam, and I^0 is the mean radiance at the upper boundary of the model. The scattering phase function p is a non-dimensional quantity that describes the probability of angular distribution of the scattered energy. The first moment of the phase function is the asymmetry factor g, which gives the overall directionality of the phase function. The first term in the right-hand side of Equation (11) represents attenuation by absorption, the second term represents the diffusive radiation increase by multiple scattering, and the last term is the contribution from single-scattering of the direct solar beam.

Before obtaining a solution of Equation (11) with a two-stream method, delta scaling of the optical paramaters for cases of highly anisotropic phase functions is necessary to improve the accuracy of the solution, based on Joseph et al. (1976):

$$g' = \frac{g}{1+g} \tag{12a}$$

$$\tau' = (1 - \omega \cdot g^2) \cdot \tau \tag{12b}$$

$$\omega' = \frac{(1-g^2)\cdot\omega}{1-\omega\cdot g^2} \quad . \tag{12c}$$

This is done to reduce the anisotropy caused by the strong forward-scattering peak characteristic of larger particles (aerosols and clouds).

For the two-stream method, the diffuse radiance is divided into up-welling and down-welling components, I^+ and I^-, respectively. This produces a pair of integral radiance equations from Eq. (11) (for detail derivation, see Meador and Weaver 1980):

$$\frac{dI^+}{d\tau} = \gamma_1 I^+ - \gamma_2 I^- - I^0 \omega \gamma_3 e^{-\tau/\mu_0} \tag{13a}$$

$$\frac{dI^-}{d\tau} = \gamma_2 I^+ - \gamma_1 I^- + I^0 \omega \gamma_4 e^{-\tau/\mu_0} \tag{13b}$$

where coefficients γ_i's are determined by the approximation used. For the Eddington approximation, I^+ and I^- are assumed to have a simple angular distribution given as

$$I^{\pm}(\tau) = I_0(\tau) \pm \mu I_1(\tau). \tag{14}$$

This yields coefficients of the radiance equations as:

$$\gamma_1 = \frac{1}{4}[7 - \omega(4+3g)]$$

$$\gamma_2 = -\frac{1}{4}[1 - \omega(4+3g)]$$

$$\gamma_3 = \frac{1}{4}(2 - 3g\mu_0)$$

$$\gamma_4 = 1 - \gamma_3 \ .$$

The coefficients I^0 and I_1 are evaluated by solving the radiative equation for I^+ and I^- subject to the boundary conditions that no diffuse radiation is incident at the top of the atmosphere, while at the bottom of the atmosphere (the Earth's surface), radiation is reflected isotropically with a known albedo. Vertical inhomogeneity of the atmosphere is

parameterized by subdivison into 120 layers, each being then taken as internally homogeneous with specified vertical optical depth, single scattering albedo, and asymmetry factor. To solve for the set of two-stream equations in this multi-layer inhomogeneous atmosphere, the method described in Toon et al. (1989) is used. The triadiagonal matrix solution of their method provides improved computational speed necessary for the large number of vertical layers in our model.

The solar actinic flux at the top of the atmosphere ($q_0 = 4\pi I^0$) used in the model is shown in Table 1 . The solar flux is in units of photons/cm^2/s, with the size of the wavelength bin taken into account ($q_0(\lambda)\Delta\lambda$). Between the wavelength of 120 to 417 nm, the solar flux is the average of the flux measured by UARS SOLSTICE from Jan. 1st through March 29th, 1995 (representing long-term solar minimum condition) and from Jan 1st through March 31st, 1992 (representing solar maximum condition) (courtesy of G. Rottmann). Also listed in Table 1 is the fractional change of the solar flux from UARS day 169 to 1050 [(max-min)/(min)] representing the long-term solar variability. For wavelengths longer then 417 nm, the solar flux data are adapted from WMO (1986). To account for the ellipticity of the earth's orbit, the solar flux is adjusted with the annual variability : [1.-0.0342*cos(2 π*day/365)], with maximum flux during the winter season and minimum flux during the summer season.

The altitude variation of the optical parameters: extinction optical depth (from absorption and scattering), single scattering albedo, and asymmetry factor, are needed to obtain the solution of the solar radiative flux. Optical depth can be calculated knowing the absorption cross sections (σ) and number densities ([n]) of absorbing particles. For a clear sky atmosphere, oxygen and ozone are the main absorbers of solar radiation in the middle atmosphere. Their wavelength dependent absorption cross sections are available from laboratory measurements, reported in DeMore et al. (1997) (Note: the particular case of the Schumann-Runge bands will be described later). For the Rayleigh scattering by air molecules, an empirical formula proposed by Nicolet (1984) is used for the cross section:

$$\sigma_{RAY} = \frac{4.02 * 10^{-28}}{\lambda^{4+x}} \text{cm}^2 \qquad (15)$$

where $x = 0.389\lambda + 0.09426/\lambda - 0.3228$ for $0.2\ \mu\text{m} < \lambda < 0.55\mu\text{m}$

$x = 0.4$ for $0.55\ \mu\text{m} < \lambda < 1\mu\text{m}$

The single scattering albedo ω is then calculated from $\tau_{scat}/(\tau_{scat}+\tau_{abs})$. The asymmetry factor *g* for Rayleigh scattering is assumed to be zero (isotropic scattering).

To simulate aerosol scattering and absorption in the UV, some additional optical parameters are needed. Different approaches can be taken to obtain the optical parameters of scattering particles, depending on the conditions of interest. For background aerosol levels, Hitchman et al. (1994) compiled from SAGE and SAM measurements the climatology of aerosol extinction coefficient (ext_{aer}) at 1 μm over a period of roughly a decade. This aerosol extinction coefficient distribution can be used to calculate the extinction optical depth of aerosols by multiplying it with the thickness of the aerosol layer. To estimate its wavelength dependency, the simplest approach is to scale the extinction coefficient (for example, at 1 μ m) by the inverse of wavelength, which is a fair assumption according to Mie scattering calculations (Pinnick et al. 1980). An alternative is to use a precalculated spectral distribution of the extinction coefficient for background aerosol levels to scale the satellite-measured extinction coefficient at a given wavelength (for example, calculations shown in Fenn et al. 1985). As for the scattering parameters, the sulfate aerosols are known to be very effective scatterers with a single scattering albedo value close to 1, and an asymmetry factor of 0.7, which are approximately independent of wavelength (Michelangeli et al. 1989).

Optical properties for water cloud absorption and scattering in the UV and visible are calculated by the parameterization scheme of Hu and Stamnes (1993) based on Mie theory. The input parameters needed to be specified for this scheme are the liquid water content, effective droplet radius, cloud location, and vertical thickness. Following Kylling (1992), a typical water cloud effective radius of 10 mm and a liquid water content of 0.15 g/m3 are used in the model.

The solar zenith angles chosen for the radiative transfer equation are a function of both latitude and time of the year. As will be mentioned in the description of chemistry, for daytime conditions, the chemical equation is integrated in time with a timestep equal to one quarter of the length of the daylight part of the day. Thus, 2 photolysis calculations are made per day for each molecule subject to photodissociation. The zenith angle Z is calculated from the formula

$$\cos Z = \sin\phi \cdot \sin\delta + \cos\phi \cdot \cos\delta \cdot \cos(h_a) \qquad (16)$$

where δ is the inclination angle which is a function of day of year only (the latitude at

which the sun is directly over head with Z=0), and h_a is the hour angle (h_a=0 at noon). The value of the hour angle at sunrise or sunset $h_{1/2day}$ as a function of day and latitude can be determined from Equation (16) by setting Z=90º. Once the hour angle at sunrise (or sunset) is determined, Z is estimated for two specific times: $h_a=1/8h_{1/2day}$, and $h_a=3/8h_{1/2day}$.

To account for the sphericity of the earth in spite of the plane-parallel approximation, the Chapman function replaces the secant of zenith angle in the calculation of the optical depth. The method described by Smith and Smith (1972) for zenith angle less than 90º is used to estimate the Chapman function (Ch(Z)):

$$Ch(Z) = \sqrt{\frac{\pi x}{2}}\ erfc\left(\sqrt{\frac{x}{2}}\cos Z\right)\ \exp\left(\frac{x}{2}\cos^2 Z\right) \qquad (17)$$

where x=(a+z)/H . For zenith angles equal to or larger then 90º, night conditions are assumed.

a. Photolysis rates.

Once the solar flux at a given level is known from the solution of the radiative equation (Equation 11), the photodissociation coefficient for a given molecule can be calculated by:

$$J_i(z, Z) = 4\pi \int \sigma_i(\lambda)\varepsilon_i(\lambda) I(\lambda, z, Z) d\lambda \qquad (18)$$

This photolysis rate J (s^{-1}) for a given species i is proportional to the solar actinic flux $4\pi I$, the absorption cross section σ_i (cm^2) and the quantum efficiency ε_i. The photodissociations considered in the model are listed in Table 2 . The sources of reference for the absorption cross sections used in our model are listed in Table 3 . Molecules cross section that exhibit temperature dependencies include: ozone in the 175.8 to 347.5 nm range, N2O, NO2, HNO3, CFC12, CFC-11, CCl4 in the 200-250 nm range, ClONO2, N2O5 in the 200-281.7 nm range, H2O2, H2CO, PAN. For some source gases such a CH3CCl3, CH3Cl, CFC-113, HCFC-22, Ha-1211, Ha-1301, CH3Br, CFC-114, and CFC-115, temperature dependent cross section parameterizations are taken from Gillotay andSimon (1988) since data presented in DeMore et al. (1997) [JPL97] are for 298 K only. Cross checking of the cross sections from Gillotay and Simon (1988) and JPL97 showed

that at 298 K, the values are close to identical. For OClO, cross sections are spectrally interpolated directly from Wahner et al. (1987) instead of from JPL97 because its data are take from band peak amplitude which tends to overestimate the cross sections. The quantum efficiency ε is equal to unity in most cases, except for O3, H2CO, CF2O, NO3, ClONO2, and HO2NO2. The sources of their ε values are listed in Table 3 .

The treatment of O2 absorption in the Schumann-Runge bands (SRB: 175-205 nm) requires special attention because of the cross section's highly variable spectral structure in this wavelength region. The parameterization of the O2 absorption developed by Kockarts (1994) is used in the model. The method uses recent spectroscopic data of O2, and accounts for the temperature dependence of the O2 cross sections. It remains valid even when the slant O2 optical depth becomes very large. The photolysis rates for any molecule (M) other than O2 in the SRB are computed by

$$J_{M|SRB|} = \sum_{\dot{n}|SRB|} q_0 \sigma_M \varepsilon_M R_{\dot{n}}(M) e^{-\tau_{\dot{n}}|O_3|} \qquad (19)$$

where

$$R_{\dot{n}}(M) = a_{1|\dot{n}|}\exp(-a_{2|\dot{n}|}N) + a_{3|\dot{n}|}\exp(-a_{4|\dot{n}|}N) + a_{5|\dot{n}|}\exp(-a_{6|\dot{n}|}N) + a_{7|\dot{n}|}\exp(-a_{8|\dot{n}|}N) + a_{9|\dot{n}|}\exp(-a_{10|\dot{n}|}N) + a_{11|\dot{n}|}\exp(-a_{12|\dot{n}|}N)$$

and N is the slant total O2 overhead content, and q_0 is the solar flux at the top of atmosphere. In the particular case of molecular oxygen (O2) , the photolysis frequency in the SRB is expressed by :

$$J_{O2|SRB|} = \sum_{\dot{n}|SRB|} q_0 R_{\dot{n}}(O_2) e^{-\tau_{\dot{n}}|O_3|} \qquad (20)$$

where

$$R_{\dot{n}}(O_2) = b_{1|\dot{n}|}\exp(-b_{2|\dot{n}|}N) + b_{3|\dot{n}|}\exp(-b_{4|\dot{n}|}N) + b_{5|\dot{n}|}\exp(-b_{6|\dot{n}|}N) + b_{7|\dot{n}|}\exp(-b_{8|\dot{n}|}N) + b_{9|\dot{n}|}\exp(-b_{10|\dot{n}|}N) + b_{11|\dot{n}|}\exp(-b_{12|\dot{n}|}N)$$

The SRB is divided into 17 (iv) wavelength subintervals, and each wavelength subinterval is assigned 12 coefficients (a1~a12, b1 ~ b12) (Table 1 and 2 in Kockarts, 1994).

The photolysis of NO in the middle atmosphere occurs primarily in the δ(0-0) band (190.9 nm) and δ(1-0) band (182.7 nm). Since thes bands coincide with the Schumann-Runge bands of oxygen, the determination of J_{NO} requires a high spectral resolution treatment of

the SRB absorption. Minschwaner and Siskind (1993) use the method of opacity distribution function to parameterize J_{NO} with the latest spectroscopic information of both O2 and NO. Their scheme is used in SOCRATES to estimate the photolysis rates of NO. The photolysis frequency of NO coincident with a given SR band of O2 [(5-0), (9-0) and (10-0)] is determined by

$$J_{NO}(z) = q_0 e^{-\tau(O_3)} P(z) \sum_{i=1}^{6} \{\exp[-\sigma_{O2}^{i} N_{O2}(z)] \sum_{j=1}^{2} W_{NO}^{i,j} \sigma_{NO}^{i,j} \exp[-\sigma_{NO}^{i,j} N_{NO}(z)]\} \quad (21)$$

where P(z) = 1 for the δ(1-0) band, and P(z)=1.65e9/(5.1e7+1.65e9+1.5e-9[N2(z)]) for δ(0-0). One given SR band is subdivided into six wavelength regions (i=1,6) and inside each of these six regions by two values (j=1, 2) of NO cross section and weighting factor (WNO). The values of these coefficients are listed in Table 1 of Minschwaner and Siskind (1993).

b. UV solar heating.

The thermal effect of the solar radiation can be calculated from the radiative transfer equation (11) for the mean radiance *I*. Solar photon absorption by O2 and O3 are the major sources of heat in the stratosphere and mesosphere. Heating in the UV by O2 and O3 knowing *I* (J/s/cm2) and the absorption cross section σ of O2 and O3 (expressed in cm2) can be determined by

$$Q_S(z,Z) = 4\pi \frac{6x10^{23}}{c_p m_{air}[M]} \{[O_2] \int_{\lambda} \frac{hc}{\lambda} \sigma_{O2} I(\lambda,z,Z) d\lambda + [O_3] \int_{\lambda} \frac{hc}{\lambda} \sigma_{O3}(\lambda) I(\lambda,z,Z) d\lambda\} \quad (22)$$

where mair is the molecular weight of air (28.8 g/mole), [M] is the air number density (in cm^{-3}), [O2] is the O2 number density (cm^{-3}), and [O3] the ozone number density (cm^{-3}). When the effect of aerosol and cloud scattering is considered in the radiative transfer equation, solar heating due to aerosol (*aer*) and cloud (*wc*) heating is determined by:

$$Q_{Slacr,wcl}(z,Z) = 4\pi\left[\int \frac{hc}{\lambda} I(\lambda;z,Z)ext_{acr,wc}(\lambda)[1-\varpi_{acr,wc}(\lambda)]d\lambda\right]\frac{6x10^{23}}{c_p m_{air}[M]} \qquad (23)$$

in units of (K/s).

In Equation (22), it is assumed that the products of O2 and O3 photolysis recombine instantly as the solar energy absorbed, so that the heat release is equal to the solar energy is absorbed. Although this is generally valid for altitudes below 80 km, the recombination may not be instantaneous at altitudes above 80 km where the atmospheric density is low. Instead, at these higher altitudes, chemical combination may occur only after some time span comparable to the transport time scale. Under this circumstance, the solar energy absorbed less the dissociation energy of photolyzed molecules shall be called 'residual heating' (Q_R), and the heat released as a result of chemical recombination called 'chemical heating' (Q_C). Thus, the residual heating is calculated by:

$$Q_R(z,Z) = 4\pi\frac{6x10^{23}}{c_p m_{air}[M]}\left[[O_2]\int_\lambda\left(\frac{hc}{\lambda}-\zeta_{O2}\right)\sigma_{O2}(\lambda)I(\lambda;z,Z)d\lambda\right.$$
$$\left.+[O_3]\int_\lambda\left(\frac{hc}{\lambda}-\zeta_{O3}\right)\sigma_{O3}(\lambda)I(\lambda;z,Z)d\lambda\right] \qquad (24)$$

where ζ is the energy required to break the O2 and O3 bonds. To estimate heating from exothermic chemical reactions, the recombination of odd oxygen species and odd hydrogen species are considered, following Brasseur and Offermann (1986):

```
O+O+M ->  O2+M          k1, e1
O+O2+M -> O3+M          k2, e2
O+O3 -> 2O2             k3, e3
H+O3 -> OH+O2           k4, e4
OH+O -> H+O2            k5, e5
HO2+O -> OH+O2          k6, e6
H+O2+M -> HO2+M         k7, e7
```

k and *e* are the reaction rate and the bond breaking energy, respectively. The rate of energy released by these chemical reactions is given by:

$$Q_C = e_1 k_1[M][O]^2 + e_2 k_2[M][O_2][O] + e_3 k_3[O_3][O] + \kappa e_4 k_4[H][O_3] + e_5 k_5[OH][O] + e_6 k_6[HO_2][O] + e_7 k_7[M][H][O_2] \quad (25)$$

For reaction *k4*, the heating term is multiplied by a solar enegry efficiency factor κ, whose value is given below. The unit of Q_C is converted from J/s/cm2 to K/s, by multiplying Q_C by $N_A/([M]m_{air}c_p)$, where N_A is Avogadro's number, m_{air} is the air molecular mass and c_p is the specfic heat at constant pressure.

In and above the mesosphere, solar energy absorbed by molecules in the form of chemical potential energy may be lost by airglow from excited photolysis products or by chemiluminescent emission from product species of exothermic chemical reactions before the energy is able to be converted to thermal energy. Mlynczak and Solomon (1993) evaluated the reduction of the solar heating efficiency by airglow processes for different absorption bands of O2 and O3, and by chemiluminescent loss for exothermic chemical reactions. They showed the heating efficiencies (η) to be less than one in the O3 Hartley band, the O2 Schumann-Runge continuum, the O2 Lyman alpha line, and in the case of H +O3 chemical reaction. These efficiencies are expressed by the following expressions:

- O3 Hartley band (200 -310 nm) - η_{O3} =co+c1x +c2x2+c3x3

  where x = $\log_{10}$p + 3 for $10^{-4} \leq p(mb) \leq 10^{-2}$

  x = $\log_{10}$p + 1 for $10^{-2} \leq p(mb) \leq 100$

  For $10^{-4} \leq p(mb) \leq 10^{-2}$, c0=0.66965, c1=-0.009682, c2=0.033093, and c3=-0.017938. For $10^{-2} \leq p(mb) \leq 100$, c0=0.92621, c1=-0.133960, c2=-0.076863, and c3=-0.006897.

- O2 SR continuum (137-183 nm) - η_{O2} =co+c1x +c2x2+c3x3

  where x = $\log_{10}$p + 3 with p in (mb)

  c0=0.75349, c1=0.0036, c2=0.059468, and c3=-0.022795.

- O2 Lyman-alpha line (121.6 nm) - $\eta_{O2} = 0.95$

- H+O3 -> OH+O2 - $\kappa = 0.6$

$\eta = 1$ for all other wavelengths. To obtain the residual solar heating rate, Equation (24) is multiplied by η at each wavelength region mentioned above. Thus,

$$Q_R(z;Z) = 4\pi[\int \eta_{O2}(\lambda)(\frac{hc}{\lambda} - \zeta_{O2})\sigma_{O2}(\lambda)I(\lambda;z;Z)d\lambda + \int \eta_{O3}(\frac{hc}{\lambda} - \zeta_{O3})\sigma_{O3}(\lambda)I(\lambda;z;Z)d\lambda] \quad (26)$$

2.1.2 Infrared (IR) radiative regime (l > 3 µm)

a. Troposphere and stratosphere

The infrared radiative transfer routine used in SOCRATES for altitudes between 0 to 50 km is the long wave band model described in Briegleb (1992). Briegleb's model computes broadband absorptivity and emissivity with a modified Malkmus random band model, corrected for overabsorption of the traditional Malkmus band transmission. The model covers a spectral region of 0 to 3000 cm^{-1} with a spectral width of 100 cm^{-1}. With this wide spectral region and a relatively high spectral resolution, minor bands of CO2 and O3, and several other radiatively active trace gases can be included in the calculation. In SOCRATES, radiative contributions from CO2, H2O,O3, CH4, N2O, CFC11, CFC12, and aerosols are included.

The optical depths for all gases are computed first, then the broadband transmission is calculated as an exponential of the summed optical depths of all gases. The optical depth for CO2, O3, CH4 and N2O for each 100 cm-1 band takes the form

$$\tau = \frac{1}{2}\frac{S_d\overline{p}^*}{S_p}[(1 + 8\frac{S_p\beta\overline{u}_a}{\overline{p}^*})^{\alpha} - 1] \quad (27)$$

where u_a is the column absorber amount (g/cm^2), S_p and S_d are band parameters [see Appendix of Brigleb (1992)] calculated as a function of line strength and half-line width taken from the HITRAN database (Rothman et. al 1987), β is the band dependent diffusivity factor to take into account the effect of solid angle integration, α is a band

dependent parameter which can be estimated from reference calculations, and p* = p+δ, where δ is an asymptotic pressure required to simulate Voigt line effects. For H2O, a different transmission function is given due to the more gradual variation of absorption strength with wavenumber and its wide wavelength absorption span:

$$\tau = \frac{1}{2}\frac{S_d \bar{\rho}}{S_p}[(1 + 4\frac{S_p \beta \bar{u}_a}{\bar{\rho}})^{1/2} - 1]. \qquad (28)$$

CFC11 and CFC12 weakly absorbs in the H2O window region between 800 to 1200 cm^{-1}, and their optical depths are given as

$$\tau = \beta(\tau)\sigma\bar{u}_a \qquad (29)$$

where σ is the absorption cross section in units of cm^2/g, and β(t) the diffusivity factor. The data for the absorption cross sections of the CFCs are from Massie et al. (1991). The diffusivity factor for the CFCs is taken from Ramanathan et al. (1985) as:

$$\beta(\tau) = 1.5 + \frac{0.5}{1 + 4\tau + 10\tau^2} \qquad (30)$$

where τ is the total optical depth of all absorbing species. Similarly, the aerosol optical depth is calculated by multiplying its spectral extinction coefficient (provided either through observation or through theoretical calculations) by the aerosol column depth.

Knowing the transmission (Γ=$e^{-\tau}$), the absorptivity (*A*) and emissivity (*E*) of the infrared radiative transfer equation is calculated by:

$$A(p,p') = \frac{1}{dB(T)/dT}\int (1 - \Gamma(p,p'))\frac{dB(T)}{dT}d\lambda \qquad (31a)$$

$$E(p,p_t) = \frac{1}{B(T_t)}\int (1 - \Gamma(p,p_t))B(T_t)d\lambda \qquad (31b)$$

B(T) is the spectrally integrated Planck function, and is the transmission for all gases absorbing between pressure *p* and *p'* for *abs*, and *p* and p_t (top boundary pressure) for *ems*, respectively. The longwave fluxes (upward + and downward -) at pressure *p* are calculated from the transfer equation by the formulation:

$$F^{-}(p) = B(T_t)E(p,p_t) + \int_{p_t}^{p} A(p,p')\frac{dB(T')}{dp'}dp' \qquad (32a)$$

$$F^{+}(p) = eB(T_g) + (1-e)F^{-}(p_s) + [B(T_s) - [eB(T_g) + (1-e)F^{-}(p_s)]]A(p,p_s)^m - \int_{p}^{p_s} A(p,p')\frac{dB(T')}{dp'}dp' \qquad (32b)$$

where subscript *g* denotes surface ground, subscript *s* denotes surface air, *e* is the broadband isotropic surface emissivity, and *m* is an empirical constant which partially corrects a bias in the surface atmosphere exchange. The upward and downward fluxes are differenced across layers to produce the longwave heating rates

$$Q_{IR} = \frac{g}{c_p}\frac{F^{-}(p_{k+1}) - F^{+}(p_{k+1}) - F^{-}(p_k) + F^{+}(p_k)}{p_{k+1} - p_k}. \qquad (33)$$

b. Mesosphere and lower thermosphere (CO2 15 μm)

The infrared radiative heating above the stratosphere is dominated by the CO2 15 μm bands, while contributions from other trace gases are negligible (Kuhn and London, 1969). Above 60 km, where the local thermodynamic equilibrium (LTE) does not necessarily apply due to low air density, a different method for the longwave radiation is required for the CO2 15 μm band. Under non-LTE conditions, the populations of the excited vibrational levels are no longer controlled by collisional processes and the source function of CO2 is no longer equal to the Planck function. For this purpose, Formichev et al. (1993) developed a parameterization scheme for the 15 μm CO2 band radiative heating rate for the middle atmosphere, which is incorporated in SOCRATES to estimate the infrared radiative heating rate above 60 km.

The parameterization scheme of Formichev et al. (1993) for altitudes 15 to 85 km is largely based on the work of Akmaev and Shved (1982), but accounts for the line overlapping in the CO2 band and for the non-LTE effects, in order for the parameterization scheme to be applicable to a wide altitude range, including a non-LTE layer (70-85 km). The cooling rate is calculated by the following formula:

$$Q_{IR}(x_0) = \frac{1}{c_p}(1 - 3\varphi_0)\sum_{j=-8}^{5}[a_j(x_0) + \varphi_0 b_j(x_0) + \varphi_0^2 c_j(x_0)]\varphi_j \quad (\mathrm{K/s}) \qquad (34)$$

where *j* is altitude index set from -8 to 5, *x=ln(1000/p(mb))* is the dimensionless height, and

$$\varphi_j = \exp(-960.24 / T_j).$$

The cooling rate accounts for the radiative exchange between a given level x0 and the other layers of the atmosphere denoted with subscript *j*. The coefficients a_j, b_j, and c_j in Equation (34) are listed in Tables A, B, and C of Formichev et al. (1993).

For the non-LTE layer between 85 to 115 km, the cooling rate calculation is based on the recurrence formula of Kutepov and Fomichev (1993), which is expressed by

$$Q_{IR}(x_j) = \frac{1}{c_p} 8.6301 \times 10^9 X_{CO_2,j} (1 - \lambda_j) \dot{\varepsilon}(x_j) \quad (K/s) \qquad (35)$$

where $X_{CO2,j}$ is the mixing ratio of CO2 at level j. The quantum probability λ_j is calculated by

$$\lambda_j = 1.5638 / [1.5638 + \exp(-x_j)[X_{N_2,j}(2.9T_j^2 - 1060T_j + 145000) + X_{O_2,j}(4.23T_j^2 - 1490T_j + 180000) + X_{O,j} k_0]] \qquad (36)$$

where $X_{N2,j}$, $X_{O2,j}$, and $X_{O,j}$ are the mixing ratios of N2, O2, and O, respectively, at level j, and k_0 is the collisional deactivation rate between O and CO2, which is not known with certainty. Currently, k_0 is set at 5×10^7 $s^{-1}atm^{-1}$. The value of $\varepsilon(x_j)$ is determined by the recurrence formula

$$A_j \dot{\varepsilon}(x_j) = A_{j-1} \dot{\varepsilon}(x_{j-1}) + D_{j-1} \varphi_{j-1} - D_j \varphi_j \qquad (37)$$

where A_j, and D_j are calculated from

$$A_j = 1 - \lambda_j (1 - \frac{1}{4} d_{j-1} - \frac{3}{4} d_j); \quad A_{j-1} = 1 - \lambda_{j-1} (1 - \frac{3}{4} d_{j-1} - \frac{1}{4} d_j);$$

$$D_j = \frac{1}{4} (d_{j-1} + 3d_j); \quad D_{j-1} = \frac{1}{4} (3d_{j-1} + d_j) \qquad (38)$$

The parameters d_j are listed in Table D of Fromichev et al. (1993).

2.2 Dynamics

The dynamical wave forcing and associated diffusion in SOCRATES are estimated as a function of the zonal wind and derived according to linear wave theories. Although it is still necessary to parameterize wave processes, the wave components are able to respond to and interact with the mean field. Three types of waves are included in the model: planetary, gravity and tidal waves. Transience, dissipation, and breaking of these waves produces convergence of the wave fluxes and deposit momentum on the zonal wind field, which is reflected in the governing equations (Eq. 2). Wave diffusive mixing is also generated in the process and principally affects the temperature distribution (Eq. 1) and chemical transport (Eq. 79). Details of how the wave forcing and diffusion are derived is described next.

2.2.1 Planetary waves

Following Smith and Avery (1987), the vorticity and thermodynamic equations for the planetary wave take the forms:

$$(\frac{\partial}{\partial t}+\frac{\bar{u}}{a\cos\phi}\frac{\partial}{\partial\lambda})q'+\frac{v'}{a}\frac{\partial\bar{q}}{\partial\phi}-f\bar{e}^{z}\frac{\partial}{\partial z}(e^{-z}w')=-(\beta+\delta)q' \qquad (39)$$

$$(\frac{\partial}{\partial t}+\frac{\bar{u}}{a\cos\phi}\frac{\partial}{\partial\lambda})T+\frac{v'}{a}\frac{\partial\bar{T}}{\partial\phi}+w'\frac{N^2H}{R}=-(\alpha+\delta)T \qquad (40)$$

The potential vorticity q is:

$$q=f+\frac{1}{a\cos\phi}\frac{\partial v}{\partial\lambda}-\frac{1}{a\cos\phi}\frac{\partial}{\partial\phi}(u\cos\phi) \qquad (41)$$

and the wave component of the meridional wind is:

$$v'=\frac{1}{fa\cos\phi}\frac{\partial\Phi'}{\partial\lambda}-\frac{1}{f^2a^2}\frac{\bar{u}}{a\cos\phi}\frac{\partial^2\Phi'}{\partial\lambda\partial\phi} \qquad (42)$$

where Φ' is the geopotential disturbance, with prime referring to wave quantities. To

represent wave dissipation from Newtonian cooling, Rayleigh friction and wave breaking, a linear damping term is added to the right hand side of equations (39) and (40), where α is the Newtonian cooling rate, β is the Rayleigh dissipation rate, and δ is the dissipation rate from planetary wave breaking (method to derive d will be described later). To derive the potential vorticity equation, *w'* is eliminated between (39) and (40), and substituted with (41) and (42) to form a single equation of the planetary wave geopotential Φ'. For a more concise formulation of the potential vorticity equation, the following transformed coordinates are defined:

$$z = -\ln(p / p_0) \qquad \text{log pressure}$$

$$s = \frac{R}{4\Omega^2 a^2}\left(\frac{\partial T}{\partial z} + \kappa T\right) \qquad \text{equivalent buoyancy frequency}$$

$$\breve{u} = \frac{\bar{u}}{a\cos\phi} \qquad \text{angular velocity}$$

Note that the log pressure *z* here is a dimensionless altitude unit used only within the wave model which is different from the pressure altitude coordinate used throughout SOCRATES. Furthermore, a new variable Ψ is introduced to define the geopotential Φ' at zonal wave number *m*, such that

$$\Phi' = \sqrt{s}e^{z/2}\Psi(\phi, z, t)e^{im\lambda}.$$

Thus, the equation can be written as:

$$\left(\frac{\partial}{\partial t} + \beta'\right)\left(A\Psi + B\frac{\partial \Psi}{\partial \phi} + \frac{\partial^2 \Psi}{\partial \phi^2}\right) + \left(\frac{\partial}{\partial t} + \alpha'\right)\left(D\frac{\partial^2 \Psi}{\partial z^2} + E\Psi\right) + \varepsilon\frac{\partial \Psi}{\partial z} + F\Psi = 0 \qquad (43)$$

where $\alpha' = \alpha + im\breve{u} + \delta$, $\beta' = \beta + im\breve{u} + \delta$, $\varepsilon = \frac{\sin^2\phi}{s}\frac{\partial \alpha}{\partial z}$, and

$$A = -\frac{m^2}{\cos^2\phi}$$

$$B = -\frac{1+\cos^2\phi}{\sin\phi\cos\phi}$$

$$D = \frac{\sin^2\phi}{s}, \quad \text{E=-1/4 D}$$

$$F = \frac{im}{\cos\phi}\frac{\partial \bar{q}}{\partial \phi} + \frac{1}{2}\frac{\sin^2\phi}{s}\frac{\partial \alpha + \delta}{\partial z}$$

In the current version of the model, we are using $s = 0.02$, independent of altitude, and only planetary wave one is considered, with $m = 1$. Then applying implicit method for time integration, Equation (43) can be rewritten as:

$$AA\frac{\partial^2\Psi}{\partial z^2} + BB\frac{\partial\Psi}{\partial z} + CC\frac{\partial^2\Psi}{\partial\phi^2} + DD\frac{\partial\Psi}{\partial\phi} + EE\Psi = FF \qquad (44)$$

where

$$AA = 1 + \Delta t \cdot \alpha'$$

$$BB = \Delta t \cdot \frac{\partial\alpha}{\partial z}$$

$$CC = (1 + \Delta t \cdot \beta')\frac{s}{\sin^2\phi}$$

$$DD = -(1 + \Delta t \cdot \beta')\frac{(1+\cos^2\phi)s}{\sin^3\phi \cdot \cos\phi}$$

$$EE = -(1 + \Delta t \cdot \beta')\frac{m^2 s}{\cos^2\phi \cdot \sin^2\phi} - \frac{1}{4}(1 + \Delta t \cdot \alpha') + \Delta t \cdot (\frac{im}{\cos\phi}\frac{\partial\overline{q}}{\partial\phi}\frac{s}{\sin^2\phi} + \frac{1}{2}\frac{\partial\alpha}{\partial z})$$

$$FF = \frac{\partial^2\Psi^{\ell-1}}{\partial z^2} + \frac{s}{\sin^2\phi}\frac{\partial^2\Psi^{\ell-1}}{\partial\phi^2} - \frac{1+\cos^2\phi}{\sin^3\phi\cdot\cos\phi}s\frac{\partial\Psi^{\ell-1}}{\partial\phi}$$

$$- (\frac{1}{4} + \frac{m^2 s}{\cos^2\phi\cdot\sin^2\phi})\Psi^{\ell-1}.$$

Using a space-centered differencing scheme, Equation (44) is solved using a numerical technique developed by Lindzen and Kuo (1969). Forcing at the lower boundary (16 km) is specified according to climatological values of wave one geopotential height at 100 mb (Randel, 1987). From the wave stream function, the wave zonal wind u' and meridional wind v' can be derived. The planetary wave momentum flux divergence, or the Eliassen-Palm (EP) flux divergence ∇ F , is then calculated from

$$F_R = \frac{1}{\rho_0 a\cos\phi}\nabla\cdot F$$

$$= -\frac{1}{a\cos^2\phi}\frac{\partial}{\partial\phi}(\overline{u'v'}\cos^2\phi) + \frac{1}{\rho_0}\frac{f}{4\Omega^2 a^2}\frac{\partial}{\partial z}(\rho_0\frac{\overline{v'\Psi_z}}{s}) \quad . \qquad (45)$$

The planetary wave diffusion coefficient Kyy and the wave breaking dissipation rate d are

derived according to methods developed by Garcia (1991). Garcia adopted barotropic instability as the criterion for planetary wave breaking, and assumed that there is dissipation when $|q'_y| \geq q_y$, generally when the zonal mean potential vorticity meridional gradient becomes negative. In this case, the dissipation rate is calculated from the WKB approximation [Eq. 17 of Garcia (1991)]:

$$\delta = c_{gy}[-\frac{5}{4}\frac{\overline{u}_y}{(\overline{u}-c)}] + c_{gz}[\frac{1}{2H} - \frac{3}{4}\frac{\overline{u}_z}{(\overline{u}-c)}] \qquad (46)$$

where c_{gy} and c_{gz} are the horizontal and vertical group velocities given by

$$c_{gy} = \frac{2kl}{k^2 + l^2 + \frac{f^2}{N^2}(m^2 + \frac{1}{4H^2})}(\overline{u}-c) \qquad (47a)$$

$$c_{gz} = \frac{2km\frac{f^2}{N^2}}{k^2 + l^2 + \frac{f^2}{N^2}(m^2 + \frac{1}{4H^2})}(\overline{u}-c). \qquad (47b)$$

The planetary wave diffusion coefficient K_{yy} coresponding to this dissipation rate is derived from

$$K_{yy} = \frac{\delta\overline{v'v'}}{k^2(\overline{u}-c)^2 + \delta^2} \qquad (48)$$

Evaluation of the dissipation rate requires knowledge of the phase speed (c), meridional wave number (l), and vertical wave number (m) for the group velocities. These quantities are likewise derived from Garcia (1991) [Eqs. (35) and (36)]:

$$l = \mathrm{Im}(\frac{\Phi'_y}{\Phi'})$$

$$m = \mathrm{Im}(\frac{\Phi'_z}{\Phi'})$$

$$c = -\frac{1}{k}\mathrm{Im}(\frac{\Phi'_t}{\Phi'})$$

where Im denotes the imaginary component.

2.2.2 Gravity waves

In the new version of the model, two options are available for the parameterization of the gravity wave breaking process. The default standard run uses the Lindzen-Holton gravity wave breaking scheme (Lindzen 1981, Holton 1982) for estimating the gravity wave forcing and vertical diffusion coefficient. In this case, the gravity wave momentum flux divergence is expressed as:

$$F_G = -A_g(\bar{u}-c)^2[(\bar{u}-c)-3H\frac{\partial \bar{u}}{\partial z}] \qquad (49a)$$

and the vertical eddy diffusion resulting from wave breaking is given by

$$K_{zz} = \frac{A_g}{Pr}\frac{(\bar{u}-c)^4}{N^2}[1-3H\frac{\partial \bar{u}/\partial z}{\bar{u}-c}], \qquad (49b)$$

where *Pr* is the Prandtl number and A_g is the amplitude coefficient. These parameters are unchanged from the previous versions of SOCRATES (Brasseur and Hitchman 1987, Brasseur et al. 1990).

A second option is to use the parameterization scheme developed primarily by Fritts and Lu (1993) (hereafter FL93), which will be described in more detail here. The Fritts-Lu gravity wave forcing parameterization scheme uses a general gravity wave spectral formulation (Fritts and VanZandt 1993) provided by the observed gravity wave spectrum to deduce how the gravity wave energy flux responds to variation in the background environment. The variation of total gravity wave energy E_0 with height is given by $E_0 \propto \int^{dz/H_E}$, where the scale height for energy growth is specified as

$$H_E = [2+\sin(\frac{\pi z}{60})]H, \qquad (50)$$

with z in kilometers. Equation (50) is slightly different from Equation (28) of Fritts and VanZandt (1993), based on more recent observations of the total energy variations (Wilson et al. 1991a,b), and produces a more realistic estimate of the gravity wave forcing profile. The lower boundary condition for gravity wave energy forcing is currently set at 30 km, and the total energy at 30 km is specified as a function of latitude and season according to Hirota (1984). With the assumption that the total energy is comprised of two component spectra propagating east and west, the energy at the lower boundary is equally

split into the east and west components, while their intrinsic phase speeds are calculated from the relation [Eq. (22) of Fritts and VanZandt (1993), $E_0/2$]

$$E_j = \frac{1}{2} c_{*j}^2 \qquad (51)$$

where j denotes the east or west direction, and c_{*j} is the intrinsic phase speed.

To determine how the total energy varies with height, with the atmospheric stratification and the local mean wind, the relationship expressed in Eq. (31) of FL93 ($E_0 \propto N^{1/2} e^{z/H_E}$) is used to obtain

$$E_0^z = E_0^{z-1} e^{1/H_E^z} \left(\frac{N^z}{N^{z-1}}\right)^{1/2} \qquad (52)$$

where the superscript z in this case denotes the altitude grid. Meanwhile, the energy spectra for each directional component (component energy) are assumed to vary with changes in the zonal wind in the vertical direction. When the vertical gradient of zonal wind is positive, the westerly phase speed c_{*w} increases with height according to

$$c_{*w}^z = \left[c_{*w}^{z0} + (\bar{u}^z - \bar{u}^{z0}) \cdot \frac{N^{z0}}{N^z}\right] \cdot \left(\frac{N^z}{N^{z0}}\right)^{1/4} \cdot e^{-dz/4H} \qquad (53)$$

with the corresponding easterly component energy E_e calculated from Equation (51). With E_e known, E_w (westerly component energy) can be calculated from E_0 - E_e. Similar conditions are applied when the vertical gradient of the zonal wind is negative, in which case c_{*e} increases with altitude.

Aside from the constraint of energy (or wave saturation) at large vertical wave number that arise from variation of wave energy with height and static stability as mentioned above, another saturation criteria set by FL93 is provided by the maximum anisotropy (α) allowed from wave propagation. Fritts and Lu assumed that no less than a fraction α of the energy may be associated with any one component ($E_j/E_0 < 1 - \alpha$), which is motivated by the insensitivity of motions of small vertical wave number to mean wind changes and the tendency of instability to occur under large wind shear conditions. In the model, we have

set a=0.25. When conditions are such that $E_j/E_0 < 1 - \alpha$, than E_j is adjusted back to $E_j = E_0 (1 - \alpha)$.

With the variation with altitude of the two energy components calculated, the momentum fluxes and its vertical divergence can be estimated. The relationships between energy (E_j), the momentum flux (F_P), and energy flux (F_E) are expressed according to FL93

$$F_P = 1/22 * (E_c - E_w) \tag{54}$$

and

$$F_E = \frac{1}{18}(c_c \cdot E_c + c_w \cdot E_w). \tag{55}$$

The gravity wave momentum flux divergence FG and the energy dissipation rate are calculated from

$$F_G = -\frac{1}{\rho_0}\frac{\partial}{\partial z}(\rho_0 F_P) \tag{56}$$

and

$$\varepsilon = -\frac{N}{\rho_0}\frac{\partial}{\partial z}(\frac{\rho_0}{N} F_E). \tag{57}$$

With the energy dissipation rate (ε) known, the gravity wave diffusion coefficient (K_{zz}) is calculated according to the relationship

$$K_{zz} = A\frac{\varepsilon}{N^2}. \tag{58}$$

As discussed in Weinstock (1984), the value of the coefficient A (equivalent to the inverse of Prandtl no.) could be as small as 1/3 or even less. In the model, we adopt the value of $A = 0.2$.

2.2.3. Tidal waves.

The parameterization of tidal wave forcing and diffusion in the 2-D model is based on the work of Lindzen (1981). Lindzen showed that under the WKBJ approximation of the linear wave equation, the momentum flux divergence from tidal gravity wave can be expressed as

$$F_T = -\frac{1}{\rho_0}\frac{\partial}{\partial z}(\rho_0 \overline{u'w'}) = -\frac{k}{2H}\frac{(-c)^3}{N(1+l^2/k^2)^{3/2}} \qquad (59)$$

and the diffusion coefficient can be written as

$$K_{zz(tides)} = \frac{kc^4}{N^3(1+l^2/k^2)^{3/2}}\frac{1}{2H} \quad . \qquad (60)$$

From theoretical calculations, it can be shown that only the first diurnal mode of the tidal waves within 30º latitude is able to propagate up into the mesosphere, and break to generate forcing and turbulence. At 85 km altitude where the waves break, with the tidal wave phase speed of 465 m/s and $k = l/6400$ for the main diurnal propagating mode, F_T = -16.3 m/s/day, and K_{zz} = 183 m^2/s, according to Eqs. (59) and (60). Above 85 km, we let F_T and K_{zz} decrease with altitude to take into account the rapid increase of the contribution from molecular viscosity and conductivity. At level z (km), above the breaking level, the momentum flux divergence F_T and diffusion coefficient K_{zz} calculated at 85 km are multiplied by exp[(85-z)/5]. Since waves are still expected to generate turbulence below the breaking level, a factor exp[(z-85)/5] is applied to F_T and K_{zz} below the breaking level (85 km).

Because the tidal wave mode that propagates up to the mesosphere is restricted to latitudes -30º < lat < 30º, a factor of exp[-(*lat*/20º)^2] is applied to F_T and K_{zz} beyond the latitudes 30º N and 30º S. Within the latitude of 30º, F_T and K_{zz} are assumed to be constant with latitude.

2.2.4. Tropospheric wave forcing and latent heating specification.

As mentioned in the Section 1, the lower boundary condition for the circulation is applied at 2 km. In order to solve the stream function equation (7), the tropospheric wave momentum flux divergence and the latent heat release rate that is particularly important in the troposphere, needs to be accounted for in the forcing term C_F. In SOCRATES, we chose to specify the EP flux divergence and latent heating rate in the troposphere according to a seasonal monthly-mean climatology.

Based on the EP flux divergence climatology established in Randel (1992), we formulated the EP flux divergence as a function of latitude, height and season as following

If $-\pi/2 < \Phi < -\pi/6$ or $\pi/6 < \Phi < \pi/2$ (mid to high latitudes):

$$\nabla \cdot F_{trop} = \frac{1}{2}\cos(3\phi - \pi)[-A_{trop} \cdot e^{-(z-8)^2/4} + 4 \cdot e^{-3(z-4)^2/2}] \qquad (61)$$

If $-\pi/6 < \Phi < \pi/6$ (tropics): EP flux divergence = 0.

The amplitude of A_{trop} varies with season and hemisphere:

- Equinox season:
  For $-\pi/2 < \Phi < -\pi/6$
  A_{trop} = 15 m/s/day
  For $\pi/6 < \Phi < \pi/2$
  A_{trop} = 28 m/s/day
- June solstice season:
  For $-\pi/2 < \Phi < -\pi/6$
  A_{trop} = 23 m/s/day
  For $\pi/6 < \Phi < \pi/2$
  A_{trop} = 16 m/s/day
- December solstice season:
  For $-\pi/2 < \Phi < -\pi/6$
  A_{trop} = 13 m/s/day
  For $\pi/6 < \Phi < \pi/2$
  A_{trop} = 40 m/s/day

The tropospheric latent heating rate due to condensation during convection events is specified to vary with latitude, height and season, based on Boville (1985) and Peixoto and Oort (1991). We use the following formulation for condensation heating rate:

At z < 12 km: $Q_{LH} = 4 \sin(\pi(z-3)/12) \exp(-\Phi^2/100)$ (K/day) (62a)

In the winter hemisphere, at latitudes less than 20^o,

At z < 5 km: Q_{LH} = 5 sin(π(z+10)/20) cos(9/4*Φ) (K/day) (62b)

In the summer hemisphere,

At z < 5 km: Q_{LH} = 8 sin(π(z+10)/20) cos(3/2*Φ) (K/day) (62b)

The latent heating rate Q_{LH} calculated from Eq. (62) is finally processed with the Gaussian filter smoothing routine, with weights of 0.25, 0.5, and 0.25, in both y and z direction for five times.

2.2.5 The circulation global mass balance correction.

The meridional circulation estimated from the stream function equation (7) is not necessarily in perfect global mass balance, either from inaccuracies in the radiative or dynamical forcing scheme, or from omitted physical processes such as small-scale turbulent processes. Thus, corrections have to be made to ensure that as the model integration proceeds, the integrated zonally-averaged mass flux between poles along a pressure surface remains equal zero. The global mass balance requirement can be written as

$$\int_{-\pi/2}^{\pi/2} \rho \overline{v}^{*} \cos\phi \cdot d\phi = 0, \qquad (63)$$

which is the latitudinal integration of area-weighted vertical residual wind along the log pressure height surface. Since w^* does not necessarily meet the condition as shown in Eq. (63), a correction α is applied to w^* such that

$$\int_{-\pi/2}^{\pi/2} \rho(\overline{v}^{*} - \alpha)\cos\phi \cdot d\phi = 0 \qquad (64)$$

where α is a function of height only. Thus, the correction factor α can be obtained from

$$\alpha = \frac{\int_{-\pi/2}^{\pi/2} \rho \overline{v}^{*} \cos\phi \cdot d\phi}{\int_{-\pi/2}^{\pi/2} \rho \cos\phi \cdot d\phi} \quad . \qquad (65)$$

2.2.6 Molecular diffusivity parameterization.

The effect of molecular diffusion on the chemical species and thermal field becomes important above the mesopause. Since the model domain of SOCRATES extends up to 120 km, the effect of molecular diffusion effect is taken into account.

Following Banks and Kockarts (1973), the vertical flux of a minor constituent (*i*) relative to air from molecular diffusion can be written as:

$$\phi_{(i)} = -K_{m(i)}\left[\frac{\partial [n]_{(i)}}{\partial z} + \frac{[n]_{(i)}}{H_{(i)}} + (1+\alpha_T)\frac{[n]_{(i)}}{T}\frac{\partial T}{\partial z}\right] \qquad (66)$$

with the molecular diffusion coefficient K_m for a particular gas *i* expressed as:

$$K_{m(i)}(cm^2/s) = 1.52 \times 10^{18}\left(\frac{1}{m_{air}} + \frac{1}{m_i}\right)^{0.5}\frac{\sqrt{T}}{[M]} \qquad (67)$$

where [*n*] is the number density of the minor consituent, $H_{(i)} = RT/(m_i g)$ is the scale height for trace species (*i*), α_T the thermal diffusion factor (-0.38 for *H*), m_{air} is the molecular weight of air (g/mole) which is specified as a function of altitude, m_i is the molecular weight of gas *i* (g/mole), and [*M*] is the number density of air (cm^{-3}). To derive the diffusivity flux formulation of Eq. (66) consistent with the chemical transport equation that will be described in section 2.3 [Equation (79)], [*n*] in Eq. (66) is substituted by the mixing ratio X_i.:

$$\phi_{(i)} = -K_{m(i)}[M]\frac{\partial X_{(i)}}{\partial z} + X_{(i)}K_{m(i)}[M]\left(\frac{1}{H} - \frac{1}{h_{(i)}}\right) \qquad (68)$$

where

$$\frac{1}{h_{ij}} = \frac{1}{H_{ij}} + \frac{(1+\alpha_T)}{T}\frac{\partial T}{\partial z}$$

Thus, if we define the vertical diffusive velocity by

$$\overline{w}_{Dij} = K_{mij}\left(\frac{1}{H} - \frac{1}{h_i}\right), \tag{69}$$

the diffusivity flux can be expressed as

$$\varphi_{ij} = [M]\cdot\left[-K_{mij}\frac{\partial X_{ij}}{\partial z} + X_{ij}w_{Dij}\right] \tag{70}$$

Since the time rate of change of mixing ratio expressed in flux form is

$$\partial X / \partial t = -(\partial\varphi / \partial z) / [M]$$

the effect of molecular diffusion on the chemical transport is given by

$$\frac{\partial \overline{X}_i}{\partial t} = \frac{1}{\rho_0}\frac{\partial}{\partial z}\left[\rho_0 \cdot K_{mij}\frac{\partial \overline{X}_i}{\partial z}\right] - \frac{1}{\rho_0}\frac{\partial}{\partial z}\left(\rho_0 \cdot \overline{w}_D \overline{X}_i\right) \tag{71}$$

where X_i represents the zonally averaged mixing ratio of gas *i*.

The thermal conductivity coefficient K_T associated with the molecular diffusion of heat in Equation (6) is adapted from the NCAR Thermospheric General Circulation Model (Alan Burns, private communication), in the form of

$$K_T\left(\frac{ergs}{cm\cdot K\cdot s}\right) = \left[(X_{O2} + X_{N2})\cdot 56 + X_O \cdot 75.9\right]\cdot T^{0.69} \tag{72}$$

where *X* represents the mixing ratio. To convert K_T to units of m^2/s for the model, Equation (72) is multiplied by a factor of $(m_{air}g^2H^2)/(P_0c_pRTe^{-z/H})$.

2.2.7. Quasibiennial oscillation simulation

The quasibiennial oscillation (QBO) of the temperature, zonal wind, and meridional circulation in the equatorial stratosphere is simulated in the 2-D model according to

Politowicz and Hitchman (1997). An analytical expression for the QBO radiative forcing is derived from a composite of observed zonal wind in the tropics, which is used to obtain the QBO forced circulation and the temperature oscillation in the stratosphere. Since the 2-D model does not explicitly deal with the zonal component of the momentum equation, using a QBO type radiative forcing in the stream function equation (Eq. 7) is a convenient way to simulate QBO processes for temperature and circulation without changes in the logistics of the model physics. The QBO forcing is specified and therefore does not respond to changes in zonal mean conditions. However, with this parameterization, the model can be used to examine various QBO radiative, transport, and chemical feedback effects on stratospheric chemistry.

From radiosonde time series at 15 tropical stations, Politowitz and Hitchman (1997) created a composite QBO for zonal wind at tropical latitudes between 16 to 40 km altitude with the formulation:

$$\bar{u}_{qbo} = -\bar{u}_{\max} \cdot \exp[-(\frac{\phi}{\phi_w})^2] \cdot \cos(\frac{\pi}{2}\frac{\phi}{\phi_w}) \cdot \cos(\frac{z - z_{\max}}{h_{qbo}}\pi) \cdot \cos(2\pi\frac{t-1}{t_{qbo}} + 2\pi\frac{z - z_{\max}}{z_{hfwd}}) \qquad (73)$$

where h_{qbo} is the QBO vertical extent of 24 km and t is the model time (in units of day with t_{qbo} in units of days). The maximum zonal wind QBO perturbation (u_{max}) is 25 m/s and is centered over the equator. The perturbation decays exponentially in latitude with a Gaussian latitude width (ϕ) of 15º, with negative tails beyond 15º on either side of the equator with the factor . The perturbation varies sinusoidally in altitude, between 16 km and 40 km, with maximum vertical amplitude at z_{max}, (28 km). A node between easterlies and westerlies descends with time, with a descent period of t_{qbo}=27 months (or 821 days) and a half width (z_{hfwd}) of 27 km.

A analytical expression for the time rate of change of temperature is derived based on the equatorial beta plane thermal wind relationship:

$$\frac{\partial \bar{u}}{\partial z} = -\frac{Ra}{2H\Omega v}\frac{\partial \bar{T}}{\partial y}. \qquad (74)$$

Assuming $T = T_0 exp(-\phi^2/\phi_w^2)$, where T_0 is the equatorial temperature with ϕ_w in radial units, the thermal wind relation can be written as

$$\overline{T} = \frac{H\Omega a \phi_w^2}{R} \frac{\partial \overline{u}}{\partial z}, \tag{75}$$

or

$$\frac{\partial \overline{T}}{\partial t} = \frac{H\Omega a \phi_w^2}{R} \frac{\partial \overline{u}}{\partial t \partial z}. \tag{76}$$

Substituting the Eq. 73 into Equation (76), the time rate of change of temperature as a function of time, latitude, and altitude can be written as

$$\frac{\partial \overline{T}}{\partial t} = -\frac{2H\Omega\phi_w^2 a \overline{u}_{\max} \pi^2}{R \cdot t_{qbo}} \exp[-(\frac{\phi}{\phi_w})^2] \cdot \cos(\frac{\pi}{2}\frac{\phi}{\phi_w}) \cdot$$
$$[\frac{1}{h_{qbo}} \sin(\frac{z - z_{\max}}{h_{qbo}}\pi) \cdot \sin(2\pi\frac{t}{t_{qbo}} + 2\pi\frac{z - z_{\max}}{z_{hfwd}}) -$$
$$\frac{2}{z_{hfwd}} \cos(\frac{z - z_{\max}}{h_{qbo}}\pi) \cdot \cos(2\pi\frac{t-1}{t_{qbo}} + 2\pi\frac{z - z_{\max}}{z_{hfwd}})] \tag{77}$$

Although in principle, temperature QBO can be derived from Equation (75) knowing the zonal wind profile, the temperature is actually derived from dynamical and thermal equations through the QBO forced meridional circulation. One option is to include the time rate of temperature change from Equation (76) as a diabatic heat forcing in the stream function equation (7) to obtain a meridional circulation forced by the QBO temperature damping rate. Another option is to include in the stream function equation a direct QBO momentum forcing with the formulation:

$$F_{QBO} = A_{qbo} \cdot \overline{u}_{\max} \cdot \frac{2\pi}{t_{qbo}} \cdot \exp[-(\frac{\phi}{\phi_w})^2] \cdot \cos(\frac{\pi}{2}\frac{\phi}{\phi_w}) \cdot \cos(\frac{z - z_{\max}}{h_{qbo}}\pi) \cdot \tag{78}$$
$$\sin(2\pi\frac{day - 1}{t_{qbo}} + 2\pi\frac{z - z_{\max}}{z_{hfwd}})$$

where A_{qbo} is an adjustable parameter to optimize the results. The QBO forced circulation is then used to integrate in time the thermodynamic equation (1), which provides the temperature. Through this procedure, both the circulation and temperature can be affected by the QBO.

2.3 Chemistry

In SOCRATES, the chemical species are grouped into three categories: long-lived species and chemical families, intermediate lifetime species, and short-lived species. For long-lived species or families with chemical lifetimes comparable to or longer than transport timescales, the full chemical continuity/transport equation is solved:

$$\frac{\partial \overline{X_i}}{\partial t} + \overline{v}^* \frac{\partial \overline{X_i}}{\partial y} + \overline{w}^* \frac{\partial \overline{X_i}}{\partial z} = \frac{P_i}{[M]} - L_i \cdot \overline{X_i} + D_{Xi} \qquad (79)$$

where X_i represents the mixing ratio of gas *i*, P_i is the chemical production rate of gas *i*, and $L_i X_i$ is the chemical loss rate of gas *i*. The transport of tracers by small scale mixing process is represented by a diffusive term D_{Xi}, written as

$$D_{Xi} = \frac{1}{\cos\phi}\frac{\partial}{\partial y}(\cos\phi \cdot K_{yy}\frac{\partial \overline{X_i}}{\partial y}) + \frac{1}{\rho_0}\frac{\partial}{\partial z}[\rho_0 \cdot (K_{zz} + K_m)\frac{\partial \overline{X_i}}{\partial z}] - \frac{1}{\rho_0}\frac{\partial}{\partial z}(\rho_0 \cdot \overline{w}_D \overline{X_i}) - w_d \overline{X_i} \qquad (80)$$

The intermediate species are chemicals with lifetimes shorter than the transport timescales, with timescales relatively insensitive to dynamical process, but sufficiently long that photochemical equilibrium cannot be assumed. These species are solved from the continuity equation without involving transport:

$$\frac{\partial \overline{X_i}}{\partial t} = P_i - L_i \cdot \overline{X_i} \qquad (81)$$

For the short-lived chemical species with lifetimes much shorter than the dynamical time constants, photochemical equilibrium conditions apply and the concentration of the trace gas i is derived from

$$P_i - L_i \cdot \overline{X_i} = 0. \qquad (82)$$

The list of the constituents included in the standard version of SOCRATES is given in

Table 4 .

2.3.1 Chemical reactions

More than 160 chemical reactions describing HOx, NOx, Clx, Brx, Ox, and hydrocarbon chemistry are included in SOCRATES. The majority of the chemical reaction rate constants are based on on the compilation published by the Jet Propulsion Laboratory (JPL) in 1997 (DeMore et al., 1997). A list of the reactions and rates is given in Table 5 .

a. Heterogeneous chemistry on polar stratospheric clouds

The parameterization of heterogeneous processes occurring on the surface of polar stratospheric clouds is based on the methods described by Chipperfield et al. (1993). Two types of PSC are considered: type II PSCs, mainly composed of water ice, and type I PSCs mainly composed of nitric acid trihydrate (NAT). For type I PSCs, the formula of Hanson and Mauersberger (1988) is used to estimate the saturation vapor pressure of HNO3 over NAT and hence the number density of condensed HNO3.3H2O species:

$$P_{HNO3} = 10^{[m(T)+\log(P_{H2O})+b(T)]} \qquad (83)$$

where and . The vapor pressure is converted into units of number density from

$$[HNO_3] = P_{HNO3} \cdot [M] / P. \qquad (84)$$

Thus the number density of condensed HNO3 3H2O species is then estimated by subtracting the "saturation number density" from the total number density of HNO3. In the case of NAT, the condensed particles are assumed to have a radius of 1 μm, with a sedimentation velocity of 0.015 km/day. Similarly, the formula for the saturation vapor pressure over ice from Murray (1967):

$$P_{H2O} = 5.715185606 \times 10^{10} \cdot \exp[-20.947031 \cdot (273.16 / T) - 3.56654 \cdot \ln(273.16 / T) - 2.01889049 \cdot (T / 273.16)] \qquad (85)$$

is used to predict the occurrence of type II PSCs. These type II PSCs are assumed to have a radius of 10 μm, and a sedimentation velocity of 1.5 km/day. The condensed HCl number density is deduced from the mole fractions of condensed HNO3 and H2O according to Hanson and Mauersberger (1990) :

$$[HCl_{ls1}] = 0.0035 \cdot [HNO_{3ls1}] + 0.0001 \cdot [H_2O_{ls1}]. \quad (86)$$

If sedimenting particles reach a level where the ambiant temperature is higher than the condensation threshold, evaporation takes place and the condensed species are returned to the gas phase. In the presence of PSCs, the following five heterogeneous reactions are assumed to occur:

- (het1) ClONO2(g)+H2O(s) -> HOCl(g)+HNO3(s)
- (het1) ClONO2(g)+H2O(s) -> HOCl(g)+HNO3(s)
- (het2) ClONO2(g)+HCl(s) -> Cl2(g)+HNO3(s)
- (het3) N2O5(g)+H2O(s) -> 2HNO3(s)
- (het4) N2O5(g)+HCl(s) -> ClNO2(g)+HNO3(s)
- (het5) HOCl(g)+HCl(s) -> Cl2(g)+H2O(s)

The first order rate constant (het1 ~ het5) for these reactions can be written as $het=\gamma vA/4$ (Cadle et al. 1975), where γ is the reaction probability, A the PSC surface area density, and v the mean molecular velocity given by $v=(8kT/\pi m)^{1/2}$. The reaction probabilities for these reactions are given in Table 6 for the two types of PSCs. Assuming that the particles are spherical, the surface area density A can be calculated knowing the radius of the two types of PSCs, and their mass and number densities.

Table 6. Reaction probabilities for heterogeneous reactions.

Reaction	Type I	Type II
het1	0.006	0.3
het2	0.3	0.3
het3	0.0006	0.03
het4	0.003	0.03
het5	0.1	0.3

b. Sulfate aerosol heterogeneous chemistry

For heterogeneous reactions on sulfate aerosol particles, six reactions are considered:

- (g1) ClONO2 + H2O(sulfate aerosol) -> HOCl +HNO3(g)
- (g2) N2O5 + H2O(sulfate aerosol) -> 2HNO3(g)

- (g3) ClONO2 + HCl (s) -> Cl2 + HNO3(g)
- (g4) HOCl + HCl (s) -> Cl2 + H2O
- (g5) BrONO2 + H2O (s) -> HOBr + HNO3(g)
- (g6) HOBr + HCl (s) -> BrCl + H2O

As for the PSC heterogeneous chemistry, the rate constants for these reactions are estimated from $g=\gamma vA/4$. The surface area density (A) of sulfate aerosols is generally attainable from extinction measurements. The reaction probability (γ) of the above reactions are based on works described in Hanson et al. (1994) and Hanson and Ravishankara (1995). The reaction probability for the g1 reaction rate is expressed as a function of sulfate aerosol composition (W: H2SO4 weight %) as

$$\gamma_1 = 10^{1.86-0.0747W} \tag{87}$$

where the aerosol composition which depends primarily on the temperature and water vapor mixing ratio is evaluated based on the study of Steele and Hamill (1981) and has been fitted to a formula as described in Hanson et al. (1994) as

$$W = \frac{[-14.458 + 0.62456 \cdot \ln(p_{h2O})] \cdot T + 3565}{44.777 + 1.3204 \cdot \ln(p_{h2O}) - 0.19988T}. \tag{88}$$

where p_{h2o} is the partial pressure for water vapor. The reaction probability of g2 is specified as 0.14, independent of the aerosol and composition, and hence, of the temperature. The reaction probability for g3 reaction is expressed as:

$$\gamma_3 = 0.018\sqrt{T \cdot [HCl]^*} \tag{89}$$

where [HCl]* is the HCl solubility in droplets calculated from the equation:

$$[HCl]^* = p_{HCl}(atm) \cdot 10^{15.514-0.1791 \cdot W}. \tag{90}$$

For g4, the reaction probability is set to be 19.1 times that of γ3. For the bromine reactions, the values adopted for the reaction probability are based on the work by Hanson and Ravishankara (1995), with γ5=0.6, and γ=10*γ4.

c. NOy production.

In addition to the major stratospheric NOy production resulting from N2O+O(1D)-> 2NO

reaction, the production source of NOy by lightning, cosmic ray, and ionic reactions are included in the model.

The rate of global lightning production is 8.7 Tg/yr, with productions occurring at latitudes less than 60^o, and at altitudes between 0 and 16 km. Between latitudes of -30 to 30 deg, the NOy production rate is specified as 2000 cm^{-3}/s. Beyond 30 deg latitude north and south, the NOy production is specified to decrease linearly from 2000 cm^{-3}/s at 30 deg to zero at 60 degrees latitude.

Production of NOy associated with the deposition of galactic cosmic rays is parameterized as a function of latitude and altitude according to Heaps (1978) for solar maximum condition, with the production of 1.3 NO molecules per ion pair produced by the cosmic rays. At altitudes less than 8 km, NOy production by cosmic ray is assumed to be zero. At other altitudes:

If 8 km < z < 19 km:

$$P_{cr} = 1.3 \cdot [1.74x10^{-18} + 1.93x10^{-17} \cdot (\sin\phi)^4] \cdot (a + bz + cz^2) \qquad (91a)$$

where

$$a = (3.03x10^{17})^{1-0.6-0.8\cos\phi}[M]^{0.6+0.8\cos\phi}[14.4 / 7x10^5(0,6+0.8\cos\phi) - 2.24]$$

$$b = (3.03x10^{17})^{1-0.6-0.8\cos\phi}[M]^{0.6+0.8\cos\phi}[-2.6 / 7x10^5(0.6+0.8\cos\phi) + 0.36]$$

$$c = (3.03x10^{17})^{1-0.6-0.8\cos\phi}[M]^{0.6+0.8\cos\phi}[0.1 / 7x10^5(0.6+0.8\cos\phi) - 0.01].$$

If z > 18 km:

$$P_{cr} = 1.3 \cdot [1.74x10^{-18} + 1.93x10^{-17} \cdot (\sin\phi)^4] \cdot [M]$$

$$\text{for } [M] < 3.03x10^{17}, \qquad (91b)$$

or

$$P_{cr} = 1.3 \cdot [1.74x10^{-18} + 1.93x10^{-17} \cdot (\sin\phi)^4] \cdot (3.03x10^{17})^{1-0.6-0.8\cos\phi}[M]^{0.6+0.8\cos\phi}$$

$$\text{for } [M] \geq 3.03x10^{17}. \qquad (91c)$$

Production of NOy by thermospheric ionic process including its production by N2 photolysis and N2 reaction with energetic electrons (e*) is specified as a function of height and latitude based on data presented by McEwan and Phillips (1975). NOy production by particle precipitation near the auroral zone in the thermosphere is confined to latitudes beyond 55 degrees, while the production by extreme UV radiation occurs at all latitudes

except for night time conditions. The magnitude of the NOy production rate is on the order of 1000 cm^{-3}/s by N2 + e*, and on the order of 10 cm^{-3}/s by N2+hv in the lower thermosphere. NOy production rates by these processes are assumed to be negligible below 90 km.

d. Tropospheric species washout rates.

Computation of the rainfall rate and wet removal rate of soluble species in the troposphere for HNO3, H2O2, CH3OOH, HCl, HO2NO2, and CH2O, is based on the parameterization described by Hough (1991). For HBr, CCl2O, CClFO, CF2O, HF, Bry and Cly, the washout rate for HCl is used; for C2H5OOH, CH3COOOH, and C3H6OHOOH, the washout rate for CH2O is used; and for NOy, the washout rates for HNO3 and HO2NO2 is used.

As described in Appendix B of Hough (1991), the rainfall rate of water vapor is written as:

$$\frac{d[H_2O]}{dt} = -\frac{[H_2O]}{7200\Delta z} \cdot \exp\left[\frac{2([H_2O]-[H_2O]_{(sat)})}{[H_2O]}\right] \quad cm^{-3}s^{-1}, \qquad (92)$$

and the water from the rainout is assumed to move vertically down to the immediate lower layer and evaporate. The washout rates of species *i* is then:

$$\frac{d[n]_i}{dt} = -\frac{1}{7200\Delta z} fx_i \qquad (93)$$

where fx_i is the fraction of species *i* in the aqueous phase derived from

$$fx_i = (lwc / d_{h2o})(H_i + lwc / d_{h2o}), \qquad (94)$$

and d_{h2o} is the density of liquid water (g/cm^3), while *lwc* is the liquid water content (g/cm^3) of the clouds.

H_i is the dimensionless Henry's Law coefficient, derived from

$$H_i = 273.15 \cdot \rho / (k_i \cdot 22.4 \cdot T \cdot \rho_0) \qquad (95)$$

where k_i is the Henry Law coefficients, listed in Table 7 for different rainout species,

while p is the local pressure and $p_0$is the standard surface pressure, both in units of Pascal. The liquid water content, *lwc* (g/cm^3),is calculated from the formula

$$lwc = \exp\left[\frac{2([H_2O]-[H_2O]_{(sat)})}{[H_2O]}\right]\cdot[H_2O]\cdot\frac{m_{h2o}}{6x10^{23}} \qquad (96)$$

where m_{h2o} is the mean molecular mass of water (18 g/mole), and $[H2O]_{(sat)}$ is the saturated concentration of water vapor derived from

$$[H_2O]_{(sat)} = [M]\cdot\frac{100\cdot10^{(-2937.4/T-4.9283\log T+23.5521)}}{p-100\cdot10^{(-2937.4/T-4.9283\log T+23.5521)}}, \qquad (97)$$

where p is the pressure in units of Pascal.

Table 7. Values of Henry's Law coefficients.

Species	k (mol l^{-1} atm^{-1})
HNO3	3.3e6
H2O2	7.36e4
CH3OOH	221
HCl	3.3e5
HO2NO2	3.3e6
CH2O	6.3e3

2.3.2 Vertical transport in the troposphere associated with convection and fronts.

Tropospheric vertical transport produced by convective and frontal activity is formulated in the 2-D model by a simple parameterization which ensures mass continuity. Assuming that the convective upward mass flux at the first model layer is known (which we shall call Φ in units of g/m2/s), mass continuity dictates that at layer i:

$$\alpha_i\Phi + \varphi_{i+1} = \varphi_i \qquad (98)$$

if α_i is the fraction of boundary mass flux that is detrained into the layer i (sumation of α_i = 1) and φ is the downward mass flux out of layer i. At the top layer of the convective layer

(denote by layer *N*), the continuity can be written as

$$\varphi_N = \alpha_N \Phi . \tag{99}$$

Substituting into Eq.98 for layer N-1 yields:

$$\varphi_{N-1} = (\alpha_N + \alpha_{N-1})\Phi . \tag{100}$$

Under the same token, at layer *i*, a recursive relationship can be obtained for the downward flux out of layer *i*:

$$\varphi_i = (\sum_{j=i}^{N} \alpha_j) \cdot \Phi . \tag{101}$$

The time rate of change of the transported chemical species, knowing the mass flux in and out of the layer *i*, can be written as:

$$\frac{\partial [n]_i}{\partial t} = \alpha_i \frac{\Phi}{\Delta z} X_1 + \frac{\varphi_{i+1}}{\Delta z} X_{i+1} - \frac{\varphi_i}{\Delta z} X_i \tag{102}$$

where $[n]_i$ is the number density of species i, and X_i the mixing ratio of the transported species at layer *i*. Substituting the relationship (101) into (102), and after converting mass flux in units of $g/m^2/s$ to units of ($cm^{-3}s^{-1}$) by multiplying it with $N_A/m_{air}/109$ yields

$$\frac{\partial [n]_i}{\partial t} = \alpha_i \frac{\Phi}{\Delta z} X_1 + \frac{\Phi}{\Delta z} (\sum_{j=i+1}^{N} \alpha_j) X_{i+1} - \frac{\Phi}{\Delta z} (\sum_{j=i}^{N} \alpha_j) X_i , \tag{103}$$

which can be rewritten as

$$\frac{\partial [n]_i}{\partial t} = \frac{\Phi}{\Delta z} [\alpha_i \cdot X_1 + (\sum_{j=i+1}^{N} \alpha_j) X_{i+1}] - [\frac{\Phi}{X_{air} \Delta z} (\sum_{j=i}^{N} \alpha_j)] \cdot [n]_i . \tag{104}$$

Thus, the convective transport effect is equivalent to a chemical production term: represented by the first term in the right-hand side of Eq. (104), and a chemical loss coefficient, represented by the coefficient of the second term on the right-hand side. These convective "production" and "loss "terms are added to the chemical production and loss rates in the continuity equation (79).

The input information needed for the transport parameterization is the upward boundary mass flux Φ , and the fraction of Φ that enters layer *i* (α_i). The convective mass flux out of the boundary layer for both deep convection and frontal circulation process is taken from Langner et al. (1990) (Table 7 in the paper). The detrainment percentages (or α_i) of the convective and frontal process as a function of season, altitude and latitude are also obtained from Langner et al. (1990) (Table 1 and 2 in the paper). The same data is used to estimate the top level (*N*) reached by convective and frontal vertical transport.

---

3. Initial and Boundary conditions.

3.1 Chemical Species

The initial conditions for the concentration of chemical species are obtained from a standard model run of four years of the date Jan 1st . Results of selected species are shown in Section 5.

Boundary conditions for the chemical species can be specified as flux or mixing ratio boundary conditions. Listed in Table 8 are the specifications of upper and lower boundary conditions for the transported species, including the dry deposition velocity (wd) at the surface. The lower boundary conditions adapted in the model are those of Hauglustaine et al. (1994) but will be described in more detail here. When fluxes are specified as boundary flux conditions (Table 8), they are generally based on Hough (1991). An uptake of methane by soils is assumed to be 30 Tg-CH4 yr^{-1}, with a latitudinal distribution adopted from Fung et al. (1991). The surface emissions of these gases are estimated based on the relative contribution of each emission category listed in Table 9 , and the latitudinal distribution of each emission category and of methane soil absorption are presented in Table 10 . The boundary fluxes of each emission category expressed in units of Tg $yr^{-1}m^{-2}$ are obtained by multiplying the values listed in Table 9 with values listed in Table 10 . The latitudinal distribution of the boundary fluxes for each species are then the addition of all emission categories. For the net surface flux of methane, the soil absorption flux is subtracted out from the emission flux. The boundary fluxes are then converted to units of $cm^{-2}s^{-1}$ and used in the chemical transport equation.

Source gases whose lower boundary conditions that are currently specified as mixing ratios according to 1990 conditions are : CO2, CFC-10, CFC-11, CFC-12, CFC-113, CFC-114, CFC-115, HCFC-22, CH3CCl3, CH3Br, CHBr3, Ha-1211, Ha-1301 and HF. For those with values varying with latitude, their surface mixing ratio are specified as follows: for CO2: [356.+b(CO2)] ppmv; for CFC-10: 108*b(CFC-10) pptv; for CFC-11: 270*b (CFC-11) pptv; for CFC-12: 465*b(CFC-12) pptv; for CFC-113: 70*b(CFC-12) pptv; for CFC-114: 10*b(CFC-12) pptv; for CFC-115: 5*b(CFC-12) pptv; for HCFC-22: 106*b (CFC-12) pptv; for CH3CCl3: 153*b(CH3CCl3) pptv; for Ha-1211: 2.9*b(CFC-12) pptv;

and for Ha-1301: 1.7*b(CFC-12) pptv. The values for the b coefficients as a function of latitude are listed in Table 11 . CH3Br is specified as 9 pptv in the Southern Hemisphere, and 11.5 pptv in the Northern Hemisphere.

As listed in Table 8 , dry deposition surface velocity are considered for species NOy, NOx, HNO3, N2O5, Ox, CO, H2O2, CH2O, PAN, and H2. The velocities for different surface types are as listed in Table 2 of Hauglustaine et al. (1994). To estimate thefraction of land, ocean, snow and sea ice as a function of surface temperature, the parameterization from Robock (1983) is used.

The upper boundary conditions at 120 km for the majority of chemical species are specified as zero fluxes (see Table 8), except for NOy, NOx, Ox, H2 and H. Downward flux of NOx and NOy at 120 km can be specified as a function of latitude and season according to Solomon et al. (1982):

$$Flux_{NOx} = -1.x10^{8} - 3.5x10^{8} \cdot \cos[\phi + 17 \cdot \cos(\frac{day - 172}{365} \cdot 2\pi)] \quad (cm^{-2}s^{-1}) \qquad (105)$$

except at polar night, where $Flux_{NOx}$=0. In the current version of the model, NO, NOx and NOy is specified as fixed mixing ratio of 5.e-5. Likewise, Ox and O(3P) is currently specified as mixing ratio. However, they can also be specified as flux at the upper boundary according to Kasting and Roble (1981) as:

$$Flux_{Ox} = (-1 + h_{1/2day}) \cdot 1.5x10^{8} - 2. \cdot h_{1/2day} \cdot 2.5x10^{11} \quad (cm^{-2}s^{-1}) \qquad (106)$$

where $h_{1/2day}$ is the half day hour angle in units of radius as mentioned in section 2.1.1.

3.2 Temperature, wind and stream function

3.2.1 Initial and boundary conditions for temperature.

The model integration time starts at January 1st, and the steady state model calculation of the temperature distribution at January 1st is used as the initial condition of temperature (Figure 2). The temperature at and below the lower boundary of the dynamical model (0, 1 and 2 km) is specified as a function of latitude and month according to Randel (1987).

3.2.2 Boundary conditions for zonal wind, and stream function.

The zonal wind in the 2-D model is derived by vertically intergrating the thermal wind equation (Eq. 4), knowing the temperature distribution. The zonal wind at the surface needed to start the vertical integration is specified as a function of latitude and month according to Fleming et al. (1988).

The boundary condition for the stream function at 2 km is calculated interactively with the cumulative wave forcing above the boundary. According to the 'downward control principle' of Haynes et al. (1991), the mass flow across an isentropic surface is controlled exclusively by the amount of eddy forcing above that surface. As in Garcia et al. (1992), the stream function at the lower boundary (z_b=2km) is calculated from:

$$\chi_{z_b} = -\frac{\cos\phi}{f \cdot \exp(-z_b / H)} \int_{z_b}^{\infty} \exp(-z / H) \cdot F_{tot} \cdot dz \ . \qquad (107)$$

This expression is derived from a linearized, steady state momentum equation , where F_{tot} is the combination of all types of wave forcing as calculated by the model, including gravity and planetary wave forcing, tropospheric wave forcing (F_{tot}=F_R+F_G+F_T...).

---

4. Numerical techniques

4.1 Thermodynamic and stream function equations (temp.f, strcal.f).

The potential temperature thermodynamic equation is solved by first applying standard 2nd order finite difference approximations to the spatial derivative.The solution and the resultant system of ODE's is approximated with a spatially split, fourth order, multi-step, backward difference scheme from Van Der Houwen (1980). In this implementation the predictor value is taken as the last known solution. The split, discrete ODE system is iterated exactly four times. When starting a calculation without using prior results the first three solutions are obtained using a simple backward Euler temporal treatment rather then the full fourth order backward formula. The resultant linear system is solved directly by a specialized banded matrix solver 'band_slv.f'.

The stream function equation, which is a 2nd-order partial differential diagnostic equation is discretized by a center finite differencing scheme. The Jacobian matrix system of equation is solved using the band sysem solver in the file 'band_slv.f'.

4.2 Chemical transport equation

The chemical transport equation (Eq. 79) can be written in a numerical operator form each representing contribution from advection, diffusion, and chemistry:

$$\frac{\partial \overline{X}_i}{\partial t} = L_{adv} \cdot \overline{X}_i + L_{diff} \cdot \overline{X}_i + L_{chem} \cdot \overline{X}_i \qquad (108)$$

where L_{adv} is the advection operator, L_{diff} is the diffusion operator, and L_{chem} is the chemical operator. We solve for the discrete analogue to Eq. 108 by:

$$\overline{X}_i^{n+1} = \prod_{j=1}^{3} \Phi_j(\Delta t) \bullet X_i^n , \qquad (109)$$

where $\Phi_1 = \Phi_{SLT}$ is the discrete analogue to L_{adv}, $\Phi_2 = \Phi_{chem}$ is the discrete analogue to

L_{chem} , and $\Phi_3 = \Phi_{diff}$ is the discrete analogue to L_{diff} . The following sections detail the numerical schemes used by each discrete operator.

4.2.1 Advection: Semi-Langrangian transport (slt.f).

The solution for the transport of chemicals by advection is obtained with the semi-Langrangian technique (Robert, 1981). This method requires a backward tracing of air parcels utilizing the residual wind (v*, w*) information, with the assumption that the tracer mixing ratio value is conserved along the trajectory. A 1 day timestep is the default for the back tracing calculation in the standard model run. Since the point of departure of a tracer parcel generally does not coincide with the model grid point, interpolations of the residual wind and the tracer mixing ratio value are necessary. The interpolation is done in subroutine LE3. To initialize for the diurnal chemistry, only the long-lived species at noon time are advected.

4.2.2 Chemical loss and production (chem_resol.f)

The changes in the concentration of long-lived and intermediate species by photochemical sources are calculated by the Euler-backward iterative method:

$$\overline{X}_i^{t+1} = \frac{\overline{X}_i^t + P_i \Delta t}{1 - L_i \Delta t} \qquad (110)$$

where Δt is the time step. The method is iterated (for a maximum of 10 times) until it is converged within 0.1%.

A different numerical method is used for selected species (O(3P), O3, OH, HO2, NO, NO2, NO3, H) during night time (night_sub.f). They belong in a special category due to large diurnal variations in their chemical lifetimes. These species which are in photochemical equilbrium in the presence of sunlight must be explicitly time integrated during the night. The system of non-linear chemical equations are transformed to a system of non-linear algebraic equations through an implicit Euler time scheme with Newton Raphson iteration:

$$F(X) = \frac{X^{t+1} - X^t}{\Delta t} - (P - LX^{t+1}) \qquad (112)$$

$$X_{it+1} = X_{it} - \frac{F(X_{it})}{F'(X_{it})} \qquad (113)$$

where *F'(X)* is the Jacobian Matrix (*dF/dX*) and *it* is the iteration number. The timesteps for the chemical equations varies according to the length of day and night, with 8 timesteps every 24 hours. For the timestep during daylight hours, the length of daylight is divided by 4; likewise, night timestep is the duration of the night divided by 4.

4.2.3 Diffusion (diffus.f)

The molecular and eddy diffusion component of transport is solved like the potential temperature by first applying standard finite difference analogues to the spatial derivatives. The resultant linear ODE system is solved through a straight forward application of backward Euler with modifications to incorporate splitting along the spatial coordinates (y and z). The combined splitting, backward Euler algorithm is iterated three times.

---

5. Selected example of model results.

In order to illustrate the type of results provided by the model, we present selected two-dimensional model distributions of model output. These results are expected to change in the future as model parameters, boundary conditions, and other inputs are modified. The results shown here are for the month of January with 1992 boundary conditions.

5.1 Dynamics.

Figures 2 to 9 present the calculated zonally averaged distributions of temperature, zonal wind, meridional and vertical wind velocities (TEM circulation), solar UV heating, terrestrial IR cooling, as well as the Rossby wave and gravity wave forcing.

Figure 2: Temperature

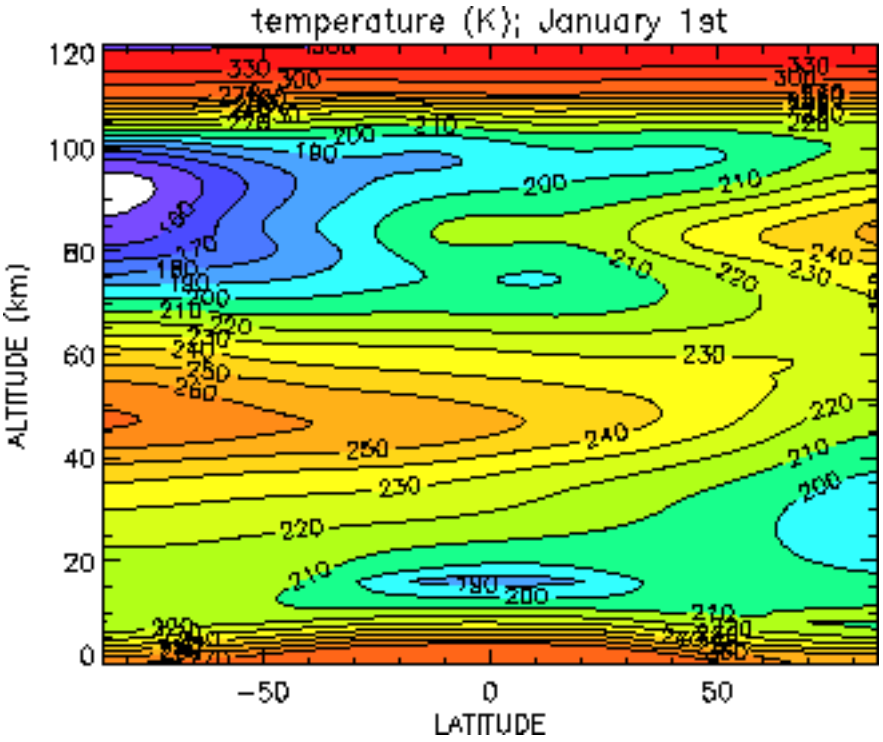

Figure 3: Zonal wind

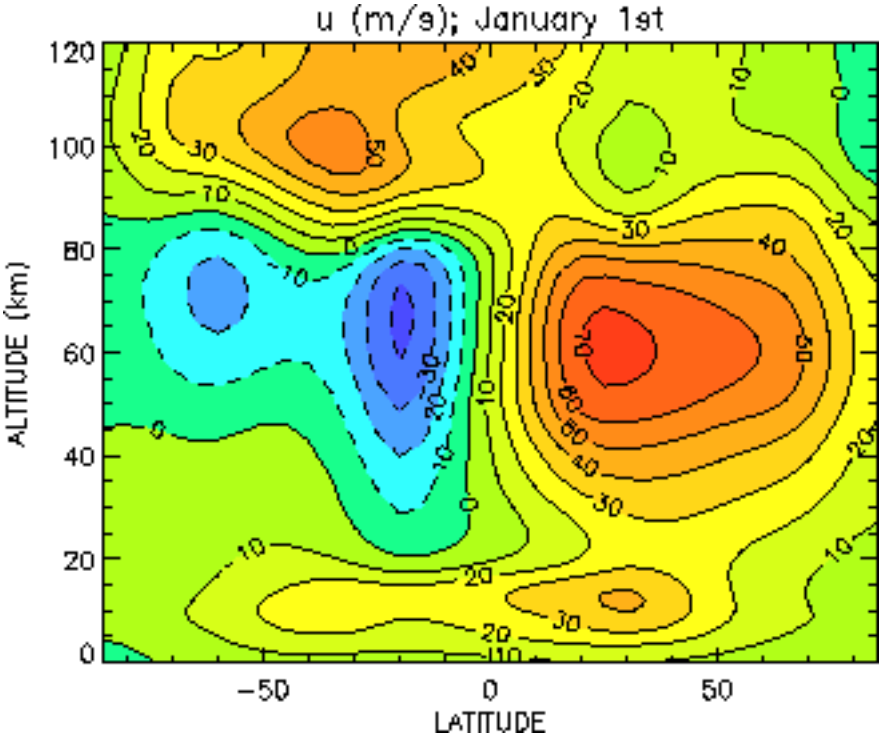

Figure 4: v*

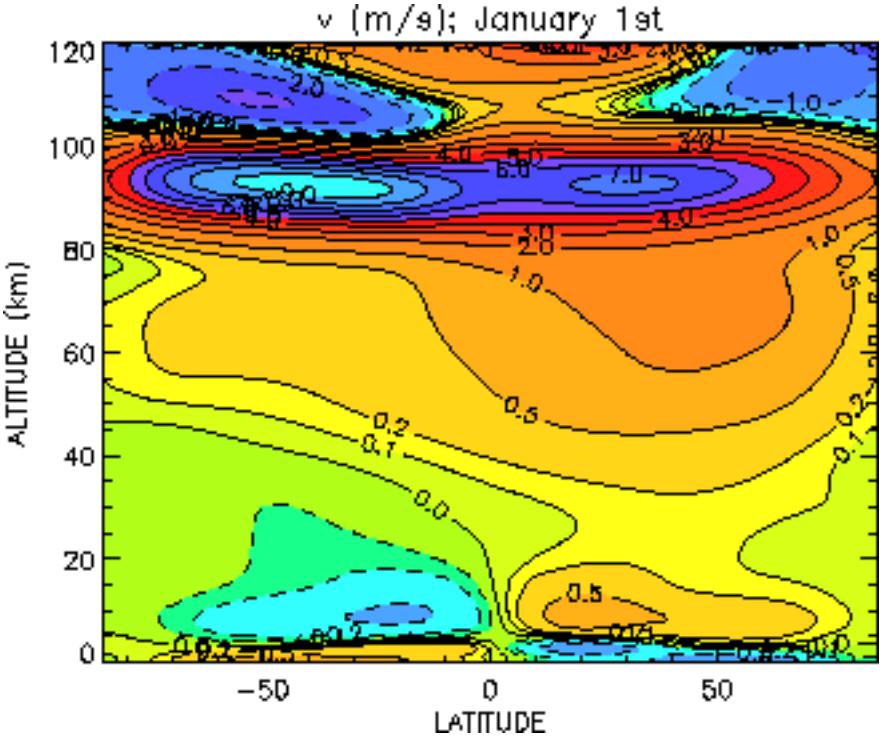

Figure 5: w*

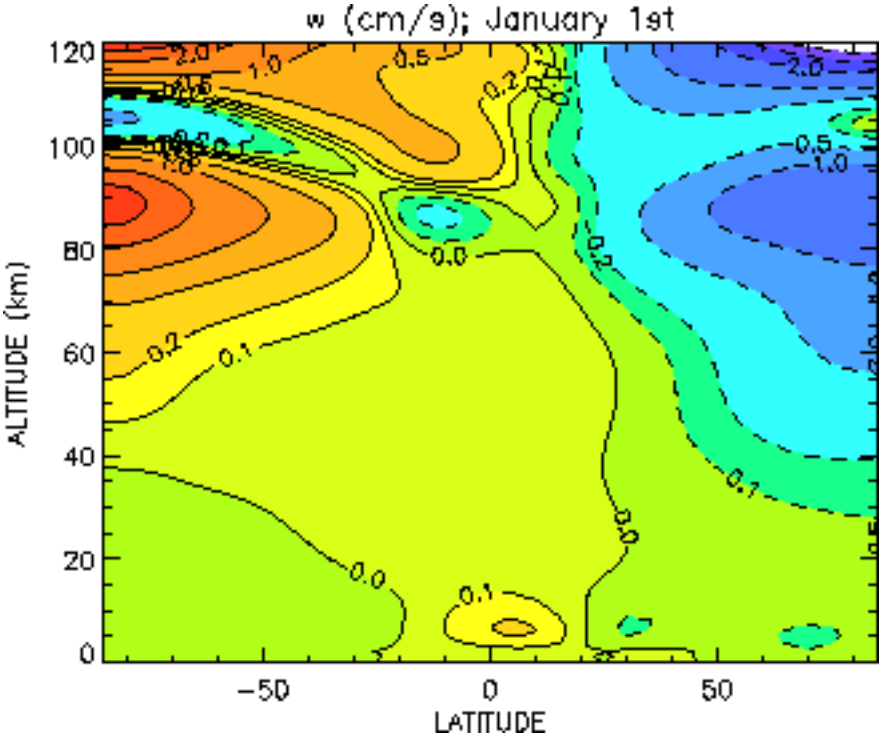

Figure 6: Solar heating rate

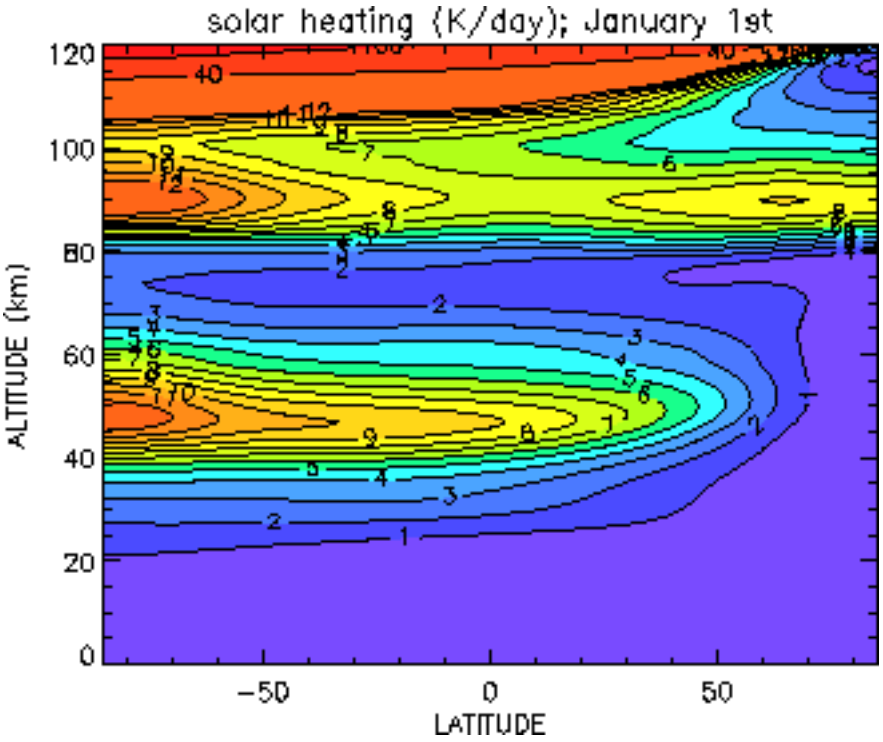

Figure 7: IR cooling rate

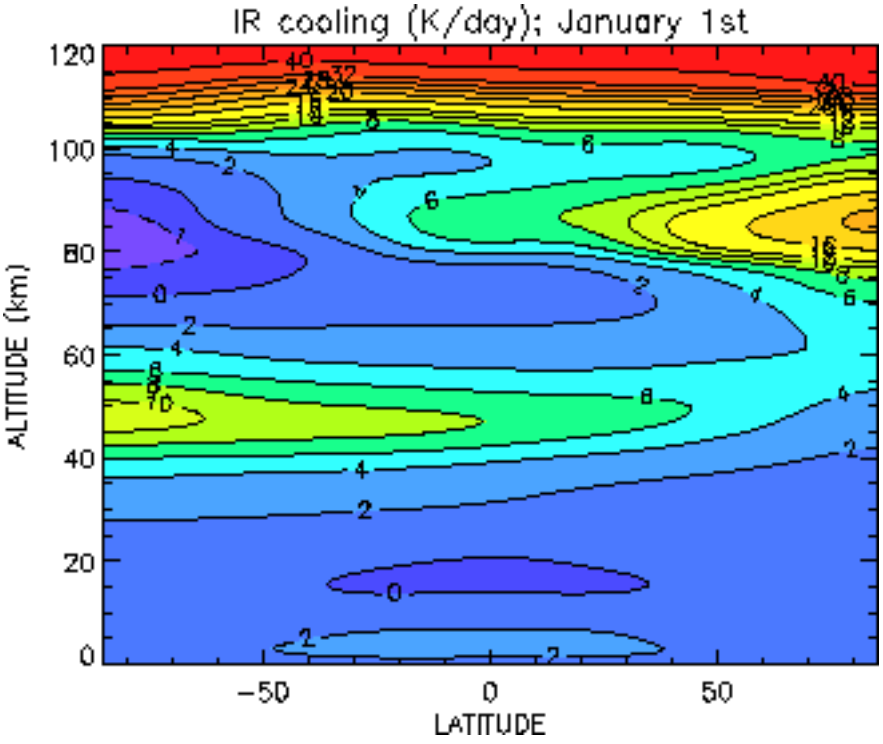

Figure 8: Rossby wave forcing

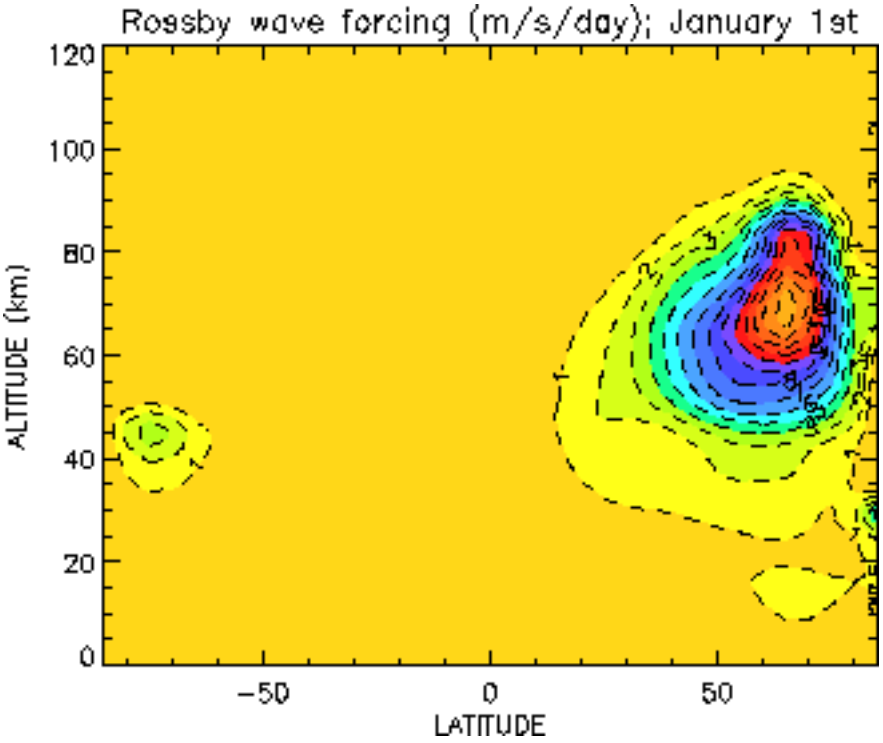

Figure 9: Gravity wave forcing

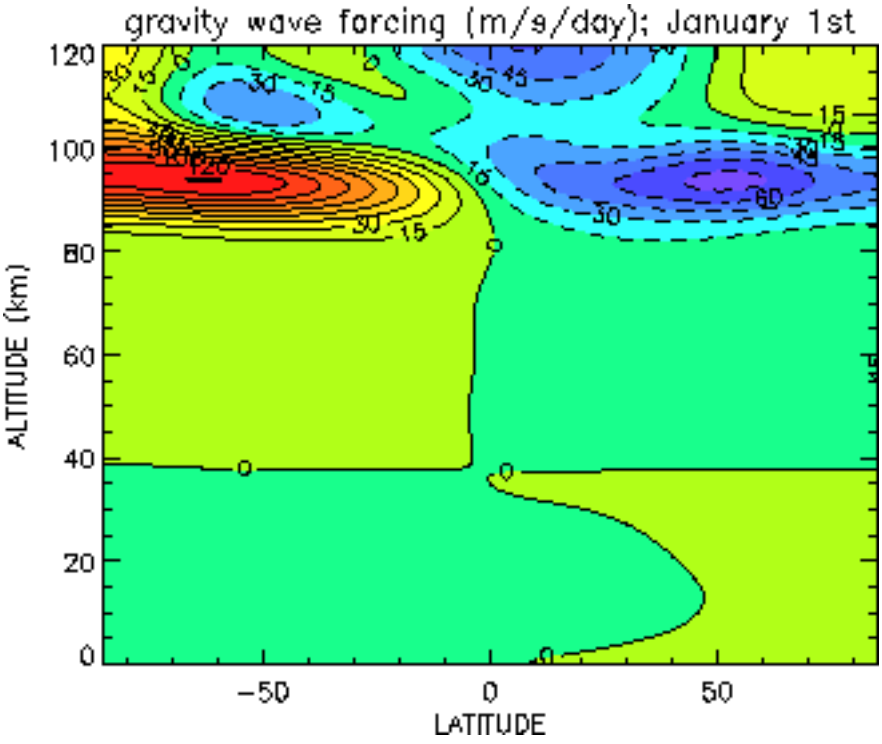

5.2 Chemistry.

Figures 10 to 21 show the calculated zonally averaged distibutions of selected chemical constituents (diurnally averaged mixing ratios) of N2O, CH4, HNO3, NOx, ClONO2, HCl, ClOx, BrOx, BrONO2, CFC-10, CH3Br, and O3.

Figure 10: N2O

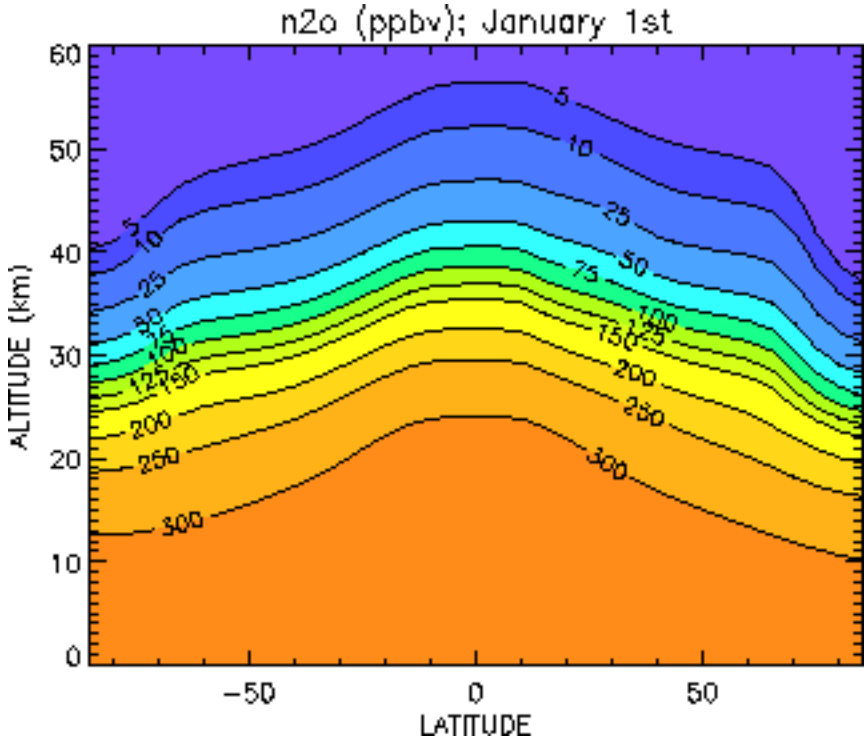

Figure 11: CH4

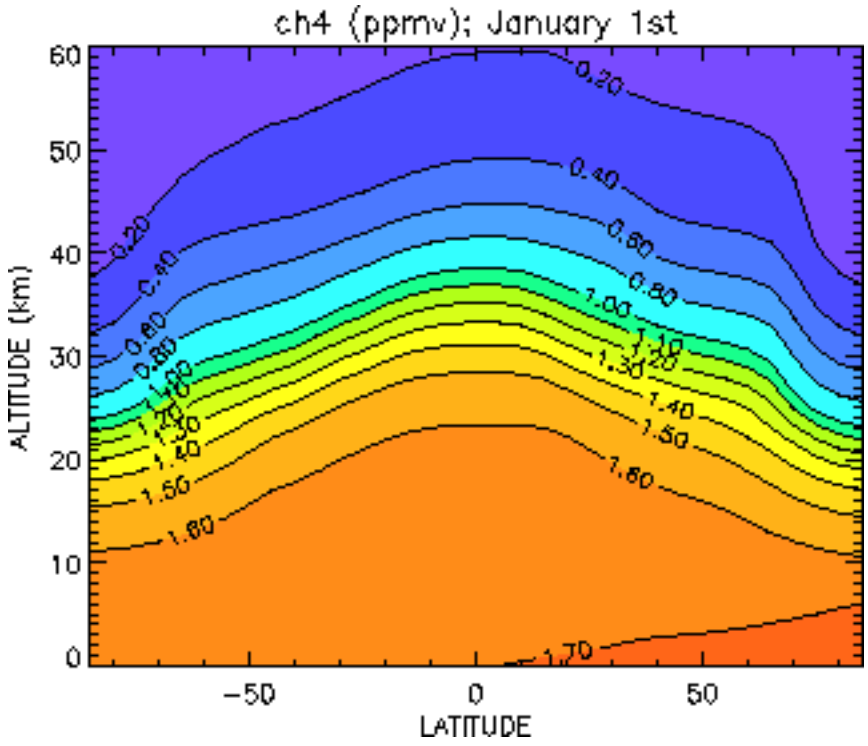

Figure 12: HNO3

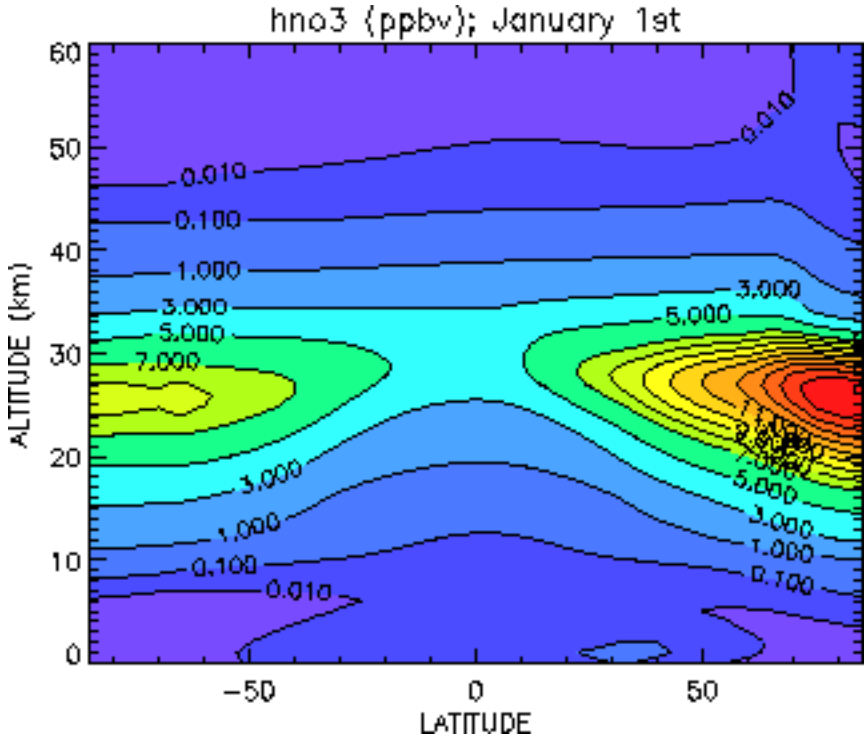

Figure 13: NOx

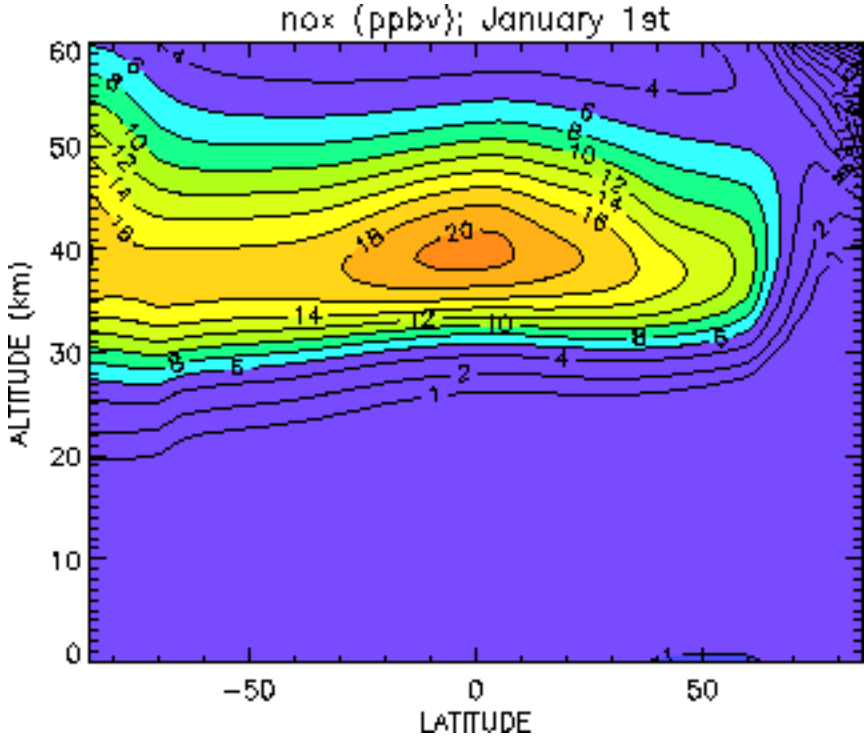

Figure 14: ClONO2

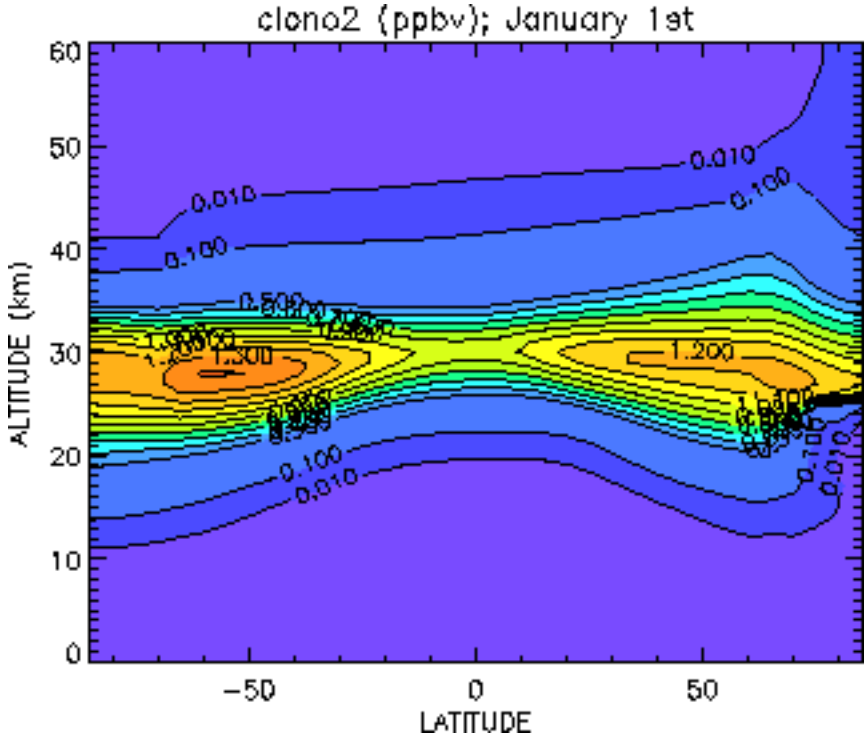

Figure 15: HCl

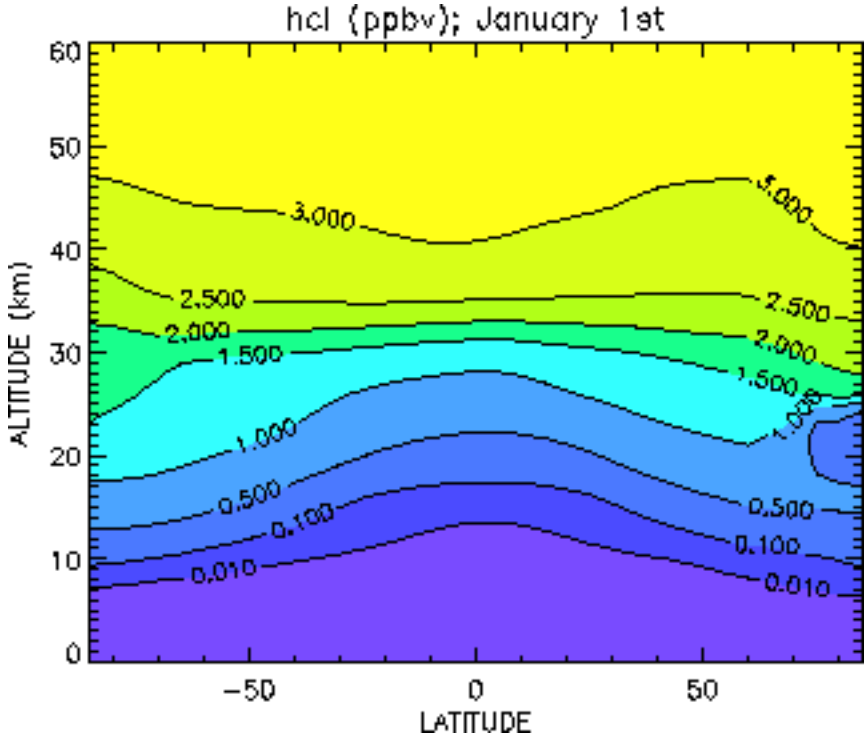

Figure 16: ClOx

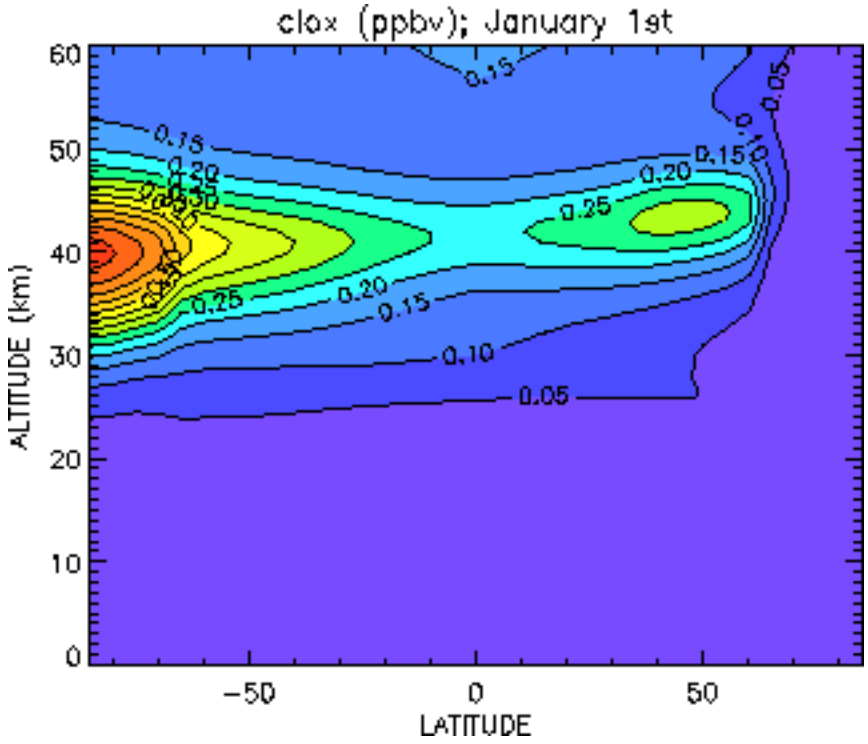

Figure 17: BrOx

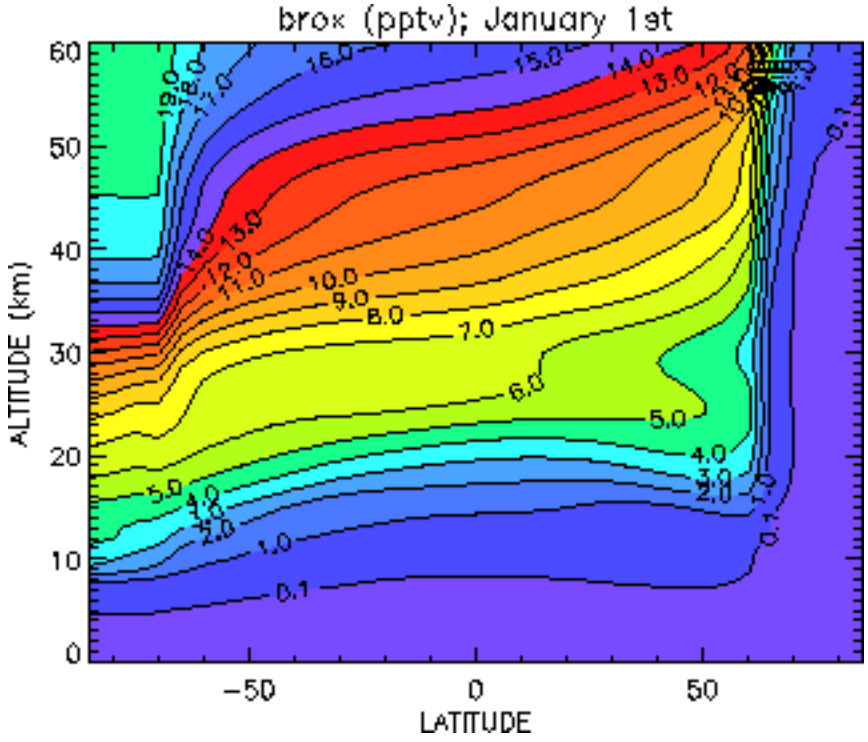

Figure 18: BrONO2

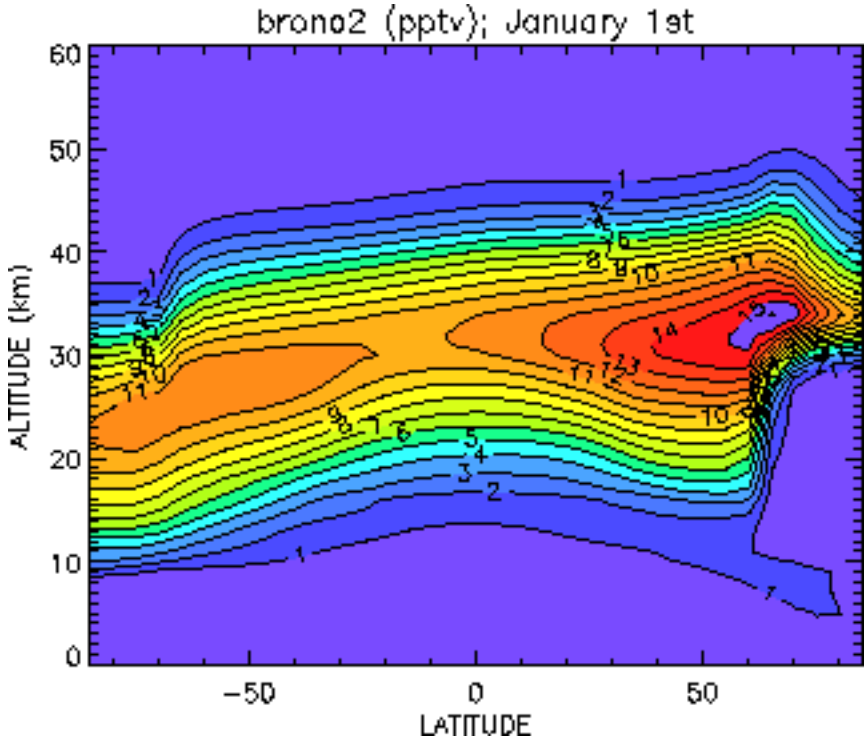

Figure 19: CFC-10

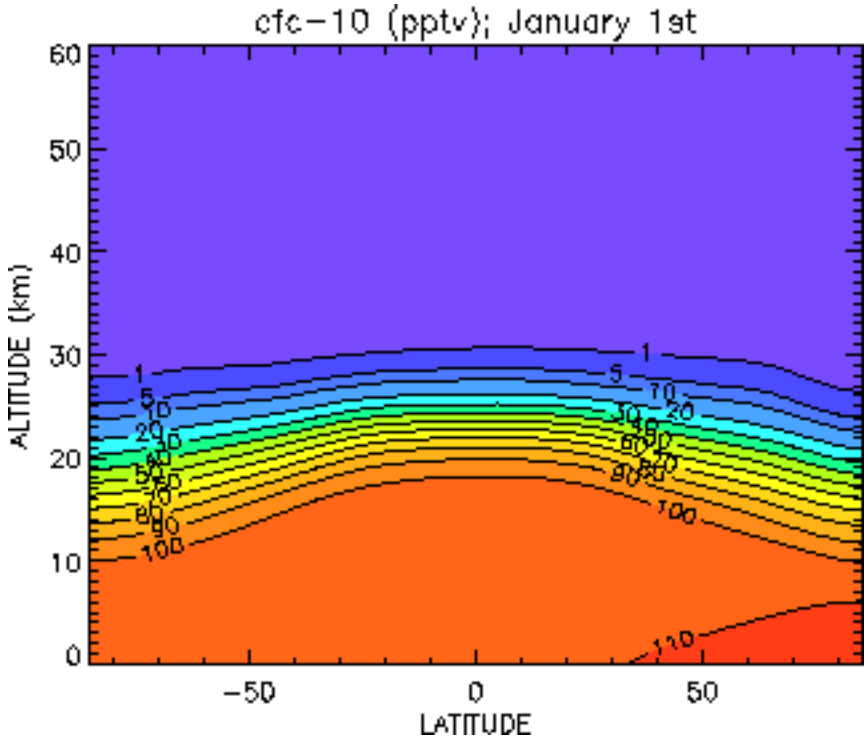

Figure 20: CH3Br

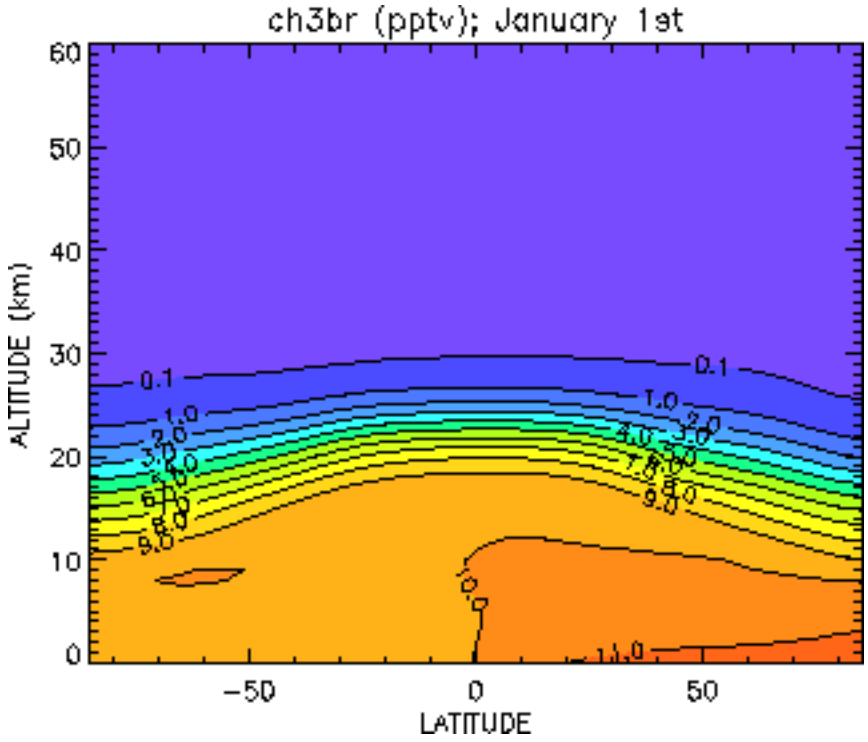

Figure 21: O3

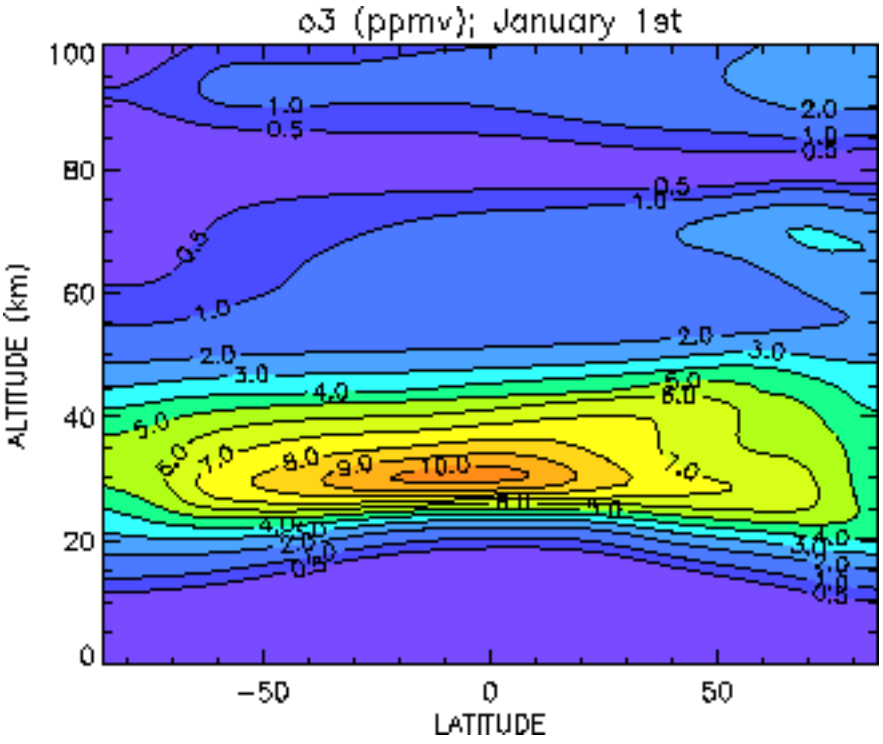
o3 (ppmv); January 1st
ALTITUDE (km)
LATITUDE
100
80
60
40
20
0
−50
0
50

6. Technical description

6.1 Introduction

The SOCRATES model is written in the Fortran 90 language. This allows :

- use of array-syntax
- use of "module" instructions instead of old, FORTRAN77 "common" instructions
- use of structured data variables, especially for date representation
- use of namelist-directed input files

It is important to understand the two last features and their implementation in the model before attempting execution. The structure of TIMING and IO_TIMING variables is explained in subsection 6.5. The format of the namelist-directed input file (e.g. "socrates.inp") where these variables are set is explained in subsection 6.6.

Another modern computing technique used by SOCRATES is netCDF, the Network Common Data Format. These libraries MUST be installed on the computer where the simulation is executed, because the initial conditions file is written in this format. Utilities built in the Fortran 90 source code are also provided for convenient output of the SOCRATES model to netCDF format.

The sequence of actions to install, compile, run and use the SOCRATES model is:
- Download and install the netCDF library (6.2)
- Download, install and compile the source code (6.4)
- Download and install the data files (6.4)
- Adapt the input file to the desired simulation (6.5 and 6.6)
- Eventually, download and install the IDL application "view2d" to visualize the output files (6.3)

6.2 What is netCDF ? How to get it ?

NetCDF (Network Common Data Format) is a format standard for binary data files. The binary format used is completely platform-independent. The data is self-describing and structured to allow easy reading and analyzis by programs written in C or Fortran, or by commercial packages (e.g. IDL, Matlab). Unidata, a division of UCAR, has developed this format and the Fortran library to read and write data to this format.
This library is available for free on all platforms : PC, Mac, Un*x workstations and CRAY computers. Your Unix admisnistrator should retrieve and install this library before you compile the SOCRATES model.

To download the library, point a World Wide Web browser to

http://www.unidata.ucar.edu/packages/netcdf/index.html

and follow the instructions.

The examples given here assume that the netCDF compiled library is available with the following path and filename :
/usr/local/lib/netcdf

The recommended filename extension for netCDF files is *.nc .

CAUTION ! The current version of netCDF is 3.3 . Although it allows faster read/write operations, a bug prevents it from being backward-compatible with previous versions. If you are using version 3.3 of the netCDF library, please compile the SOCRATES model using the module file src/modules/netcdf33.mod.f. If you are using a version of netCDF with a different version number, compile the SOCRATES model using the module file src/modules/netcdf.mod.f.

If you have already installed the NetCDF library, but it is a version older than 2.4.2, please update the library at the Unidata Web site given above.

6.3 Post-processing of netCDF files through "view2d", an IDL application

A direct advantage of using netCDF is the ability to write powerful and fast applications to perform graphical analysis on model data output.
Such an application has been written for the SOCRATES model. It is a set of IDL routines (IDL is a commercial product for scientific and graphical data analysis).
The name of the application is "view2d", packed to the file 'view2d.tar.gz' .
"view2d" allows the user to draw contour plots or one-dimensional plots from a netCDF output file from SOCRATES, and to compare two different netCDF files, through a Graphical User Interface.
The documentation is contained in the package (file README.txt) .
If your institution does not own an IDL license but uses a similar product (e.g. Matlab, or NCAR graphics), "view2d" can be used as a template to write a similar application.

6.4 Installation, compilation and execution of the SOCRATES model

The file socrates.tar.gz contains all the source code of the SOCRATES model version 1.0 . After uncompressing (e.g. "gunzip socrates.tar.gz") and unpacking (e.g. "tar -xlf socrates.tar) the contents are :

```
./socrates.inp                --> a typical simulation input file
                                  (see section 6.6)
./2dsoc.sh                    --> A C-shell script to compile and execute
                                  the model on CRAY computers
./src/*.f                     --> Fortran 90 source code for the main,
                                  subroutines and functions
./src/Makefile.ibm            --> to compile the model on an IBM RS/6000
                                  workstation
./src/modules/*.mod.f         --> Fortran 90 source code for the modules
./src/modules/Makefile.ibm    --> to compile the model on an IBM RS/6000
                                  workstation
```

To compile and execute the model on a CRAY computer, adapt and execute 2dsoc.sh.

To compile and execute the model on a Unix workstation, adapt the Makefiles to your environment (fortran 90 compiler command and options). The sequence of commands on an IBM RS/6000 workstation is then :

```
$HOME/.../src/modules> make -f Makefile.ibm
$HOME/.../src> make -f Makefile.ibm
$HOME/...> xlf src/*.o src/modules/*.o -o socrates  -L/usr/local/lib -lnetcdf
$HOME/...> nohup socrates < socrates.inp > socrates.out &
```

Makefiles for DEC alpha computers are available as well.

NOTE: If any of the module files is changed, it is advisable that all the source code be recompiled again.

The SOCRATES model requires a set of data files to run. These are packed in the file socrates_data.tar.gz . It should be downloaded, decompressed and unpacked to a separate directory. The simulation input files provided here assume that the data files are in the directory ./data , at the same directory level than /.src .

6.5 Structured variables of type TIMING and IO_TIMING

In SOCRATES, structured variables have been used to specify the date of the bginning of the simulation, the date of the end of the simulation, and the dates of desired output.
A date in the model is described by a structured variable of type TIMING (defined in the module TIME_CONTROLS, file src/modules/main.mod.f).
A structured variable is a group of subvariables, called "fields" of the structured variable. Each variable of type TIMING contains eight fields:

type TIMING

```
  integer :: year               --> Full year, e.g. 1996
  integer :: month              --> From 1 to 12
  integer :: day                --> If mode="date", day of the month (1 to 31)
                                    If mode='days', number of days since the
                                    beginning of simulation
  integer :: days0              --> Absolute measure of time: number of days
                                    since date 0/0/0000. Managed within the
                                    model.
  integer :: cal_day            --> Julian day of the year (1 to 365)
  integer :: index              --> Number of 5-day timesteps since beginning
                                    of simulation
  logical :: active             --> Managed by the model : will be set to .true.
                                    if the variable has been specified by the
                                    user and checked valid by the model.
  character(len=5) :: mode      --> set to "index", "days" or "date" depending
                                    of the way the variable is specified
```

The three different modes allow the user to define a date in several different ways. For example, assuming that the simulation begins January 1, 1995, the three following settings define the same date for the end of the simulation:

```
   sim_stop_time = 1997, 1,   1, 0, 0,   0, .true., 'date'    ...or...
   sim_stop_time =    0, 0, 730, 0, 0,   0, .true., 'days'    ...or...
   sim_stop_time =    0, 0,   0, 0, 0, 146, .true., 'index'
```

The values 0 are just blank fields which will be calculated by the model, depending on the mode ('date', 'days' or 'index') specified by the user. Note that when using the 'date' mode, the first integer sets the year, the second integer sets the month and the third integer sets the day of the month.

The model has two important variables of type TIMING : sim_start_time and sim_stop_time. Both must be specified by the user as elements of the namelist CONTROL_PARMS in the simulation input file (see next subsection). Contrarily to sim_stop_time (see example above), sim_start_time must be specified with the mode 'date'.
Furthermore, the "internal" initial conditions contained in the file data/initcond.nc correspond to the date January 1. If the user starts from

these conditions and not from a restart file calculated previously, the date set by sim_start_time must be January 1. The year can be chosen freely by the user, keeping in mind that the initial conditions correspond to the atmospheric composition typical of the 1990's. The usual starting date is thus:

```
    sim_start_time = 1995, 1, 1, 0, 0, 0, .true., 'date'
```

The user can set precise simulation dates at which printed, archived (diurnal averages or diurnal variations) or saved output are required (see next subsection). These variables have the type TIMING, and are named respectively ran_printout, ran_archive, ran_dvarch and ran_save.
It is also possible to output data at regular intervals between two specified dates, through the variables intv_printout, intv_archive and intv_save.
These variables have the type IO_TIMING, defined in the module TIME_CONTROLS (file ./src/modules/main.mod.f) :

```
type IO_TIMING
  type( TIMING ) :: start_time          --> set by any of the three modes
  type( TIMING ) :: stop_time           --> set by any of the three modes
  integer :: increment                  --> in 5-days timesteps
  logical :: active                     --> must be set to .true.
  character(len=5) :: mode              --> must be set to 'index'
```

Although these variables are vectors dimensioned to 10, only the first element of the vector is taken in account in the present version of the model.

6.6 Writing the namelist-directed simulation input files

Runs of the SOCRATES model require an input file, named 'socrates.inp' in the present description. This file contains the settings of basic parameters of the simulation, and the settings of variables of type TIMING and IO_TIMING. These variables are set through the use of namelists, a feature of Fortran90 which allows setting variables in a random order, with no formatting, by naming the variables to set.

'socrates.inp' contains two namelists: CONTROL_PARMS and IO_PARMS.
CONTROL_PARMS contains the settings of the simulation start date, stop date and basic parameters, whose names and possible values are given in the headers of the file src/main.f .

IO_PARMS contains the settings of the data directory name, and of the variables to specify what, when and where to output data. There are four possible output files, described in Table 12.

Table 12. Characteristics of SOCRATES-generated output files

Type of output	Format	output to file...	Data written in the file	TIMING variables	IO_TIMING variables
printed	ASCII	Standard out	dynamical and/or chemical variables (diurnal averages)	ran_printout(50)	intv_printout(10)
archived (diurnal average)	NetCDF	set by arch_filespec	dynamical and chemical variables (diurnal averages)	ran_archive(50)	intv_archive(10)
archived (diurnal cycle)	NetCDF	set by dvarch_filespec	temperature and chemical variables (diurnal cycles)	ran_dvarch(10)	none
saved	NetCDF	set by save_filespec	Everything needed to restart from last saved date	ran_save(50)	intv_save(10)

To explain the structure of an input file, we will comment the example input file named "socrates.inp", a typical two-year simulation requiring all the possible output files.

```
 &control_parms                                  --> settings for CONTROL_PARMS
namelist
 sim_start_time%year = 1995,                     --> arbitrary, left to user's
choice.
 sim_start_time%month = 1,                       --> mandatory to use internal
initial conditions
 sim_start_time%day = 1,                         --> mandatory to use internal
initial conditions
 sim_stop_time%year = 1997,                      --> simulation will end for
year 1997...
 sim_stop_time%month = 1,                        --> ... month of january...
 sim_stop_time%day = 6,                          --> ... first day of that month
 sim_stop_time%mode = 'date',                    --> this is an absolute date
 particle = 1,                                   --> turn ON sulfate aerosol
heterogeneous chemistry
 aero = .false.,                                 --> turn OFF aerosol effect on
photodissociatiation
                                                     and heating rates
calculation
 polar = 1,                                      --> turn ON heterogeneous
chemistry on Polar
                                                     Stratospheric Clouds
 liste = .true.,                                 --> output the initial values
 /                                               --> end of CONTROL_PARMS
namelist
 &io_parms                                       --> settings for IO_PARMS
namelist
 data_dir = 'data/',                             --> name of the directory
containing data files
 run_label = 'run30',                            --> label to identify version
number
 prntsw = 1,                                     --> generate ASCII output...
 dynprt = 1,                                     --> ... of dynamical
variables ...
 chmprt = 0,                                     --> ... but not of chemical
variables
```

```
 intv_printout(1) = 1995, 1,  1,  0, 0,  0, .true.,  'date' ,   --> ASCII output begins 1st
day of simulation...
                    0, 0,  0,  0, 0, 12, .true., 'index' ,   --> ... and ends after 12 (5-
days) timesteps
                   1,                                        --> between these two dates,
write at each timestep
                   .true.,                                   --> mandatory for variables of
type IO_TIMING
                   'index',                                  --> mandatory for variables of
type IO_TIMING
 ran_printout(1:3) = 1996, 6, 20, 0, 0,  0, .true., 'date' ,   --> add ASCII printout for 20
June 1996
                    0, 0, 90, 0, 0,  0, .true., 'days' ,   --> add ASCII printout 90 days
after simulation begins
                    0, 0,  0, 0, 0, 73, .true., 'index',   --> .. and 73 (5-days)
timesteps after simulation begins
 filesw = 1,                                               --> do NetCDF output of all
diurnally averaged variables
 arch_filespec = 'results/archive.nc',                     --> directory and file name
for NetCDF archive file
 intv_archive(1) =  1995, 1,  1,  0, 0, 0, .true., 'date' ,    --> archived output begins 1st
day of simulation...
                   1997, 1,  6,  0, 0, 0, .true., 'date' ,    --> ... and ends last day of
simulation
                   2,                                        --> between those two date,
output every other timestep
                   .true.,                                   --> mandatory for variables of
type IO_TIMING
                   'index',                                  --> mandatory for variables of
type IO_TIMING
 dvarchsw = 1,                                             --> do NetCDF output of
diurnal cycles of chemical vars
 diuvarch_filespec = 'results/diuvarch.nc',                --> directory and file name
for NetCDF archive file
 ran_dvarch(1:2) =  1996,  6, 20, 0, 0,  0, .true., 'date' ,    --> output for 20 june 1996
                   1996, 12, 17, 0, 0,  0, .true., 'date' ,    --> output for 17 december 1996
 savesw = 1,                                               --> save all variables to
```

```
restart from a "restart" file
 save_filespec = 'results/save30.nc',                          --> directory and file name
for NetCDF "restart" file
 intv_save(1) =  1995, 3,  1,  0, 0, 0, .true., 'date' ,       --> begin to save at 1 march
1995
                 1997, 1,  6,  0, 0, 0, .true., 'date' ,       --> stop savings at end of
simulation
                 12,                                           --> save every 12 (5-days)
timesteps
                 .true.,                                       --> mandatory for variables of
type IO_TIMING
                 'index',                                      --> mandatory for variables of
type IO_TIMING
 ran_save(1) = 1997, 1, 1, 0, 0, 0, .true., 'date',            --> make sure to save
simulation at 1 January 1997
/                                                              --> end of IO_PARMS namelist
```

The example provided above makes use of the "internal" initial conditions file 'data/initcond.nc' . The user can start the simulation with any other "restart" file saved from previous runs, provided that he knows the date of the last conditions saved in the "restart" file generated by the previous run.

Let us suppose that the user wants to use a restart file containing the conditions saved by a previous run, for the date 20 june 1995.
First, this must be the date of the start of his run:

```
 &control_parms
 sim_start_time%year = 1995,
 sim_start_time%month = 1,
 sim_start_time%day = 1,
```

The following line must be inserted in the CONTROL_PARMS namelist settings:

```
 restrt = .true.,
```

The path and name of the "restart" file must be set in the IO_PARMS namelist .

```
If the "restart" file is named 'save29.nc' and is in the directory 'results',
the next line should be inserted in the IO_PARMS namelist settings:
 rstrt_filespec = 'results/save29.nc'
```

References:

Akmaev, R. A., and G. M. Shved, Parameterization of the radiative flux divergence in the 15 mm CO2 band in the 30-75 km layer, J. Atmos. Terr. Phys., 44, 993-1004, 1982.

Andrews, D. G., J. R. Holton, and C. B. Leovy, Middle Atmospheric Dynamics, 489 pp., Academic Press, 1987.

Banks, P. M., and G. Kockarts, Aeronomy, Academic Press, 1973.

Boville, B. A., The thermal balance of the NCAR community climate model. J. Atmos. Sci., 42, 695-709, 1985.

Brasseur G. and D. Offermann, Recombination of atomic oxygen near the mesopause: Interpretation of rocket data. J. Geophys. Res., 91, 10818-10824, 1986.

Brasseur, G. and S. Solomon, Aeronomy of the middle atmosphere, 452 pp, D. Reidel Publishing Company, 1986.

Brasseur, G. and M. H. Hitchman, The effect of breaking gravity waves on the distribution of trace species in the middle atmosphere, in Transport Processes in the Middle Atmosphere, edited by G. Visconti and R. Garcia, pp. 215-227, D. Reidel, Hingham, Mass., 1987.

Brasseur, G., M. H. Hitchman, S. Walters, M. Dymek, E. Falise, and M. Pirre, An interactive chemical dynamical radiative two-dimensional model of the middle atmosphere, J. Geophys. Res., 95, 5639-5655, 1990.

Briegleb, B. P., Longwave band model for thermal radiation in climate studies, J. Geophys. Res., 97, 11475-11485, 1992.

Cadle, R. D., P. Crutzen, and D. Ehhalt, Heterogeneous chemical reactions in the stratosphere, J. Geophys. Res., 80, 3381-3385, 1975.

Cess, R. D., Climate change: An Appraisal of atmospheric feedback mechanisms employing zonal climatology. J. Atmos. Sci., 33, 1831-1843, 1976.

Chipperfield, M. P., D. Cariolle, P. Simon, R. Ramaroson, D. J. Lary, A three-dimensional modeling study of trace species in the Arctic lower stratosphere during winter 1989-1990. J. Geophys. Res., 98, 7199-7218, 1993.

DeMore, W. B., S. P. Sander, D. M. Golden, R. F. Hampson, M. J. Kurylo, C. J. Howard, A. R. Ravishankara, C. E. Kolb, M. J. Molina, Chemical kinetics and photochemical data for use in stratospheric modeling, JPL Publication 97-4, 1997.

Fleming, E. L., S. Chandra, M. R. Schoeberl, and J. J. Barnett, Monthly mean global climatology of temperature, wind, geopotential height, and pressure for 0-120 km. NASA Tech. Memorandum 100697, 1988.

Formichev, V. I., A. A. Kutepov, R. A. Akmaev, and G. M. Shved, Parameterization of the 15 mm CO2 band cooling in the middle atmosphere (15-115 km), J. Atmos. Terr. Phys., 55, 7-18, 1993.

Fritts, D. C., and T. E. VanZandt, Spectral estimates of gravity wave energy and momentum fluxes. Part I: Energy dissipation, acceleration, and constraints. J. Atmos. Sci., 50, 3685-3694, 1993.

Fritts, D. C., and W. Lu, Spectral estimates of gravity wave energy and momentum fluxes. Part II- Parameterization of wave forcing and variability, J. Atmos. Sci., 50, 3695-3713, 1993.

Fung, I., J. John, J. Lerner, E. Matthews, M. Prather, L.P. Steele, and P. J. Fraser, Three-dimensional model synthesis of the global methane cycle. J. Geophys. Res., 96, 13033-10365, 1991.

Garcia, R. R., Parameterization of planetary wave breaking in the middle atmosphere, J. Atmos. Sci., 48, 1405-1419, 1991.

Garcia, R. R., F. Stordal, S. Solomon, and J. T. Kiehl, A new numerical model of the middle atmosphere, 1, Dynamics and transport of tropospheric source gases. J. Geophys. Res., 97, 12967-12992, 1992.

Gillotay D. and P. C. Simon, Ultraviolet cross-sections of halocarbons of stratospheric interest, Aeronomica Acta A - No 336, Belgian Space Aeronomy Institute, Brussels, Belgium, 1988.

Hanson, D., and K. Mauersberger, Laboratory studies of the nitric acid tridydrate: Implications for the south polar stratosphere, Geophys. Res. Lett., 15, 855-858, 1988.

Hanson, D., and K. Mauersberger, HCl/H2O solid-phase vapor pressures and HCl solubility in ice. J. Phys. Chem, 94, 4700-4705, 1990.

Hanson, D. R., A. R. Ravishankara, and S. Solomon, Heterogeneous reactions in sulfuric acid aerosols: A framework for model calculations, J. Geophys. Res., 99, 3615-3629, 1994.

Hanson, D. R., and A. R. Ravishankara, Heterogeneous chemistry of bromine species in sulfuric acid under stratospheric conditions, Geophys. Res. Lett, 22, 385-388.

Hauglustaine, D. A., C. Granier, G. Brasseur, and G. Megie, The importance of atmospheric chemistry in the calculation of radiative forcing on the climate system. J. Geophys. Res., 99, 1173-1186, 1994.

Heaps, M. G., A parameterization of cosmic ray ionization, Planet. Space Sci., 26, 513, 1978.

Hirota, Isamu, Climatology of gravity waves in the middle atmosphere. J. Atmos. Terr. Phys., 46, 767-773, 1984.

Hitchman, M. H., M. McKay, and C. R. Trepte, A climatology of stratospheric aerosol. J. Geophys. Res., 99, 20689-20700, 1994.

Holton, J. R., The role of gravity wave induced drag and diffusion in the momentum budget of the mesosphere, J. Atmos. Sci., 39, 791-799, 1982.

Hough, A. M., Development of a two-dimensional global tropospheric model: Model chemistry, J. Geophys. Res., 96, 7325-7362, 1991.

Hu Y. X., and K. Stamnes, An accurate parameterization of the radiative properties of

water clouds suitable for use in climate models. J. Climate, 6, 728-742, 1993.

Hubinger, S., and J. B. Nee, Absorption spectra of Cl2, Br2, and BrCl between 1990 and 600 nm, J. Photochem. Photobiol. A: Chem., 86, 1-7, 1995

Joseph, J. H., W. J. Wiscombe and J. A. Weinman, The delta-Eddingtion approximation for radiative flux transfer. J. Atmos. Sci., 33, 2452-2450, 1976.

Kockarts, G., Penetration of solar radiation in the Schumann-Runge bands of molecular oxygen: a robust approximation. Ann. Geophysicae, 12, 1207-1217, 1994.

Kuhn, W. R., and J. London, Infrared radiative cooling in the middle atmosphere (30-110 km), J. Atmos. Sci., 26,189-204, 1969.

Kutepov, A. A., and V. I. Formichev, Application of the second-order escape probability approximation to the solution of the NLTE vibration-rotational band radiative transfer problem, J. Atmos. Terres. Phys., 55, 1-6, 1993.

Kylling, A., Radiation transport in cloudy and aerosol loaded atmosphere. Ph.D. thesis, University of Alaska, 1992.

Langner, J., H. Rodhe, and M. Olofsson, Parameterization of subgrid scale vertical tracer transport in a global two-dimensional model of the troposphere. J. Geophys. Res., 95, 13691-13706, 1990.

Lindzen, R. S., and H. -L. Kuo, A reliable method for the numerical intergration of a large class of ordinary and partial differential equations. Mon.Wea. Rev., 97, 732-734, 1969.

Lindzen, R. S., Turbulence and stress owing to gravity wave and tidal breakdown, J. Geophys. Res., 86, 9707-9714, 1981.

Liu, S. C., and T. M. Donahue, The aeronomy of hydrogen in the atmosphere of the earth. J. Atmos.Sci., 31, 1118-1136, 1974.

Magnotta, F. and H. S. Johnston, Photodissociation quantum yields for the NO3 free radical, Geophys. Res. Lett., 7, 769-772,1980

Maric, D., J. P. Burrows, and G. K. Moortgat, A study of the UV-visible absorption

spectra of Br2 and BrCl, J. Photochem. Photobiol. A: Chem, 83, 179-192, 1994.

Massie, S. T., A. Goldman, A. H. McDaniel, C. A. Cantrell, J. A. Davidson, R. E. Shetter, and J. G. Calvert, Temperature dependent infrared cross secions for CFC-11, CFC-12, CFC-13, CFC-14, CFC-22, CFC-113, CFC-114, and CFC-155, NCAR Tech. Note NCAR/TN-358+STR, 67 pp., Natl. Cent. for Atmos. Res., Boulder, Colo., 1991.

McEwan, M. J., and L. F. Philips, Chemistry of the atmosphere, Edward Arnold Ltd. Publishers, London U.K., 301pp., 1975.

Meador, W. E., and W. R. Weaver, Two-stream approximations to radiative transfer in planetary atmosphere: A unified description of existing methods and a new improvement, J. Atmos. Sci., 37, 630-643, 1980.

Michelangeli, D., M. Allen, and Y. L. Young, El Chichon volcanic aerosols: Impact of radiative, thermal and chemical perturbations. J. Geophys. Res., 94, 18429-18443, 1989.

Minschwaner, K., and D. Siskind, A new calculation of nitric oxide photolysis in the stratosphere, mesosphere, and lower thermosphere. J. Geophys. Res., 98, 20401-20412, 1993.

Molina, L. T., and M. J. Molina, Absolute absorption cross sections of ozone in the 185- to 350- nm wavelength range. J. Geophys. Res., 91, 14501-14508, 1986.

Murray, F. W., On the computation of saturation vapor pressure. J. Appl. Meteor., 6, 203-204, 1967.

Mylnczak, M. G. and S. Solomon, A detailed evaluation of the heating efficiency in the middle atmosphere, J. Geophys. Res., 98, 10517-10541, 1993.

Nicolet, M., On the molecular scattering in the terrestrial atmosphere: an empirical formula for its calculation in the homosphere. Planet. Space Sci., 32, 1467-1468.

Orlando, J. J., and J. B. Burkholder, Gas-phase uv/visible absorption sepctra of HOBr and Br2O, J. Phys. Chem., 99, 1143-1150, 1995.

Peaceman, D. W., and H. H. Rachford, Jr., The numerical solution of parabolic and elliptic

differential equations, J. Soc. Indust. Appl. Math., 3, 28-41, 1955.

Peixoto, J. P., and A. H. Oort, Physics of Climate, 520 pp., American Institute of Physics, 1991.

Pinnick, R. G., S. G. Jennings, and P. Chylek, Relationships between extinction, absorption, backscattering, and mass content of sulfuric acdid aerosols. J. Geophys. Res., 85, 4059-4066, 1980.

Politowicz, P. A., and M. H. Hitchman, Exploring the effects of forcing quasibiennial oscillations in a two-dimensional model, J. Geophys. Res., 102, 16481-16498, 1997.

Ramanathan, V., R. J. Cicerone, H. B. Singh, and J. T. Kiehl, Trace gas trends and their potential role in climate change, J. Geophys. Res., 90, 5547-5566, 1985.

Randel, W. J., Global atmospheric circulation statistics, 1000 - 1 mb, NCAR Tech. Note TN-295, 245 pp., Natl. Cent. for Atmos. Res., Boulder, Colo., 1987.

Randel, W. J., Global atmospheric circulation statistics, 1000 - 1 mb, NCAR Tech. Note, TN-366+STR, 256 pp., Natl. Cent. for Atmos. Res., Boulder, Colo., 1992.

Robock, A., Ice and snow feedbacks and the latitudinal and seasonal distribution of climate sensitivity, J. Atmos. Sci., 40, 986-997, 1983.

Robert, A., A stable numerical integration scheme for the pimitive meteorological equations, Atmos. - Ocean, 10, 35-46, 1981.

Rothman, L. S., et al., The HITRAN database: 1986 edition, Appl. Opt., 26, 4058-4097, 1987.

Shettle, E. P., and J. A. Weinman, The transfer of solar irradiance through inhomogeneous turbid atmospheres evaluated by Eddingtion's approximation. J. Atmos. Sci., 27, 1048-1055, 1970.

Smith, A. K., and S. K. Avery, A resonant wave in a numerical model of the 1979 sudden stratospheric warming. J. Atmos. Sci., 44, 3150-3161, 1987.

Smith III, F. L. and C. Smith, Numerical evaluation of Chapman's grazing incidence

integral ch(X,c). J. Geophys. Res., 77, 3592-3597, 1972.

Solomon, S., P. J. Crutzen, and R. G. Roble, Photochemical coupling between the thermosphere and the lower atmosphere. 1. Odd nitrogen from 50 to 120 km. J. Geophys. Res., 87, 7206-7220, 1982.

Steele, H. M., and P. Hamill, Effects of temperature and humidity on the growth and opitcal properties of sulphuric acid-water droplets in the stratosphere. J. Aerosol Sci., 12, 517-528, 1981.

Talukdar, R. K., J. B. Burkholder, A. Schmoltner, J. M. Roberts, R. R. Wilson, and A. R. Ravishankara, Investigation of the loss processes of peroxyacetyl nitrate in the atmosphere: UV photolysis and reaction with OH, J. Geophys. Res., 100, 14163-14174, 1995.

Toon, O. B., C. P. McKay, T. P. Ackerman, and K. Santhanam, Rapid calculation of radiative heating rates and photodissociation rates in inhomogeneous multiple scattering atmosphere, J. Geophys. Res., 94, 16287-16301, 1989.

Wahner, A., G. S. Tyndall, and A. R. Ravishankara, Absorption cross sections for OClO as a function of temperature in the wavelength range 240-480 nm, J. Phys. Chem., 91, 2734-2738, 1987.

Weinstock, J., Gravity wave saturation and eddy diffusion in the middle atmosphere, J. Atmos. Terr. Phys., 46, 1069-1082, 1984.

Wilson, R., M. L. Chanin, and A. Hauchecorne, Gravity waves in the middle atmosphere observed by Rayleigh lidar. 1. Case studies. J. Geophys. Res., 96, 5153-5167, 1991a.

Wilson, R., M. L. Chanin, and A. Hauchecorne, Gravity waves in the middle atmosphere observed by Rayleigh lidar. 2. Climatology. J. Geophys. Res., 96, 5169-5183, 1991b.

World Meteorological Organization, Atmospheric Ozone 1985, WMO Rep. 16, Global Ozone Res. and Monit. Proj., Geneva, Switzerland, 1986.

List of Tables

Back to Table of content.

List of Tables

Back to Table of content.

Figure 1. Numerical algorithm of the 2-D Model

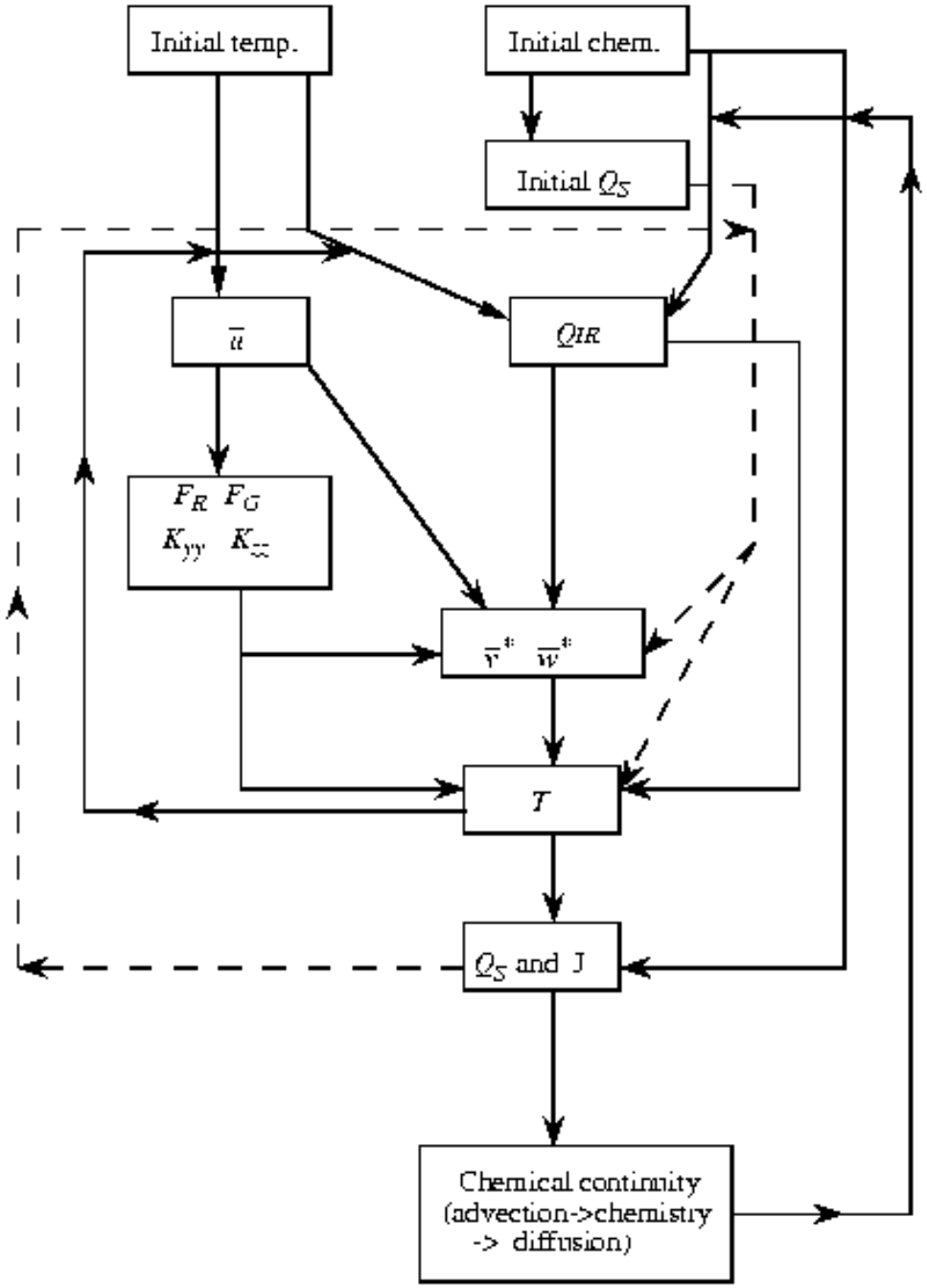

Table 1. Solar flux

no.	Wavelength(nm)		phot/s/cm2	solar variability
1	116.3	117.0	6.880E+08	
2	117.0	117.6	2.790E+09	
3	117.6	118.3	7.300E+08	
4	118.3	119.0	6.510E+08	
5	119.0	119.8	2.575E+09	0.43
6	119.8	120.5	2.970E+09	0.49
7	120.5	121.2	9.500E+09	0.71
8	121.6	121.6	4.880E+11	0.70
9	121.2	122.0	6.485E+09	0.61
10	122.0	122.7	3.475E+09	0.36
11	122.7	123.5	1.680E+09	0.30
12	123.5	124.2	2.225E+09	0.42
13	124.2	125.0	1.575E+09	0.35
14	125.0	125.8	1.380E+09	0.30
15	125.8	126.6	2.650E+09	0.43
16	126.6	127.4	1.210E+09	0.33
17	127.4	128.2	1.335E+09	0.28
18	128.2	129.0	9.315E+08	0.21
19	129.0	129.9	1.275E+09	0.34
20	129.9	130.7	1.008E+10	0.28
21	130.7	131.6	2.975E+09	0.28
22	131.6	132.4	1.305E+09	0.14
23	132.4	133.3	2.150E+09	0.22
24	133.3	134.2	1.455E+10	0.35
25	134.2	135.1	1.415E+09	0.19
26	135.1	136.0	2.940E+09	0.15
27	136.0	137.0	2.150E+09	0.18
28	137.0	137.9	2.020E+09	0.17
29	137.9	138.9	2.240E+09	0.15
30	138.9	140.8	1.189E+10	0.41
31	140.8	142.8	6.795E+09	0.15
32	142.8	144.9	8.515E+09	0.15
33	144.9	147.0	1.032E+10	0.14
34	147.0	149.2	1.515E+10	0.12
35	149.2	151.5	1.625E+10	0.12
36	151.5	153.8	2.265E+10	0.17
37	153.8	156.2	4.295E+10	0.21
38	156.2	158.7	3.610E+10	0.14

39	158.7	161.3	4.165E+10	0.13
40	161.3	163.9	5.705E+10	0.14
41	163.9	166.7	9.360E+10	0.15
42	166.7	169.5	1.095E+11	0.11
43	169.5	172.4	1.780E+11	0.09
44	172.4	173.9	1.016E+11	0.09
45	173.9	175.4	1.295E+11	0.09
46	175.4	177.0	1.770E+11	0.08
47	177.0	178.6	2.240E+11	0.10
48	178.6	180.2	2.440E+11	0.11
49	180.2	181.8	3.250E+11	0.11
50	181.8	183.5	3.810E+11	0.10

no.	Wavelength(nm)		phot/s/cm2	solar variability
51	183.5	185.2	3.570E+11	0.07
52	185.2	186.9	4.255E+11	0.07
53	186.9	188.7	5.635E+11	0.07
54	188.7	190.5	6.585E+11	0.07
55	190.5	192.3	7.715E+11	0.06
56	192.3	194.2	7.685E+11	0.06
57	194.2	196.1	1.095E+12	0.07
58	196.1	198.0	1.240E+12	0.07
59	198.0	200.0	1.380E+12	0.06
60	200.0	202.0	1.665E+12	0.06
61	202.0	204.1	2.000E+12	0.05
62	204.1	206.2	2.450E+12	0.05
63	206.2	208.3	2.870E+12	0.05
64	208.3	210.5	5.080E+12	0.02
65	210.5	212.8	8.395E+12	0.01
66	212.8	215.0	9.120E+12	0.01
67	215.0	217.4	9.370E+12	0.01
68	217.4	219.8	1.200E+13	0.02
69	219.8	222.2	1.230E+13	0.02
70	222.2	224.7	1.715E+13	0.01
71	224.7	227.3	1.425E+13	0.01
72	227.3	229.9	1.510E+13	0.00
73	229.9	232.6	1.705E+13	0.01
74	232.6	235.3	1.400E+13	0.01
75	235.3	238.1	1.765E+13	0.01
76	238.1	241.0	1.475E+13	0.01
77	241.0	243.9	2.290E+13	-0.01

78	243.9	246.9	2.065E+13	0.00
79	246.9	250.0	2.110E+13	0.01
80	250.0	253.2	2.005E+13	0.02
81	253.2	256.4	2.845E+13	0.00
82	256.4	259.7	5.425E+13	0.01
83	259.7	263.2	4.265E+13	0.02
84	263.2	266.7	1.160E+14	0.00
85	266.7	270.3	1.250E+14	0.02
86	270.3	274.0	1.165E+14	0.01
87	274.0	277.8	1.080E+14	0.02
88	277.8	281.7	7.205E+13	0.03
89	281.7	285.7	1.505E+14	0.01
90	285.7	289.9	2.245E+14	0.01
91	289.9	294.1	3.640E+14	0.02
92	294.1	298.5	3.540E+14	0.02
93	298.5	303.0	3.230E+14	0.02
94	303.0	307.7	4.520E+14	0.00
95	307.7	312.5	4.885E+14	0.00
96	312.5	317.5	5.615E+14	0.00
97	317.5	322.5	6.180E+14	0.00
98	322.5	327.5	7.045E+14	0.00
99	327.5	332.5	8.610E+14	0.00
100	332.5	337.5	7.930E+14	0.00

no.	Wavelength(nm)		phot/s/cm2	solar variability
101	337.5	342.5	8.510E+14	0.00
102	342.5	347.5	8.370E+14	0.00
103	347.5	352.5	8.675E+14	0.00
104	352.5	357.5	9.150E+14	0.00
105	357.5	362.5	8.375E+14	0.00
106	362.5	367.5	1.060E+15	0.00
107	367.5	372.5	1.110E+15	0.02
108	372.5	377.5	1.020E+15	0.00
109	377.5	382.5	1.175E+15	-0.01
110	382.5	387.5	9.040E+14	-0.01
111	387.5	392.5	1.195E+15	-0.01
112	392.5	397.5	9.105E+14	0.00
113	397.5	402.5	1.685E+15	-0.01
114	402.5	407.5	1.755E+15	0.01
115	407.5	412.5	1.800E+15	0.01
116	412.5	417.5	1.935E+15	-0.01

117	417.5	422.5	1.860E+15
118	422.5	427.5	1.760E+15
119	427.5	432.5	1.630E+15
120	432.5	437.5	1.960E+15
121	437.5	442.5	2.010E+15
122	442.5	447.5	2.170E+15
123	447.5	452.5	2.330E+15
124	452.5	457.5	2.280E+15
125	457.5	462.5	2.350E+15
126	462.5	467.5	2.340E+15
127	467.5	472.5	2.340E+15
128	472.5	477.5	2.380E+15
129	477.5	482.5	2.460E+15
130	482.5	487.5	2.250E+15
131	487.5	492.5	2.390E+15
132	492.5	497.5	2.500E+15
133	497.5	502.5	2.400E+15
134	502.5	507.5	2.460E+15
135	507.5	512.5	2.500E+15
136	512.5	517.5	2.350E+15
137	517.5	522.5	2.420E+15
138	522.5	527.5	2.440E+15
139	527.5	532.5	2.600E+15
140	532.5	537.5	2.590E+15
141	537.5	542.5	2.550E+15
142	542.5	547.5	2.610E+15
143	547.5	552.5	2.590E+15
144	552.5	557.5	2.610E+15
145	557.5	562.5	2.570E+15
146	562.5	567.5	2.640E+15
147	567.5	572.5	2.630E+15
148	572.5	577.5	2.690E+15
149	577.5	582.5	2.700E+15
150	582.5	587.5	2.750E+15

no.	Wavelength(nm)	phot/s/cm2	solar variability

151	587.5	592.5	2.630E+15
152	592.5	597.5	2.660E+15
153	597.5	602.5	2.620E+15
154	602.5	607.5	2.690E+15
155	607.5	612.5	2.680E+15

156	612.5	617.5	2.630E+15
157	617.5	622.5	2.710E+15
158	622.5	627.5	2.610E+15
159	627.5	632.5	2.620E+15
160	632.5	637.5	2.640E+15
161	637.5	642.5	2.660E+15
162	642.5	647.5	2.660E+15
163	647.5	655.0	5.210E+15
164	655.0	665.0	5.060E+15
165	665.0	675.0	5.240E+15
166	675.0	685.0	5.260E+15
167	685.0	695.0	5.100E+15
168	695.0	705.0	5.790E+15
169	705.0	715.0	5.060E+15
170	715.0	725.0	4.990E+15
171	725.0	735.0	4.970E+15

Table 2. Photodissociation process

```
1.........O2 + hv  -> O + O
2.........O3 + hv  -> O(3P) + O2
3.........H2O + hv  -> OH + H
4.........N2O + hv -> N2 + O(1D)
5.........CO2 + hv  -> CO + O
6.........CH4 + hv -> CH2+H2
7.........NO2 + hv -> NO + O(3P)
8.........HNO3 + hv -> OH + NO2
9.........CFC-12 (CCl2F2) + hv -> CClF2 + Cl
10.........CFC-11 (CCl3F) + hv -> CFCl2 + Cl
11.........CFC-10 (CCl4 )+ hv  -> CCl3 + Cl
12.........HOCl + hv -> OH + Cl
13.........CH3CCl3 + hv -> CH3CCl2 + Cl
14.........HO2NO2 + hv -> HO2+NO2
15.........CH3Cl + hv -> CH3O2 + Cl
16.........ClONO2 + hv -> ClO+NO2
17.........N2O5 + hv -> NO2 + NO3
18.........O3 + hv -> O(1D) + O2
19.........CFC-113 (CCl2FCClF2)+ hv -> products
20.........HCFC-22 (CHF2Cl) + hv  ->   products
21.........Ha-1211 (CF2ClBr) + hv ->   products
22.........Ha-1301 (CF3Br) + hv -> products
23.........H2O2 + hv -> OH + OH
24.........CH2O + hv -> CO + HO2 + H
25.........BrONO2 + hv -> 0.71(BrO +NO2)+  0.29(Br +NO3)
26.........HOBr + hv -> OH + Br
27.........CH3Br + hv -> CH3O2 + Br
28.........OClO + hv -> O + ClO
29.........Cl2O2 + hv -> 2Cl + O2
30.........Cl2    + hv -> Cl + Cl
31.........CCl2O + hv -> products
32.........CClFO + hv -> products
33.........CF2O + hv -> products
34.........CFC-114 (CClF2CClF2)+ hv -> products
35.........CFC-115 (CClF2CF3) + hv ->  products
36.........HCl + hv -> H + Cl
37.........CH2O + hv -> CO + H2
38.........CH3OOH + hv -> CH3O+OH
39.........CH3CO3 + hv -> products
40.........PAN (CH3C(O)OONO2)+ hv ->   0.8 ( CH3C(O)O2 + NO2 )+ 0.2 ( CH3C(O)O +
NO3 )
41.........ClNO2  + hv -> Cl + NO2
42.........  NO3  + hv -> NO2 + O
43.........NO + hv -> N + O
44.........BrCl + hv -> Br + Cl
45.........BrO + hv -> Br + O
```

```
46.........HO2NO2+ hv  -> OH+NO3
47.........ClONO2 + hv -> Cl + NO3
48.........NO3  + hv -> NO + O2
49.........CHBr3  + hv -> products
50.........O2 + hv  ->  O(1D) + O(3P)
```

Table 3 Cross section and quantum yield source references

	Cross sections	Quantum yield
1.....O2		
	116.3-175.4 nm : Brasseur and Solomon (1986)	1
	175.4-204.1 nm : Kockarts (1994)	NA
	204.1-244 nm : JPL97	1
2.....O3 -> O(3P)		
JPL97		
	116.3-175.4 nm : Brasseur and Solomon (1986)	1
	175.8-347.5 nm : Molina and Molina (1986)	JPL97
	347.5-735 nm : Brasseur and Solmon (1986)	1
3.....H2O	JPL97	1
4.....N2O	JPL97	1
5.....CO2	Brasseur and Solomon (1986)	1
6.....CH4	Source NA	1
7.....NO2	JPL97	JPL97
8.....HNO3	JPL97	1
9.....CFC-12	JPL97	1
10.....CFC-11	JPL97	1
11.....CCl4	JPL97, Gillotay and Simon (1988)	1
12.....HOCl	JPL97	1
13.....CH3CCl3	JPL97	1
14.....HO2NO2 -> NO2	JPL97	JPL97
15.....CH3Cl	JPL97	1
16.....ClONO2 -> NO2	JPL97	JPL97
17.....N2O5	JPL97	1
18.....O3 -> O(1D)	Same as 2) O3->O(3P)	JPL97
19.....CFC-113	JPL97, Gillotay and Simon (1988)	1
20.....HCFC-22	JPL97, Gillotay and Simon (1988)	
1		
21.....Ha-1211	JPL97, Gillotay and Simon (1988)	1
22.....Ha-1301	JPL97, Gillotay and Simon (1988)	1
23.....H2O2	JPL97	1
24.....CH2O->H+HCO	JPL97	JPL97
25.....BrONO2	JPL97	1
26.....HOBr	JPL97	1
27.....CH3Br	Gillotay and Simon (1988)	1
28.....OClO	Wahner et al. (1987)	1
29.....Cl2O2	JPL97	1
30.....Cl2	Hubinger and Nee (1995)	1
31.....CCl2O	JPL97	1
32.....CClFO	JPL97	1
33.....CF2O	JPL97	JPL97
34.....CFC-114	JPL97, Gillotay and Simon (1988)	1
35.....CFC-115	JPL97	1
36.....HCl	JPL97	1

37.....CH2O->H2+CO	JPL97	JPL97
38.....CH3OOH	JPL97	1
39.....CH3CO3	NA	NA
40.....PAN	Talukdar et al. (1995), JPL97	1
41.....ClNO2	JPL97	1
42.....NO3	Magnotta and Johnston (1980)	included in crs sec.
43.....NO	Minschwaner and Siskind (1993)	NA
44.....BrCl	Maric et al. (1994), JPL97	1
45.....BrO	JPL97	1
46.....HO2NO2 -> NO3	JPL97	JPL97
47.....ClONO2 -> NO3	JPL97	JPL97
48.....NO3	Magnotta and Johnston (1980)	included in crs sec.
49.....CHBr3	JPL97	1

Table 4. SOCRATES chemical species

Table 4a. Long-lived species

1.....N2O
2.....CH4
3.....H2O
4.....NOy=NO+NO2+HNO3+
      2*N2O5+HO2NO2+NO3+N+
      ClONO2+BrONO2+ClNO2
5.....HNO3
6.....N2O5
7.....Cly=ClO+OClO+
      2*Cl2O2+HCl+ClONO2+HOCl+
      2*Cl2+ClNO2
8.....Ox=O3+O(3P)+O(1D)
9.....CO
10.....OClO
11.....TRACER
12.....AEROSOLS
13.....HCl
14.....ClONO2
15.....HOCl
16.....Cl2
17.....H2O2
18.....ClNO2
19.....HBr
20.....BrONO2
21.....NOx =NO +NO2
22.....HO2NO2
23.....ClOx =Cl + ClO
24.....BrOx =Br + BrO
25.....Cl2O2
26.....HOBr
27.....CO2
28.....C2H6
29.....C2H4
30.....C3H6
31.....CH2O
32.....PAN   (CH3CO3NO2)
33.....H2
34.....HOx

35.....CFC-10 (CCl4)
36.....CFC-11 (CCl3F)
37.....CFC-12 (CCl2F2)
38.....CFC-113 (C2Cl3F3)
39.....CFC-114 (C2Cl2F4)
40.....CFC-115 (C2ClF5)
41.....HCFC-22 (CHClF2)
42.....CH3CCl3
43.....CH3Cl
44.....CCl2O
45.....CClFO
46.....CF2O
47.....Ha-1211 (CF2ClBr)
48.....Ha-1301 (CF3Br)
49.....HF
50.....CH3Br
51.....Bry=Br+BrO+HOBr+
HBr+BrONO2+BrCl
52.....CHBr3

Table 4b Intermediate lifetime species
1.....CH3O2
2.....CH3OOH
3.....C2H5O2
4.....C2H5OOH
5.....CH3CHO
6.....CH3CO3
7.....CH3COOOH
8.....C3H6OHO2
9.....C3H6OHOOH
10.....BrCl

Table 4c Short-lived species
1.....O(1D)
2.....OH
3.....Cl
4.....O(3P)
5.....O3
6.....HO2
7.....NO2

```
8.........NO
9.........Br
10.........N
11.........ClO
12.........BrO
13.........NO3
14.........H
```

Table 5. SOCRATES Chemical reactions.

Odd hydrogen reactions

a1	H + O2 + M -> HO2 + M	*	k0(300)=5.7e-32	n=1.6
			kinf(300)=7.5e-11	m=0
a1et	O1D + H20 -> OH + OH		2.2e-10	
a2	H + O3 -> OH + O2		1.4e-10 exp(-470/T)	
a2et	O1D + CH4 -> OH + CH3O2		1.5e-10	
a3et	O1D + H2 -> OH + H		1.0e-10	
a5	O + OH -> O2 + H		2.2e-11 exp(120/T)	
a6	OH + O3 -> HO2 + O2		1.6e-12 exp(-940/T)	
a6b	HO2 + O3 -> OH + 2O2		1.1e-14 exp(-500/T)	
a7	O + HO2 -> OH + O2		3. e-11 exp(200/T)	
a17	OH + HO2 -> H2O + O2		4.8e-11 exp(250/T)	
a19	OH + H2 -> H2O + H		5.5e-12 exp(-2000/T)	
a23a	H + HO2 -> OH + OH		8.1e-11*0.9	
a23b	H + HO2 -> H2 + O2		8.1e-11*0.08	
a23c	H + HO2 -> H2O + O		8.1e-11*0.02	
a24	H2 + O -> OH + H		8.8e-12 exp(-4200/T)	
a26	NO + HO2 -> NO2 + OH		3.5e-12 exp(250/T)	
a27	HO2 + HO2 -> H2O2 + O2	**	k1=1.7e-33 exp(1000/T)[M]	
			k2=2.3e-13 exp(600/T)	
			fh2o=1+1.4e-21 exp(2200/T)[H2O]	
a30	OH + H2O2 -> H2O + HO2		2.9e-12 exp(-160/T)	
a36	OH + CO -> CO2 + H		1.5e-13*(1+0.6p(mb)/1013)	
a40	HO2+HO2+H2O -> H2O2+O2+H2O			
a81	O+H2O2 -> OH+HO2		1.4e-12 exp(-2000/T)	
a82	OH+OH -> H2O + O		4.2e-12 exp(-240/T)	
a83	OH+OH+M -> H2O2 + M	*	k0(300)=6.9e-31	n=0.8
			kinf(300)=1.5e-11	m=0

Odd nitrogen reactions

b3	O + NO2 -> NO+ O2		6.5e-12 exp(120/T)	
b4	O3 + NO -> NO2 + O2		2.0e-12 exp(-1400/T)	
b6	N + NO -> N2 + O		2.1e-11 exp(100/T)	
b7	N + O2 -> NO + O		1.5e-11 exp(-3600/T)	
b9	O3 + NO2 -> NO3 + O2		1.2e-12 exp(-2450/T)	
b12	NO2 + NO3 + M -> N2O5 + M	*	k0(300)=2.2e-30	n=3.9
			kinf(300)=1.5e-12	m=0.7
b22	OH + NO2 + M -> HNO3 + M	*	k0(300)==2.6e-30	n=3.2
			kinf(300)=2.4e-11	m=1.3
b23	HO2 + NO2 + M -> HO2NO2 + M	*	k0(300)=1.8e-31 n=3.2	
			kinf(300)=4.7e-12	m=1.4
b24	HO2NO2 + M -> HO2 + NO2 + M		b23/Keq Keq=2.1e-27 exp(10900/T)	
b27	HNO3 + OH -> H2O + NO3	***	k0=7.25e-15 exp(785/T)	
			k2=4.1e-16 exp(1440/T)	
			k3=1.9e-33 exp(725/T)	

b28	OH + HO2NO2-> H2O+NO2+O2		1.3e-12 exp(380/T)	
b32	N2O5 + M -> NO2 + NO3 + M	b12/Keq	Keq=2.7e-27exp(11000/T)	
b38	O1D + N2O -> N2 + O2		4.9e-11	
b39	O1D + N2O -> NO + NO		6.7e-11	
b71	NO3+O -> NO2+O		1.0e-11	
b72	NO3+OH -> NO2+HO2		2.2e-11	
b73a	NO3+HO2 -> OH+NO2+O2		3.5e-12*0.8	
b73b	NO3+HO2 -> HNO3+O2		3.5e-12*0.2	
b81	O+NO2+M -> NO3+M	*	k0(300)=9.0e-32	n=2
			kinf(300)=2.2e-11	m=0
b82	NO+O+M -> NO2+M	*	k0(300)=9.0e-32	n=1.5
			kinf(300)=3.0e-11	m=0
b84	NO+NO3 -> 2NO2		1.5e-11 exp(170/T)	

Carbon reactions

c1	CH4 + O1D -> CH3O2 + OH		1.5e-10	
c1a	CH4 + O1D -> CH2O +H2		1.5e-11	
c2	CH4 + OH -> CH3O2 +H2O		2.45e-12 exp(-1775/T)	
c5	CH3O2 + NO -> CH2O+HO2+NO2		4.2e-12 exp(180/T)	
c7	CH3O2 + HO2 -> CH3OOH+O2		3.8e-13 exp(800/T)	
c8	CH2O + OH -> CO+HO2+H2O		1.e-11	
c9	CH2O + O -> CO+HO2+OH		3.4e-11 exp(-1600/T)	
c10	CH2O + NO3 -> CO+HO2+HNO3		6.e-13 exp(-2058/T)	
c14	CH3O2 + CH3O2 -> 0.6CH3OH+1.4CH2O+0.8HO2			
			2.5e-13 exp(190/T)	
c17	CH3O2H + OH -> CH3O2+H2O		0.58*3.8e-12 exp(200/T)	
c44	CH3O2H + OH-> CH2O+H2O+OH		0.42*3.8e-12 exp(200/T)	
c50	C2H6 + OH -> C2H5O2+H2O		8.7e-12 exp(-1070/T)	
c51	C2H6 + Cl -> HCl + C2H5		7.7e-11 exp(-90/T)	
c52	C2H5O2 + NO -> CH3CHO+HO2+NO2		2.6e-12 exp(365/T)	
c53	C2H5O2 + HO2 -> C2H5OOH+O2		7.5e-13 exp(700/T)	
c54	C2H5O2 + CH3O2 -> 0.7CH2O+0.8CH3CHO+HO2+0.3CH3OH			
	+0.2C2H5OH		3.75e-13 exp(-40/T)	
c55	C2H5O2 + C2H5O2 -> 1.6CH3CHO+1.2HO2			
	+0.4C2H5OH+O2		1.5e-13 exp(-270/T)	
c56	C2H5O2H + OH -> 0.5(C2H5O2+CH3CHO+OH)+H2O		7.0e-12 exp(235/T)	
c57	CH3CHO + OH -> CH3COO2+H2O		5.6e-12 exp(270/T)	
c57et	CH3CHO + NO3 -> CH3COO2+HNO3		1.4e-12 exp(-1900/T)	
c58	CH3CO3H + OH -> CH3COO2+H2O		1.e-11	
c59	CH3CO3 + NO -> CH3O2+NO2+CO2		5.3e-12 exp(360/T)	
c60	CH3CO3 + NO2 +M -> PAN + M	*	k0(300)=9.7e-20	n=5.6
			kinf(300)=9.0e-12	m=1.5
c61	CH3CO3 + HO2 -> 2/3(CH3CO3H+O2)+1/3(CH3COOH+O3)			
			4.5e-13 exp(1000/T)	
c62	CH3CO3 + CH3O2 -> CH3O2 + CH2O + CO2 + HO2			
		*****	c62 = k*kratio/(1+kratio)	
c63	CH3CO3 + CH3O2 -> CH3CO2H + CH2O + O2			
		*****	c63 = k/(1	
+kratio)				
c64	CH3CO3 + CH3CO3 -> 2CH3O2+2CO2		2.9e-12 exp(500/T)	

c65	PAN + OH -> CH2O2CO3NO2+H2O		1.1e-12 exp(-650/T)	
c66	PAN + M -> CH3COO2+NO2+M	****	k0=5.2e-2 exp(-12875/T) k°=2.2e16 exp(-13435/T) fc=0.27	
c67	PAN + NO -> products		1.0e-12	
c68	C2H4 + OH + M -> 2/3(C3H6OHO2)+M	****	k0=9.5e-20 (300/T)3.1 k°=9.5e-12 fc=exp(-T/840)	
c69	C2H4 + O3 -> CH2O+0.4HCOOH+0.52HO2+0.4OH +0.18CO2+0.42CO+0.12H2+0.02H2O		1.2e-14 exp(-2630/T)	
c70	C3H6 + OH + M -> C3H6OHO2+M	****	k0=8.0e-27 (300/T)3.5 kinf=3.0e-11 fc=exp(-T/433)	
c71	C3H6 + O3-> 0.1CH3COOH+0.08CH4+0.585HO2+0.2875CH3O2 +0.37CO+0.5325CH2O+0.4575OH+0.06H2 +0.5CH3CHO+0.2HCOOH+0.33CO2		6.5e-15 exp(-1900/T)	
c72	C3H6 + NO3 -> C3H6NO3		4.0e-15	
c73	C3H6OHO2 + NO -> CH3CHO+CH2O+NO2+HO2		4.2e-12 exp(180/T)	
c74	C3H6OHO2 + HO2 -> C3H6OHOOH+O2		6.5e-13 exp(650/T)	
c75	C3H6OHOOH + OH -> 0.5(C3H6OHO2+CH3COCH2OH+OH) +H2O		3.8e-12 exp(200/T)	

Chlorine reactions

d0	OH + CH3Cl -> CH2Cl + H2O		4.1e-12 exp(-1400/T)	
d2	Cl + O3 -> ClO + O2		2.9e-12 exp(-260/T)	
d3	ClO + O -> Cl + O2		3.0e-11 exp(70/T)	
d4	ClO + NO -> NO2 + Cl		6.4e-12 exp(290/T)	
d5	Cl + CH4 -> HCl + CH3O2		1.1e-11 exp(-1400/T)	
d6	Cl + H2 -> HCl + H		3.7e-11 exp(-2300/T)	
d7	Cl + HO2 -> HCl + O2		1.8e-11 exp(170/T)	
d8	ClO + OH -> Cl + HO2		1.1e-11 exp(120/T)*0.93	
d10	Cl + CH2O -> HCl+CO+HO2		8.1e-11 exp(-30/T)	
d11	OH + HCl -> H2O + Cl		2.6e-12 exp(-350/T)	
d31	ClO + NO2 + M -> ClONO2 + M	*	k0(300)=1.8e-31 kinf(300)=1.5e-11	n=3.4 m=1.9
d32	O + ClONO2 -> NO3 + ClO		2.9e-12 exp(-800/T)	
d33	ClO + HO2 -> HOCl + O2		4.8e-13 exp(700/T)	
d34	OH + HOCl -> H2O + ClO		3.0e-12 exp(-500/T)	
d35	O + HOCl -> OH + ClO		1.7e-13	
d36	Cl + NO2 + M -> ClNO2 + M	*	k0(300)=1.8e-31 kinf(300)=1.0e-10	n=2 m=1
d37	Cl + HOCl -> OH + Cl2		2.5e-12 exp(-130/T)	
d46	ClO+OH -> HCl+O2		1.1e-11 exp(120/T)*0.07	
d47	ClO+ClO -> Cl+OClO		3.5e-13 exp(-1370/T)	
d48	ClO+ClO -> Cl2+O2		1.0e-12 exp(-1590/T)	
d50	CH3CCl3 + OH -> 3 Cl + products		1.8e-12 exp(-1550/T)	
d52	HCFC22 + OH -> Cl + products		1.0e-12 exp(-1600/T)	
d60	ClO + ClO + M -> Cl2O2 + M	*	k0(300)=2.2e-32	n=3.1

			kinf(300)=3.5e-12	m=1
d61	Cl2O2 + M -> ClO + ClO + M	d60/Keq	Keq=1.3e-27 exp(8744/T)	
d62	OClO + OH -> HOCl + O2		4.5e-13 exp(800/T)	
d63	Cl + OClO -> ClO + ClO		3.4e-11 exp(160/T)	
d64	OClO + O -> ClO + O2		2.4e-12 exp(-960/T)	
d65	OClO + NO -> NO2 + ClO		2.5e-12 exp(-600/T)	
d71	O1D+Cl2 -> ClO+Cl		2.8e-10	
d72	Cl2O2+Cl -> Cl2+Cl+O2		1.0e-10	
d73	NO3+Cl -> NO2+ClO		2.4e-11	
d74	NO3+ClO -> NO2+Cl+O2		4.7e-13	
d75	O1D+HCl -> OH+Cl		1.5e-10	
d81	OH+Cl2 -> HOCl +Cl		1.4e-12 exp(-900/T)	
d82	Cl + ClONO2 -> Cl2 + NO3		6.5e-12 exp(135/T)	
d83	HO2+Cl -> OH+ClO		4.1e-11 exp(-450/T)	
d84	Cl+H2O2 -> HCl+HO2		1.1e-11 exp(-980/T)	
d85	O+HCl -> Cl+OH		1.0e-11 exp(-3300/T)	
d87	ClONO2+OH -> HOCl + NO3		1.2e-12 exp(-330/T)	
d90	O1D + CFCl3 -> products		2.3e-10	
d91	O1D + CF2Cl2 -> products		1.4e-10	
d101	CFC10 + O(1D) -> CCl2O + Cl2		3.3e-10	
d102	CFC11 + O(1D) -> CClFO + Cl2		2.3e-11	
d103	CFC12 + O(1D) -> CF2O + Cl2		1.4e-10	
d104	CFC113 + O(1D) -> CClFO + CF2O + Cl2		2.e-10	
d105	CFC114 + O(1D) -> 2 CF2O + Cl2		1.3e-10	
d106	CFC115 + O(1D) -> CF2O + HF + Cl		5.e-11	
d107	HCFC-22 + O(1D) -> CF2O + Cl		1.e-10	
d108	CCl2O + O(1D) -> Cl2 + products		3.6e-10	
d109	CClFO + O(1D) -> HF + Cl + products		1.9e-10	
d110	CF2O + O(1D) -> 2 HF + products		7.4e-11	

Bromine reactions

e0	CH3Br + OH -> H2O + Br + products		4.0e-12 exp(-1470/T)	
e1	CHBr3 + OH -> H2O + 3 Br + products		1.6e-13 exp(-710/T)	
e2	Br + O3 -> BrO + O2		1.7e-11 exp(-800/T)	
e3	BrO + O -> Br + O2		1.9e-11 exp(230/T)	
e4	BrO + NO -> NO2 + Br		8.8e-12 exp(260/T)	
e5a	BrO + ClO -> OClO + Br		1.6e-12 exp(430/T)	
e5b	BrO + ClO -> Br + Cl + O2		2.9e-12 exp(220/T)	
e5c	BrO + ClO -> BrCl + O2		5.8e-13 exp(170/T)	
e6	BrO + BrO -> 2Br + O2		1.5e-12 exp(230/T)	
e7	Br + HO2 -> HBr + O2		1.5e-11 exp(-600/T)	
e8	Br + OClO -> BrO + ClO		2.6e-11 exp(-1300/T)	
e9	Br+CH2O -> HBr+ CO + HO2		1.7e-11 exp(-800/T)	
e11	OH + HBr -> H2O + Br		1.1e-11	
e13	BrO + NO2 + M -> BrONO2 + M	*	k0(300)=5.2e-31	n=3.2
			kinf(300)=6.9e-12	m=2.9
e15	BrO + HO2 -> HOBr + O2		3.4e-12 exp(540/T)	
e71	O1D+HBr -> OH+Br		1.5e-10	
e72	BrO+OH -> HO2+Br		7.5e-11	
e81	O+HBr -> Br+OH		5.8e-12 exp(-1500/T)	

e91	ha-1301 + O(1D) -> Br + 3HF + prod.	1.e-10
e92	ha-1211 + O(1D) -> Br + Cl + prod.	1.5e-10
e93	CH3Br + O(1D) -> Br + prod.	1.8e-10

Oxygen reactions

hk1	O + O + M -> O2 + M	4.23e-28 [M]/T2
hk2	O + O2 + M -> O3 + M	6.0e-34*(300/T)2.3*[M]
hk3	O + O3 -> O2 + O2	8.0e-12 exp(-2060/T)
hk4	O1D + N2 -> O + N2	1.8e-11 exp(110/T)
hk5	O1D + O2 -> O + O2	3.2e-11 exp(70/T)
hk7	O1D + O3 -> O2 + O2	1.2e-10
hk21	O1D+N2 +M -> N2O +M	3.5e-37*(300*T)0.6*[M]

Table 6. Reaction probabilities for heterogeneous ractions .

Reaction	Type I	Type II
het1	0.006	0.3
het2	0.3	0.3
het3	0.0006	0.03
het4	0.003	0.03
het5	0.1	0.3

Table 7. Values of Henry's Law coefficients.

Species	*k* (mol l^{-1} atm^{-1})
HNO3	3.3e6
H2O2	7.36e4
CH3OOH	221
HCl	3.3e5
HO2NO2	3.3e6
CH2O	6.3e3

Table 8. Lower and upper boundary conditions for the transported species and families.
Flux in units of cm-2s-1.

	Boundary Conditions		
	0 km	120 km	dry deposition at surface
N2O	flux (see text)	flux = 0.	wd = 0.
CH4	flux (see text)	flux = 0.	wd = 0.
H2O	m.r. (see text)	flux = 0.	wd = 0.
NOy	flux (see text)	flux (see text)	wd (see text)
HNO3	flux = 0.	flux = 0.	wd (see text)
N2O5	flux = 0.	flux = 0.	wd (see text)
Cly	flux = 0.	flux = 0.	wd = 0.
Ox	flux = 0.	m.r. O(3P)	wd (see text)
CO	flux (see text)	flux = 0.	wd (see text)
OClO	flux = 0.	flux = 0.	wd = 0.
HCl	flux = 0.	flux = 0.	wd = 0.
ClONO2	flux = 0.	flux = 0.	wd = 0.
HOCl	flux = 0.	flux = 0.	wd = 0.
Cl2	flux = 0.	flux = 0.	wd = 0.
H2O2	flux = 0	flux = 0.	wd (see text)
ClNO2	flux = 0.	flux = 0.	wd = 0.
HBr	flux = 0.	flux = 0.	wd = 0.
BrONO2	flux = 0.	flux = 0.	wd = 0.
NOx	flux (see text)	m.r. of NO	wd (see text)
HO2NO2	flux = 0.	flux = 0.	wd = 0.
ClOx	flux = 0.	flux = 0.	wd = 0.
BrOx	flux = 0.	flux = 0.	wd = 0.
Cl2O2	flux = 0.	flux = 0.	wd = 0.
HOBr	flux = 0.	flux = 0.	wd = 0.
CO2	m.r.(see text)	flux = 0.	wd = 0.2
C2H6	flux (see text)	flux = 0.	wd = 0.
C2H4	flux (see text)	flux = 0.	wd = 0.
C3H6	flux (see text)	flux = 0.	wd = 0.
CH2O	flux = 0	flux = 0.	wd (see text)
PAN	flux = 0	flux = 0.	wd (see text)
H2	flux (see text)	m.r. = 1.66e-6	wd (see text)
HOx	flux = 0	flux = 0.	wd = 0.
CFC-10	m.r. (see text)	flux = 0.	wd = 0.
CFC-11	m.r. (see text)	flux = 0.	wd = 0.
CFC-12	m.r. (see text)	flux = 0.	wd = 0.
CFC-113	m.r. (see text)	flux = 0.	wd = 0.
CFC-114	m.r. (see text)	flux = 0.	wd = 0.
CFC-115	m.r. (see text)	flux = 0.	wd = 0.
HCFC-22	m.r. (see text)	flux = 0.	wd = 0.
CH3CCl3	m.r. (see text)	flux = 0.	wd = 0.

CH3Cl	m.r. = 6.e-10	flux = 0.	wd = 0.
CCl2O	m.r. ClONO2 *0.014	flux = 0.	wd = 0.
CClFO	m.r. ClONO2 *0.033	flux = 0.	wd = 0.
CF2O	m.r. ClONO2 *0.1	flux = 0.	wd = 0.
Ha-1211	m.r. (see text)	flux = 0.	wd = 0.
Ha-1301	m.r. (see text)	flux = 0.	wd = 0.
HF	m.r. Cly *0.25	flux = 0.	wd = 0.
CH3Br	m.r. (see text)	flux = 0.	wd = 0.
Bry	flux = 0.	flux = 0.	wd = 0.
CHBr3	m.r. = 2.e-12	flux = 0.	wd = 0.
O(3P)	flux = 0.	m.r. = 0.99 - N2 - O2	wd = 0.
O3	flux = 0.	flux = 0.	wd (see text)
NO2	flux (see text)	flux = 0.	wd (see text)
NO	flux (see text)	m.r. = 5.e-5	wd (see text)
H	flux = 0.	m.r. = 5.e-6	wd = 0.

Table 9. Global surface emission of source gases

	Emissions from each category						
Species	industrial	ruminants	vegetation	soil/fauna	wetland	rice paddy	biomass burning	ocean
N2O(Tg-N yr-1)	1.2	0	0	0.5	0	0	0.05	0.3
CH4(Tg yr-1)	130.9	76	0	34	91	88	42.8	9.8
H2(Tg yr-1)	20	0	0	3	0	0	10	3
CO(Tg yr-1)	381.6	0	666	0	0	0	710.5	13
NOx(Tg-N yr-1)	23.3	0	0	6.6	0	0	4.9	0
C2H6(Tg-C yr-1)	6	0	0.8	0	0	0	4.7	0.8
C2H4(Tg-C yr-1)	4.3	0	4.3	0	0	0	14.8	8.2
C3H6(Tg-C yr-1)	1.7	0	0.8	0	0	0	6.5	9.9

Table 10. Latitudinal distribution of emissions and methane soil uptake (in units of m-2).

	Emissions category								
Latitude	industrial	ruminants	veget.	soil/fauna	wetland	paddy	biomass b.	ocean	CH4 soil abs.
-85	0	0	0	0	0	0	0	2.1e-16	0
-80	0	0	0	0	0	0	0	4.3e-16	0
-75	0	0	0	0	0	0	0	1.1e-15	0
-70	0	0	0	0	0	0	0	1.7e-15	0
-65	0	0	0	0	0	0	0	2.8e-15	0
-60	0	0	0	0	0	0	0	3.9e-15	0
-55	6.6e-17	4.9e-18	0	4.6e-17	0	0	0	4.3e-15	0
-50	1.3e-16	8.0e-18	0	9.2e-17	0	0	0	4.7e-15	0
-45	4.0e-16	1.6e-16	3.9e-17	2.3e-16	1.8e-16	0	1.2e-16	4.3e-15	0
-40	6.6e-16	3.2e-16	7.8e-17	3.7e-16	3.6e-16	0	2.3e-16	3.9e-15	3.2e-16
-35	4.4e-16	1.2e-15	2.3e-16	1.0e-15	7.2e-16	0	8.9e-16	3.2e-15	5.9e-16
-30	4.8e-16	2.1e-15	3.9e-16	1.7e-15	1.1e-15	0	1.5e-15	2.5e-15	8.4e-16
-25	4.0e-16	2.4e-15	1.5e-15	2.1e-15	1.2e-15	1.3e-15	2.0e-15	2.2e-15	1.1e-15
-20	3.1e-16	2.7e-15	2.6e-15	2.5e-15	1.4e-15	2.7e-15	2.5e-15	1.8e-15	1.5e-15
-15	1.5e-16	2.3e-15	3.9e-15	2.6e-15	1.6e-15	3.9e-15	3.1e-15	1.8e-15	2.0e-15
-10	0	1.9e-15	5.1e-15	2.6e-15	1.8e-15	5.1e-15	3.8e-15	1.8e-15	1.5e-15
-5	8.9e-17	1.7e-15	5.4e-15	2.8e-15	1.8e-15	3.1e-15	3.0e-15	1.8e-15	9.8e-16
0	1.7e-16	1.6e-15	5.6e-15	2.9e-15	1.8e-15	1.1e-15	2.2e-15	1.8e-15	9.7e-16
5	2.6e-16	1.6e-15	5.2e-15	2.8e-15	1.4e-15	3.2e-15	3.0e-15	1.8e-15	9.8e-16
10	3.5e-16	1.6e-15	4.8e-15	2.8e-15	1.0e-15	5.4e-15	3.7e-		

15 1.8e-15 1.2e-15
15 5.1e-16 1.7e-15 3.6e-15 2.9e-15 8.9e-16 5.5e-15 3.5e-15 1.7e-15 1.5e-15
20 6.6e-16 1.8e-15 2.5e-15 3.1e-15 7.2e-16 5.5e-15 3.2e-15 1.6e-15 1.4e-15
25 2.0e-15 2.0e-15 1.7e-15 3.1e-15 7.2e-16 4.0e-15 2.9e-15 7.9e-16 1.3e-15
30 3.4e-15 2.2e-15 9.4e-16 3.1e-15 7.2e-16 2.5e-15 2.7e-15 1.4e-15 2.2e-15
35 5.6e-15 3.1e-15 7.8e-16 2.7e-15 8.9e-16 1.9e-15 2.4e-15 1.3e-15 3.2e-15
40 7.8e-15 4.0e-15 6.2e-16 2.4e-15 1.0e-15 1.3e-15 2.1e-15 1.2e-15 3.9e-15
45 9.3e-15 5.0e-15 4.7e-16 2.2e-15 4.3e-15 6.4e-16 1.9e-15 1.1e-15 4.8e-15
50 1.0e-14 6.0e-15 3.1e-16 2.0e-15 7.5e-15 0 1.6e-15 9.9e-16 6.2e-15
55 8.9e-15 4.8e-15 3.1e-16 1.7e-15 9.5e-15 0 1.4e-15 7.1e-16 8.1e-15
60 6.8e-15 3.5e-15 3.1e-16 1.4e-15 1.1e-14 0 1.2e-15 4.3e-16 8.3e-15
65 4.2e-15 2.1e-15 2.3e-16 1.2e-15 8.6e-15 0 8.9e-16 2.8e-16 8.6e-15
70 1.6e-15 8.1e-16 1.5e-16 9.2e-16 5.7e-15 0 5.9e-16 1.4e-16 5.3e-15
75 1.0e-15 5.6e-16 7.8e-17 6.9e-16 4.6e-15 0 4.1e-16 1.2e-16 0
80 3.5e-16 3.2e-16 0 4.6e-16 3.6e-15 0 2.3e-16 9.4e-17 0
85 1.8e-16 1.6e-16 0 3.4e-16 1.8e-15 0 1.2e-16 4.7e-17 0

Table 11. Boundary coefficients as a function of latitude.

	Coefficients				
Latitude	b(CO2)	b(CFC-10)	b(CFC-11)	b(CFC-12)	b(CH3CCl3)
-85	-1.7	0.96	0.87	0.91	0.85
-80	-1.7	0.96	0.87	0.91	0.85
-75	-1.7	0.96	0.87	0.91	0.85
-70	-1.7	0.96	0.87	0.91	0.85
-65	-1.7	0.96	0.87	0.91	0.85
-60	-1.7	0.96	0.87	0.91	0.85
-55	-1.7	0.96	0.87	0.91	0.85
-50	-1.7	0.97	0.88	0.92	0.85
-45	-1.6	0.97	0.88	0.92	0.86
-40	-1.6	0.97	0.88	0.92	0.86
-35	-1.5	0.97	0.88	0.92	0.87
-30	-1.4	0.98	0.9	0.93	0.88
-25	-1.2	0.98	0.9	0.93	0.88
-20	-1.1	0.99	0.9	0.93	0.89
-15	-0.8	0.99	0.92	0.95	0.9
-10	-0.6	0.99	0.92	0.95	0.92
-5	-0.4	0.99	0.94	0.97	0.93
0	-0.1	0.99	0.96	0.98	0.96
5	0.1	0.99	0.98	0.99	1.
10	0.4	1.01	1.	1.	1.02
15	0.7	1.01	1.01	1.01	1.05
20	0.9	1.01	1.03	1.01	1.08
25	1.1	1.01	1.07	1.02	1.1
30	1.3	1.02	1.09	1.05	1.12
35	1.5	1.02	1.1	1.06	1.13
40	1.6	1.03	1.2	1.15	1.15
45	1.7	1.03	1.2	1.15	1.15
50	1.8	1.03	1.2	1.15	1.15
55	1.9	1.03	1.2	1.15	1.15
60	1.9	1.04	1.2	1.15	1.15
65	1.9	1.04	1.2	1.15	1.14

70	2.	1.05	1.2	1.15	1.14
75	2.	1.05	1.2	1.15	1.13
80	2.	1.06	1.1	1.06	1.12
85	2.	1.06	1.08	1.04	1.11

SOCRATES

Table of Contents